Vertical plate motions in the West Siberian Basin and Northern Europe as indicators of mantle-induced dynamic topography

Yulia Vibe

München 2017

Vertical plate motions in the West Siberian Basin and Northern Europe as indicators of mantle-induced dynamic topography

Yulia Vibe

Dissertation
An der Fakultät für Geowissenschaften
der Ludwig-Maximilians-Universität
München

vorgelegt von
Yulia Vibe
aus Nowosibirsk

München, 13.09.2017

Erstgutachter: Prof. Dr. Hans-Peter Bunge

Zweitgutachter: Dr. Stuart R. Clark

Tag der mündlichen Prüfung: 05.02.2018

Acknowledgements

I would like to express my sincere gratitude to my supervisors **Dr. Stuart R. Clark** and **Prof. Dr. Hans-Peter Bunge** for all the support and guidance over the last years. I am very thankful for everything you taught me as a researcher and as a person.

Also, I would like to thank my parents for always helping me in everything I do. Your example of dedication, hard work and passion to learn has always been my main inspiration in work and life.

This thesis would be impossible without the help of **Prof. Dr. Anke Friedrich, Dr. Lorenzo Colli, Dr. Stefanie Rieger and Dr. Christoph Moder**. Thank you very much for the knowledge you gave me and for your contribution and support during this project.

And, of course, thanks to my beloved friends and family: to the family Schmidt for being my home in Munich and to Bernardo and Teodora for making my PhD years joyful.

Summary

Motion of the lithospheric plates is a reflection of the convective circulation of the Earth's mantle. Plate divergence is attributed to the mantle upwellings, while plate convergence to the mantle's downwellings. In addition to the horizontal movement, plates move vertically. Vertical plate motions are documented both at the tectonic boundaries and in the plate interior. The marginal vertical motions can be explained by changes of the stress state in the plate boundary setting. Yet, a mechanism responsible for the intra-plate vertical motions still remains unclear. Understanding this mechanism would shed the light on the nature of anomalous topographic features and improve the knowledge of the poorly constrained Earth's mantle parameters. Moreover, it would have implications for minimizing the risks associated with explorations of natural energy resources.

In this work we study the character of intraplate vertical motions and their driving forces in the West Siberian Basin (WSB) and Northern Europe. We begin by constraining the tectonic subsidence history of the WSB. The WSB's sedimentary cover represents an archive of the basin's vertical motions for the last 250 million years. Due to the basin's intraplate location and the large scale, it serves as a perfect location to study the vertical motions isolated from the effects of plate boundary stresses. Our analysis shows that the WSB experienced anomalous subsidence interrupted by repeated episodes of uplift, consistent with uplift events reported in the Barents Sea and at the North Atlantic passive margin.

We extend our study by exploring the vertical motions in the northern Europe and the North Atlantic. To illustrate the regional topographic evolution, we construct the digital continent-scale erosional surface maps for 5 stratigraphic boundaries of Cenozoic. The maps reveal that northern Europe experienced increased erosion in the late Paleocene – late Eocene and in the Miocene. These time intervals also correspond to the episodes of increased North Atlantic spreading velocity. Accordingly, our work shows a strong agreement between the two trends. In addition, we find that these results agree with the dynamic topography trend inferred by the output of a mantle convection model. We connect these findings through a common mantle-related mechanism.

We suggest that observed trend may indicate a fast, plume-fed flow in the thin asthenospheric channel beneath Northern Europe. The topographic signal may reflect a mantle flow driven by the pressure gradient related to Iceland. Such flow serves as a link between the horizontal and vertical plate motions and could have implications for the paleo-topographic and basin development studies in Europe and in other regions.

Contents

Introduction

Preface

This work addresses the fundamental questions related to the vertical plate tectonics. Vertical motions of plates are observed worldwide. They play an important role in shaping the Earth's surface as we see it today. Besides that, vertical motions are directly related to the formation of the hydrocarbon resources that bring energy to the modern life. Despite the huge impact on our world, their nature is not fully understood. The major challenge to overcome is the complexity of the Earth systems consisting of many inter-related parameters, some of which are concealed in the depth of the Earth. In this thesis we attempt to make a step in understanding the character of the vertical motions and their driving mechanisms.

Background

i.   Plate tectonics

At the beginning of the twentieth century, a German researcher Wegener (1880 – 1930) published a book "The Origin of Continents and Oceans" (Wegener, 1920). This book presented a theory that all continents were once joined into one origin continent and then consequently drifted apart. The theory of continental drift was supported by paleontological and geological evidence matching on adjacent continents that were supposedly connected in the past. Nevertheless, during Alfred's life his theory was met with criticism and rejection. Almost fifty years later, with the development of technologies facilitating geophysical explorations, the idea of continental drift was accepted leading to the rise of the field of Plate Tectonics.

Plate Tectonics studies motions of plates – rigid blocks of the Earth's outer shell (Morgan, 1968). The outer shell resembles lithosphere – the outermost layer, which covers the Earth interior layers – the mantle and the core (Figure 1). Unlike the theory of continental drift, plate tectonics also studies the mechanisms that drive the plates. Nowadays it is widely accepted that the major source of energy responsible for the motions of plates is the heat of the Earth's interior (Turcotte and Schubert, 2014). This heat is generated by the radioactive decay inside the core and then transferred to the

outer layers. The heat transfer at the core-mantle boundary occurs by the means of **conduction.** This type of heat transfer is a result of the microscopic collision of particles and movement of the electrons within a body. Once the mantle is heated up, the heat is further transferred through the mantle by the means of **advection**. Advection is another type of heat transfer, occurring by the bulk motion of the material. The combination of conduction at the core-mantle boundary and advection throughout the mantle constitutes the process of mantle **convection**.
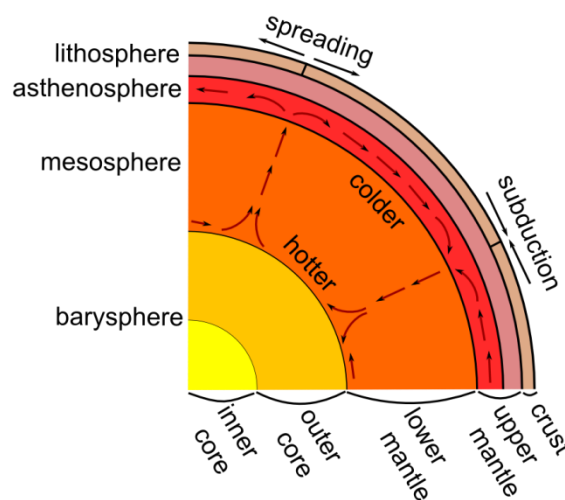
Figure 1. Schematic drawing of the Earth's layers. A simplified mantle convection cartoon illustrates how mantle drives plate tectonics. The hotter mantle rises up forcing plates apart at spreading ridges and colder mantle sinks down dragging plates at subduction zones.

Mantle convection is induced by buoyancy – a body force described by Archimedes' principle (Fowler, 2004; Turcotte and Schubert, 2014). The principle states: "Any object, wholly or partially immersed in a stationary fluid, is buoyed up by a force equal to the weight of the fluid displaced by the object." Thus, buoyancy is driven by the weight – or better said – density differences. The Earth's solid mantle behaves as a viscous fluid on a geological time scale of millions of years (Cathles, 1975). In the mantle, hotter and less dense material rises upwards by buoyancy and, oppositely, colder and denser material sinks down. Such motion of the mantle is a principle mechanism responsible for plate tectonics (Turcotte and Schubert, 2014). When the hot mantle material reaches the Earth's surface it creates the new oceanic floor and pushes the plates apart at the mid-oceanic ridge, a process known as oceanic spreading. As the material cools down and

becomes denser it sinks down at subduction zones (Figure 1). This is a basic mechanism driving the plates horizontally.

ii.   Vertical Plate motions

As mentioned above, mantle convection drives the plates in horizontal perspective, but the plates also move vertically. Vertical plate motions are common at the plate boundaries. Mountain building is an example of an upward vertical plate motion, or uplift, occurring when plates converge and collide. Moreover, convergence of plates can trigger the downward plate motion – subsidence. The mechanisms of subsidence in the vicinity of convergent boundaries include flexure of lithosphere, foreland and fore-arc basin development (Allen and Allen, 2013; Watts, 2001). The divergent plate boundaries are also associated with vertical motions. In this case, the ridge uplift occurs when mantle material rises up to the surface, lifting the ocean floor (Phipps Morgan et al., 1987). After reaching the surface, the mantle material becomes a part of the sea-floor, moves away from the spreading center and subsides due to cooling (Allen and Allen, 2013).

In some cases, vertical motions are observed away from the plate boundaries. A well-known mechanism of the intraplate vertical movement is the removal of a large amount of weight from the Earth's surface. When the weight is removed, the crust is going to rise in order to achieve a new equilibrium in the process called "isostatic rebound". Isostatic equilibrium is a gravitational balance between the Earth's layers – crust and mantle, where crust is "floating" in the underlying denser mantle (Watts, 2001). A good example of the isostatic rebound is post-glacial uplift, occurring when the ice-sheets of the glacial period retreat causing the underlying crust to re-adjust (Sigmundsson, 1991).

Interestingly, vertical motions of plates are also observed in the locations remote from tectonic boundaries and not associated temporarily or spatially with the glacial rebound. For example, the Earth's surface has experienced large amounts of subsidence in the plate interior, forming depressions (Pysklywec and Mitrovica, 1998). In the process of subsidence such depressions accumulate sediments, leading to the development of intra-plate sedimentary basins. The intra-plate basins occur on all continents, and the largest of them is the West Siberian Basin (WSB) (Leighton, 1991) (Figure 2). The WSB covers the territory of about 3 million km2, which is approximately the size of Western Europe (Vyssotski et al., 2006). Forces, responsible for the downward motion of such

large areas remain debated. Moreover, geological observations suggest that at some time periods intra-plate basins were subjected to intense uplift. The uplift of intra-plate basins inhibited further accumulation of sediments and led to erosion. Processes governing the uplift of intra-plate basin are not yet clear either.
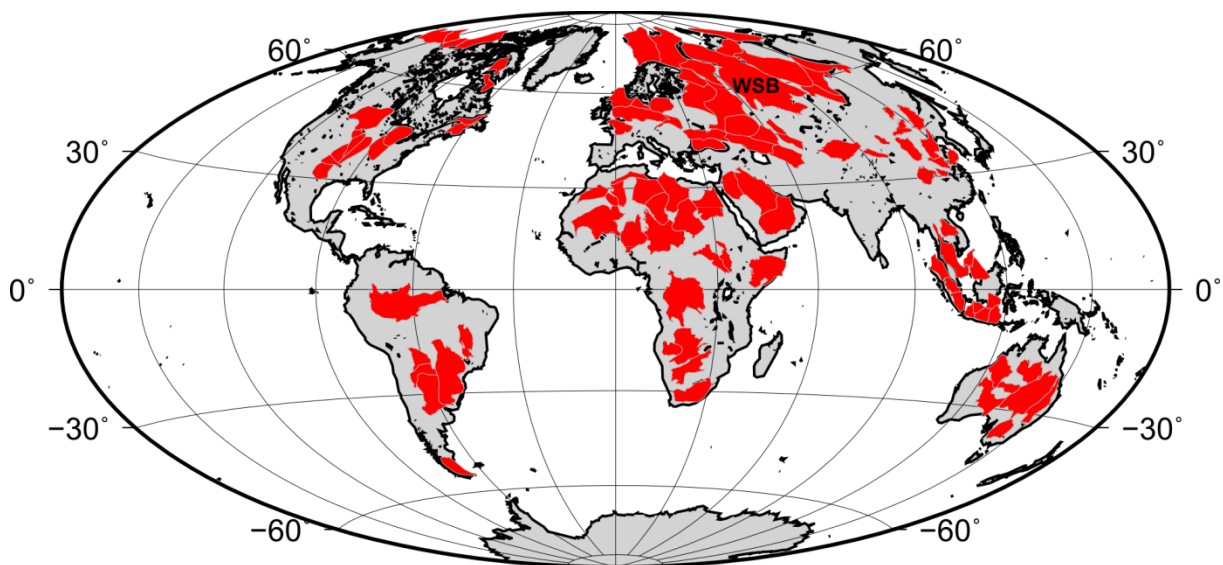
Figure 2. World map of intra-plate basins. The compilation of basins is based on the set of intracontinental basins (Heine, 2007), interior cratonic basins (Leighton, 1996) and basin polygons provided by Statoil. The largest intra-plate basin – the West Siberian Basin (WSB) – is later used in the study.

Some studies (e.g., Cloetingh, 1988) relate intra-plate vertical motions to the far-field effects of the changes at the plate boundaries. However, in many cases subsidence and uplift affect areas that are further away from the possible influence of the stresses at plate boundaries (See Chapter 1). In addition, the timing of the intra-plate vertical motions and tectonic events at the plate boundaries does not always agree. In these cases it is difficult to establish an accurate relation between the two events. A potential explanation of vertical motions in such regions is the stress exerted on the plates by the underlying mantle. This mechanism overcomes the spatial limitation related to the distance to plate boundaries, since the mantle flow is present globally. Its role in the vertical displacement of crust in response to mantle flow is a topic of active research and is referred to as dynamic topography.

iii.   **Dynamic topography**

Dynamic topography is a deflection of the Earth's surface in response to the underlying mantle flow. The term "dynamic" is chosen due to the fact that on the geological time scale the mantle is constantly in motion. If present, the vertical component of the mantle flow may produce topographic signals. Hence, the signals may vary spatially and temporally, depending on the mantle state. Dynamic topography and its scales can be inferred from numerical models and geophysical observations. A prominent example of dynamic topography is the anomalously high elevation of the southeast of Africa associated with a hot mantle anomaly revealed by seismic tomography (Lithgow-Bertelloni and Silver, 1998). Also, geological data indicates differential vertical plate motions in the interior of the North American continent. Namely, the Western Interior Seaway of North America was actively subsiding in the late Cretaceous, but was uplifted in the Tertiary (Bond, 1976; Liu and Nummedal, 2004). According to these observations, the wavelength of dynamic topography varies from ~100 km to ~1000 km and its amplitude is in the order of 1-2 km (Flament et al., 2013).

The exact mechanism of dynamic topography is a question of active research. Recent numerical models significantly advanced our understanding of the mantle convection. Nevertheless, the lack of accurate constraints on the density and viscosity structure of the mantle remains an obstacle to fully understand and model the mantle flow. The present day mantle structure can be to some degree constrained by the seismic tomography (Kárason and Van Der Hilst, 2000). However, reconstructing the mantle flow of older geological ages is a more complex task, because the past mantle structure is unknown. It involves implementation of sophisticated numerical algorithms and often relies on the global plate motion models and theoretical assumptions. As a consequence, the uncertainties related to the mantle induced topography become significant. Classification of the available algorithms and their limitations is presented by Flament et al. (2013).

iv.   **Surface observations**

Just as the mantle flow models can be used to constrain dynamic topography, also information on the topography evolution can improve our knowledge of the mantle processes. This is done by comparing the surface expressions of dynamic topography

with topography predicted by mantle models. Thus, surface observations serve as a valuable source of information in understanding the deep Earth's processes.

At the moment, the geological constraints of the dynamic topography evolution are of a local character. Moreover, detecting the dynamic component of vertical motions on a local scale is often difficult because at times it is not easily distinguishable from other tectonic mechanisms. Therefore, the most informative regions to observe dynamic topography are larger-scale plate interiors where effects of other tectonic controls are smaller (Gurnis, 1992). The record of the vertical motions is preserved by the sedimentary basins and can be restored from their cover.

The aim of this thesis is to contribute to the global database of dynamic topography evolution by studying the anomalous vertical motions of the largest intra-continental sedimentary basin – the West Siberian Basin (Chapter 1). We then extend our analysis of vertical motions to the Barents Sea and Northern Europe. In order to understand the relation of vertical motions and the mantle, we juxtapose the trends of the observed vertical motions and available mantle flow indicators. The latter include vertical motions predicted by the mantle convection model and relative velocity of Eurasian plate. More details on the hypotheses, methods and results of this work are provided in the Summary of chapters.

Summary of chapters
Chapter 1 – Anomalous subsidence history of the West Siberian Basin as an indicator for mantle-induced dynamic topography

The West Siberian Basin is a good example of the intra-continental region that has experienced vertical motions. The basin's sedimentary cover recorded the history of subsidence and uplift from the Permo-Triassic and until the late Paleogene. Although the basin has been extensively explored, its development mechanisms are not very clear. The traditional view on its formation process presumes the post-rift thermal accommodation subsidence (Lobkovsky et al., 1996). We contributed by calculating the tectonic component of the basin's subsidence and uplift on the scale of the whole basin based on geological data.

Furthermore, we assessed whether the calculated subsidence would agree with the model of the post-rift thermal basin subsidence. Our results demonstrated that calculated and modelled subsidence trends differ in several aspects. The subsidence of the West Siberian Basin was about twice larger and lasted longer than the thermal subsidence. Also, the basin experienced migration of the subsidence center and repeated uplift events. Such observations indicate that thermal subsidence is unlikely to be the only mechanism responsible for the basin's development and the vertical motions reflect the underlying mantle processes.

Chapter 2 – Kalkulo Report on the vertical motions in the Barents Sea

Mantle convection is a process, operating on a very large continent scale (Jones et al., 2011). Therefore, the mantle-induced vertical motions in the West Siberian Basin may be also reflected in the proximate regions. An area to the northwest of the WSB – the Barents Sea contains several deep intracratonic basins, where this hypothesis can be tested. Due to a very high hydrocarbon potential, the Barents Sea has been extensively explored, and a large amount of data is freely available (Henriksen et al., 2011). Thus, tectonic events and vertical motions of the Barents Sea basins are relatively well constrained. We dedicate Chapter 2 to reviewing the data and models of the Barents Sea geology to understand the character of its vertical motions. The data indicate the following pattern: Permo-Triassic rifting followed by intense Triassic subsidence; a rifting event at the end of Jurassic – beginning of Cretaceous accompanied by an uplift of highs; moderate subsidence in the Cretaceous and the late Cretaceous – Paleogene uplift and the Neogene intense uplift. We have found that the character of the vertical motions in the Barents Sea resembles the one in the WSB. This is a very strong indication that the vertical motions in these regions are governed by a common mechanism likely manifesting the mode of the underlying mantle flow.

Chapter 3 – Repeated Cenozoic erosional events in northwestern Eurasia during episodes of faster spreading: implications for the common driving mechanism

In the two previous chapters we have learned that large parts of Eurasia are affected by coeval vertical motion. Moreover, coeval vertical motions have been reported along the

North Atlantic margin – in Greenland, the British Isles and Norway (Japsen and Chalmers, 2000). In this chapter we constrained the evolution of European topography by the means of digital hiatus surface maps at the bases of 5 distinct Cenozoic epochs. These results show two episodes of the areal increase in erosion occurring at the Paleocene-Eocene boundary and in the Miocene. In order to understand the role of the mantle convection flow in the European topography we compare this trend to the indicators of the underlying mantle flow. The hiatal area curve is very close qualitatively and also quantitatively (since Miocene) to the dynamic topography predicted by the mantle convection model. Moreover, the observed trends are in strong qualitative agreement with the North Atlantic spreading velocity trend. Our work links the vertical and horizontal plate motions in the North Atlantic through a pressure-driven mantle flow triggered by the mantle anomaly associated with the Icelandic mantle plume.

Conclusion

The outcome of our work provides estimates of the spatial and temporal pattern of vertical motions in Western Siberia since the Permo-Triassic and in northwestern Eurasia since the late Cretaceous. Our results reveal a remarkable closeness in the character of certain subsidence and uplift events in various locations of the study area. The large spatial extent of the corresponding vertical tectonics indicates their strong relation to the deep Earth's processes. This hypothesis was further supported by the mantle convection model output and the analysis of the plate velocity variations in the North Atlantic, which directly reflect the mantle convection mode in the region. The analysis demonstrated that episodes of velocity increase of Eurasia relative to North America corresponded to an overall increase of uplifted area in northwestern Eurasia. We interpret this outcome as an indication of a common mechanism, relating the spreading velocity variations and topography variations.

A number of analytical and numerical solutions proposed that a pressure driven flow in the mantle asthenosphere could link the changes of horizontal and vertical plate motions (Höink et al., 2012; Höink and Lenardic, 2010). Moreover, these models also set constraints on the asthenospheric structure characterized by lower viscosity and thinner channel shape (Weismüller et al., 2015). These models demonstrate that the flow in the thin low-viscosity asthenosphere would have a strong pressure-driven

component associated with higher flow velocities. On its way through the asthenosphere, the pressure-driven flow would also induce vertical plate motions. In the case of North Atlantic, the pressure gradient may arise due to the mantle anomaly related to the Iceland plume. The rising anomaly would cause a topographic signal, first focused on the plume area and moving radially away from the plume (Friedrich et al., 2017). Such anomaly would also cause changes of the spreading velocities. Our work is a systematic approach to support this theory by the surface observations.

We observed that the pattern of dynamic topography is in a good agreement with the suggested mantle flow mechanism. An important consequence of this agreement is the possibility to elaborate the constraints on the mantle structure. Better constraints of mantle parameters would allow more accurate mantle convection models improving our knowledge of the deep Earth processes. Thus, the focus of the future work should be on the analytical estimation of elements characterizing the mantle convection system in order to minimize the misfit between the modelled and observed topography.

Deeper understanding of the laws governing the vertical motions and the mantle flow would also have a practical value in the energy field. Knowing the processes underlying the sedimentary basins' development would facilitate decision making process in the hydrocarbon domain. This knowledge would reduce the costs of exploration drilling and also decrease the risks associated with it.

References

Allen, P.A., Allen, J.R., 2013. Basin analysis: Principles and application to petroleum play assessment. John Wiley & Sons.

Bond, G., 1976. Evidence for continental subsidence in North America during the Late Cretaceous global submergence. Geology 4, 557–560.

Cathles, L.M., 1975. Viscosity of the Earth's Mantle. Princeton University Press.

Cloetingh, S., 1988. Intraplate stresses: a new element in basin analysis, in: New Perspectives in Basin Analysis. Springer, 205–230.

Flament, N., Gurnis, M., Müller, R.D., 2013. A review of observations and models of dynamic topography. Lithosphere 5, 189–210.

Fowler, C.M.R., 2004. The Solid Earth, An Introduction to Global Geophysics, 2nd Edition. Cambridge University Press.

Friedrich, A.M., Bunge, H.-P., Rieger, S.M., Colli, L., Ghelichkhan, S., Nerlich, R., 2017. Stratigraphic framework for the plume mode of mantle convection and the analysis of interregional unconformities on geological maps. Gondwana Res.

Gurnis, M., 1992. Long-term Controls Eustatic and Epeirogenic Motions by Mantle Convection. GSA TODAY 2.

Heine, C., 2007. Formation and evolution of intracontinental basins, PhD Thesis, School of Geosciences, The University of Sydney, Australia.

Henriksen, E., Ryseth, A., Larssen, G., Heide, T., Roenning, K., Sollid, K., Stoupakova, A., 2011. Chapter 10 Tectonostratigraphy of the greater Barents Sea: implications for petroleum systems. Geol. Soc. Lond. Mem. 35, 163–195.

Höink, T., Lenardic, A., 2010. Long wavelength convection, Poiseuille–Couette flow in the low-viscosity asthenosphere and the strength of plate margins. Geophys. J. Int. 180, 23–33.

Höink, T., Lenardic, A., Richards, M., 2012. Depth-dependent viscosity and mantle stress amplification: implications for the role of the asthenosphere in maintaining plate tectonics. Geophys. J. Int. 191, 30–41.

Japsen, P., Chalmers, J.A., 2000. Neogene uplift and tectonics around the North Atlantic: overview. Glob. Planet. Change 24, 165–173.

Jones, S.M., Lovell, B., Crosby, A.G., 2011. Temporal and Spatial Scales of Sub-Continental Mantle Convection: Comparison of Modern and Geological Observations of Dynamic Support. AGU Fall Meet. Abstr, 11.

Kárason, H., Van Der Hilst, R.D., 2000. Constraints on Mantle Convection from Seismic Tomography, in: Richards, M.A., Gordon, R.G., Van Der Hilst, R.D. (Eds.), The History and Dynamics of Global Plate Motions. American Geophysical Union, 277–288.

Leighton, M.W., 1996. Interior cratonic basins: a record of regional tectonic influences. Spec. Pap.-Geol. Soc. Am., 77–94.

Leighton, M.W., 1991. Interior cratonic basins. American Association of Petroleum Geologists.

Lithgow-Bertelloni, C., Silver, P.G., 1998. Dynamic topography, plate driving forces and the African superswell. Nature 395, 269-272.

Liu, S., Nummedal, D., 2004. Late Cretaceous subsidence in Wyoming: Quantifying the dynamic component. Geology 32, 397–400.

Lobkovsky, L.I., Cloetingh S., Nikishin A.M., Volozh Yu.A., Lankkreijer A.C., Belyakov S.L., Groshev V.G., Fokin P.A., Milanovsky E.E., Pevzner L.A., Gorbachev V.I., Korneev M.A., 1996, Extensional basins of the former Soviet Union - structure, basin formation mechanisms and subsidence history, Tectonophysics 266, 251-285

Morgan, W.J., 1968a. Rises, trenches, great faults, and crustal blocks. J. Geophys. Res. 73, 1959–1982.

Phipps Morgan, J., Parmentier, E.M., Lin, J., 1987. Mechanisms for the origin of Middle ocean ridge axial topography: Implications for the thermal and mechanical structure of accreting plate boundaries. J. Geophys. Res. Solid Earth 92, 12823–12836.

Pysklywec, R.N., Mitrovica, J.X., 1998. Mantle flow mechanisms for the large-scale subsidence of continental interiors. Geology 26, 687–690.

Sigmundsson, F., 1991. Post-glacial rebound and asthenosphere viscosity in Iceland. Geophys. Res. Lett. 18, 1131–1134.

Turcotte, D., Schubert, G., 2014. Geodynamics. Cambridge University Press.

Vyssotski, A.V., Vyssotski, V.N., Nezhdanov, A.A., 2006. Evolution of the West Siberian Basin. Mar. Pet. Geol. 23, 93–126.

Watts, A.B., 2001. Isostasy and Flexure of the Lithosphere. Cambridge University Press.

Wegener, A., 1920. Die entstehung der kontinente und ozeane. Braunschweig Druck und Verlag von Friedr. Vieweg & Sohn

Weismüller, J., Gmeiner, B., Ghelichkhan, S., Huber, M., John, L., Wohlmuth, B., Rüde, U., Bunge, H.-P., 2015. Fast asthenosphere motion in high-resolution global mantle flow models. Geophys. Res. Lett. 42.

Chapter 1

Anomalous subsidence history of the West Siberian Basin as an indicator for episodes of mantle-induced dynamic topography

Yulia Vibe[a,b,*], Hans-Peter Bunge[b] and Stuart R. Clark[a]

[a] Kalkulo AS, Simula Research Laboratory, P.O. Box 134, 1325 Lysaker Norway

[b] Department of Earth and Environmental Sciences, Geophysics, Munich University, Theresienstr. 41, 80333, Munich, Germany

[*] Corresponding author

Email addresses: julia@simula.no (Y. Vibe), bunge@lmu.de (H.-P. Bunge), stuart@simula.no (S. R. Clark)

This chapter presents estimates of tectonic subsidence of the West Siberian Basin based on available geological data. The obtained tectonic subsidence estimates are then compared to a model of post-rift subsidence, which has previously been suggested to be the main mechanism of the basin's development. Significant differences in the patterns of observed and predicted subsidence indicate an imprint of an additional mechanism, likely related to the sublithospheric processes.

Anomalous subsidence history of the West Siberian Basin as an indicator for episodes of mantle-induced dynamic topography

Abstract

Vertical intraplate motions are not easily related to plate tectonics. Understanding their underlying mechanism is further complicated by poor constraints on the magnitude and timing of these motions. Western Siberia is a prominent intraplate area affected by vertical tectonics. Shortly after the assemblage of Pangaea, the region experienced substantial uplift followed by a long period of subsidence that led to formation of the world's largest sedimentary basin–the West Siberian Basin. Its sedimentary cover has been extensively explored and described in the Soviet literature. Here we digitise compilations of stratigraphic data to calculate the basin's subsidence history by backstripping analysis. Our results confirm the prolonged and high amplitude regional subsidence that has been noted before and constitutes the basin's first-order vertical motion. However, our backstripping results also reveal a secondary mode of shorter spatial and temporal scales induced by the migration of the maximum subsidence across the basin. Importantly, the generally slow subsidence of the basin was interrupted by uplift events in the early and late Cretaceous and in the middle Oligocene. While the secondary mode of vertical motion is not easily understood in terms of traditional subsidence models restricted to lithospheric cooling after stretching, it is consistent with rapid uplift events that have been reported for other locations, such as elevated passive continental margins. We discuss the geodynamic implications and conclude that the basin may hold important constraints on dynamic topography induced by sublithospheric mantle flow processes.

Introduction

Plate tectonics (Morgan, 1968) is a powerful framework for understanding horizontal motions of Earth's surface, whereas the vertical movements of the plate interior are more difficult to comprehend. Their underlying geodynamic mechanisms are unclear,

because the forces commonly assumed to govern vertical movements of tectonic plates, for instance lithospheric flexure or isostasy (see Cloetingh and Ziegler (2007) for a review) are usually associated with plate margin processes such as subduction or mountain building. Nevertheless, intraplate regions are known to have experienced significant uplift or subsidence events, even though located far away from tectonic boundaries.

Soviet scholars recognized the importance of vertical motions early on. Favouring a *fixistic* concept of global deformation, they acknowledged that "the fundamental and most universal tectonic motions of the Earth crust are vertical oscillatory movements" (Khain and Ryabukhin, 2002). While their view was partly motivated by observations from the Russian cratonic interiors, where the effects of vertical motions are evident from the stratigraphic record, the mechanism for intraplate vertical motions remained unexplained.

Geodynamicists have long known that viscous flow in the Earth's mantle can cause sizeable vertical movement of the Earth's surface in addition to driving the horizontal component of plate motion. They introduced the concept of dynamic topography (Hager and Gurnis, 1987) to refer to mantle induced vertical deflections of the lithosphere (see Flament et al. (2013) and Braun (2010) for recent reviews). Because these deflections produce gravity anomalies of comparable amplitude to the primary flow inducing mass anomalies associated with mantle heterogeneity, it is essential that one takes them into account in dynamic models of the Geoid (Colli et al., 2016; Ricard et al., 1984; Richards and Hager, 1984).

Geologic inferences about dynamic topography have grown rapidly in recent years. They are drawn from a variety of indicators, such as regional velocity-depth anomalies in North Sea Chalk (e.g., Japsen (1998)), residual depth measurements (Hoggard et al., 2016), the subsidence pattern of intra continental basins (Heine et al., 2008) and marginal seas in SE Asia (Yang et al., 2016), or the stratigraphic record along passive continental margins (e.g., Autin et al. (2013), Dressel et al. (2015), Guillocheau et al. (2012), Paton et al. (2008), Praeg et al. (2005), Reeve et al. (2016), Said et al. (2015), Kukla et al. (this volume)). There is also evidence for episodes of burial and exhumation along passive continental margins (e.g., Anell et al. (2009), Dressel et al. (2016), Japsen et al. (2012a), Japsen and Chalmers (2000)), as well as reports of transient uplift events

in the sedimentary basins of the North Atlantic (e.g., Hartley et al. (2011)) with amplitudes approaching 1 km. In the South Atlantic region, moreover, spreading rate changes appear to correlate with uplift events, presumably owing to variations in pressure driven upper mantle flow (Colli et al., 2014). Dynamic topography may thus provide important clues on the convective circulation of the sublithospheric mantle. Its temporal changes have implications for past mantle flow, which one can constrain from retrodictions (Colli et al., 2015), inverse flow modeling techniques (Bunge et al., 2003), backward advection (Moucha and Forte, 2011).

The West Siberian Basin (WSB) is an ideal location to study intraplate vertical motions. It is the largest petroleum basin in the world, located on the Eurasian plate, and bounded by the East European Craton from the West and the Siberian Craton from the East (Vyssotski et al., 2006) (Figure 1). The basin's subsidence initiated after a Permo-Triassic uplift event, which left evidence in the form of rift structures and the well-known Siberian trap basalts (Reichow et al., 2005). Many authors have suggested that the Permo-Triassic uplift event and magmatism are consequences of a plume arrival (Dobretsov et al., 2013; Holt et al., 2012; Saunders et al., 2005). The subsidence, delayed in the majority of the basin until Jurassic (200 Ma), continued until the middle Oligocene (~ 30 Ma), leading to the accumulation of up to 12 km of sediments that archive the basin's tectonic history (Vyssotski et al., 2006). The structure of the basin's sedimentary cover was documented by extensive drilling and seismic experiments in the 1950's. In total, the overall volume of exploratory drilling accounted for 6500 kilometers in borehole length. As well, 90% of the basin's area was covered by regional seismic imaging (Kontorovich et al., 1975). While the original borehole and seismic data is not readily available, detailed interpretations have been published in the Soviet literature.

In this paper, we digitise these compilations of sedimentary data and constrain the tectonic vertical motions in the WSB using backstripping analysis. This method determines pure tectonic subsidence of a basin and corrects for the effects of sediment loading (Steckler and Watts, 1978). While previous attempts to analyse the basin's vertical motions performed backstripping in 1D for single well data (Armitage and Allen, 2010; Saunders et al., 2005), we extend the analysis to 2D by using our digitised maps that cover the WSB. Furthermore, we compare the obtained backstripping results to the

empirical thermal subsidence model from McKenzie (1978). Data and workflow for this study are discussed in the Data and Methods section.
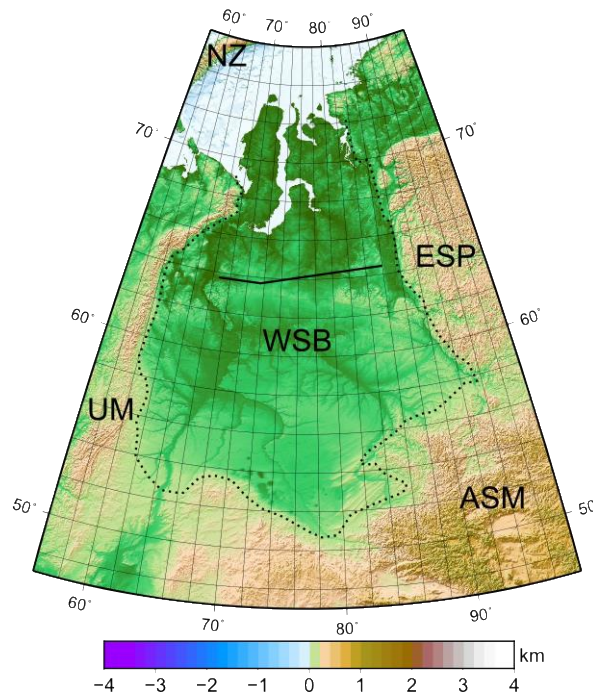
Figure 1. Geographic map of the basin. Geographic map showing topography and outline (digitised after Cherepanova et al. (2013) of the West Siberian Basin (WSB). ESP - East Siberian Platform, UM - Ural Mountains, ASM - Altay–Sayan Mountains. Much of the basin is low-lying at less than 150 m elevation. The black line shows location of the regional seismic profile from Figure 7.

Data and Methods

The sedimentary thickness data was obtained by geo-referencing and digitising isopach maps (Rudkevich, 1976; Rudkevich et al., 1988). The resulting data consists of grids for each of the 12 sedimentary cycles, which are geological time intervals defined by their common depositional characteristics. Each grid point contains the value of the sediment thickness, the lithological parameters (density, initial porosity and porosity coefficients) and paleo-water depth for that location. The resulting digitised isopach maps are presented in Figure 2, while Table 1 summarizes the lithology of the maps and the corresponding lithological parameters.

For each of the grid points we calculated the tectonic subsidence of the WSB by backstripping the sediment thicknesses at the time intervals dictated by the age of the sedimentary cycles. We use the porosity (ϕ) – depth (z) relationship (Athy, 1930):

$$\phi(z) = \phi_0 e^{-cz},$$

where ϕ_0 is the initial or surface porosity and c is the compaction coefficient, to calculate the total layer thickness, which is the sum of the net sediment thickness and the pore space. Backstripping is performed assuming Airy isostasy, because the basin is approximately in isostatic equilibrium as its crust is not sufficiently strong to support the sediment load (Saunders et al., 2005). We implement an iterative approach for each layer, where subsequent decompactions are applied for each layer removed (Said et al., 2015). Tectonic uplift is derived from the local paleo-water depth gradient, and therefore stands for the minimum estimate of uplift.

Water weight also contributes to loading the lithosphere and therefore paleo-water depth is added to the decompacted sequence at each time step in backstripping. An indicator for paleo-water depth comes from the amount and type of foraminifera in the sediment. Bulinnikova et al. (1978) provides water depth values for different depositional environments of the WSB based on the foraminifera content. Combined with knowledge of the basin's depositional environments from Kontorovich et al. (1975) we constructed curves of basin paleo-water depth. Figure 3 shows the mean paleo-water depth and its standard deviation.

To estimate the contribution of post-rift thermal subsidence in the development of the basin, we applied a lithospheric cooling model from McKenzie (1978). This model, which assumes uniform stretching, is a simplified way to test whether thermal subsidence is the main driving mechanism of the basin's tectonic subsidence without going into many technical details of depth or rheology dependant stretching models (e.g. Brune et al. (2017), Huismans and Beaumont (2011), Watts and Burov (2003)).

The model requires an assumption about the β-factor, which is the measure of the crustal stretching estimated by a ratio of unstretched relative to stretched crust. The present day crustal thickness in the WSB is described by Cherepanova et al. (2013) (Figure 4) and ranges from 25 km in the northern parts of the basin to 43 km in the

periphery. The original thickness of crust prior to the formation of the rifts in the West Siberian basement is not known. To be conservative, we assume it to be 45 km as a mean, as suggested by the crustal thickness in the surrounding areas. A summary of β-factors and other parameters applied in the thermal subsidence model is listed in Table 2.
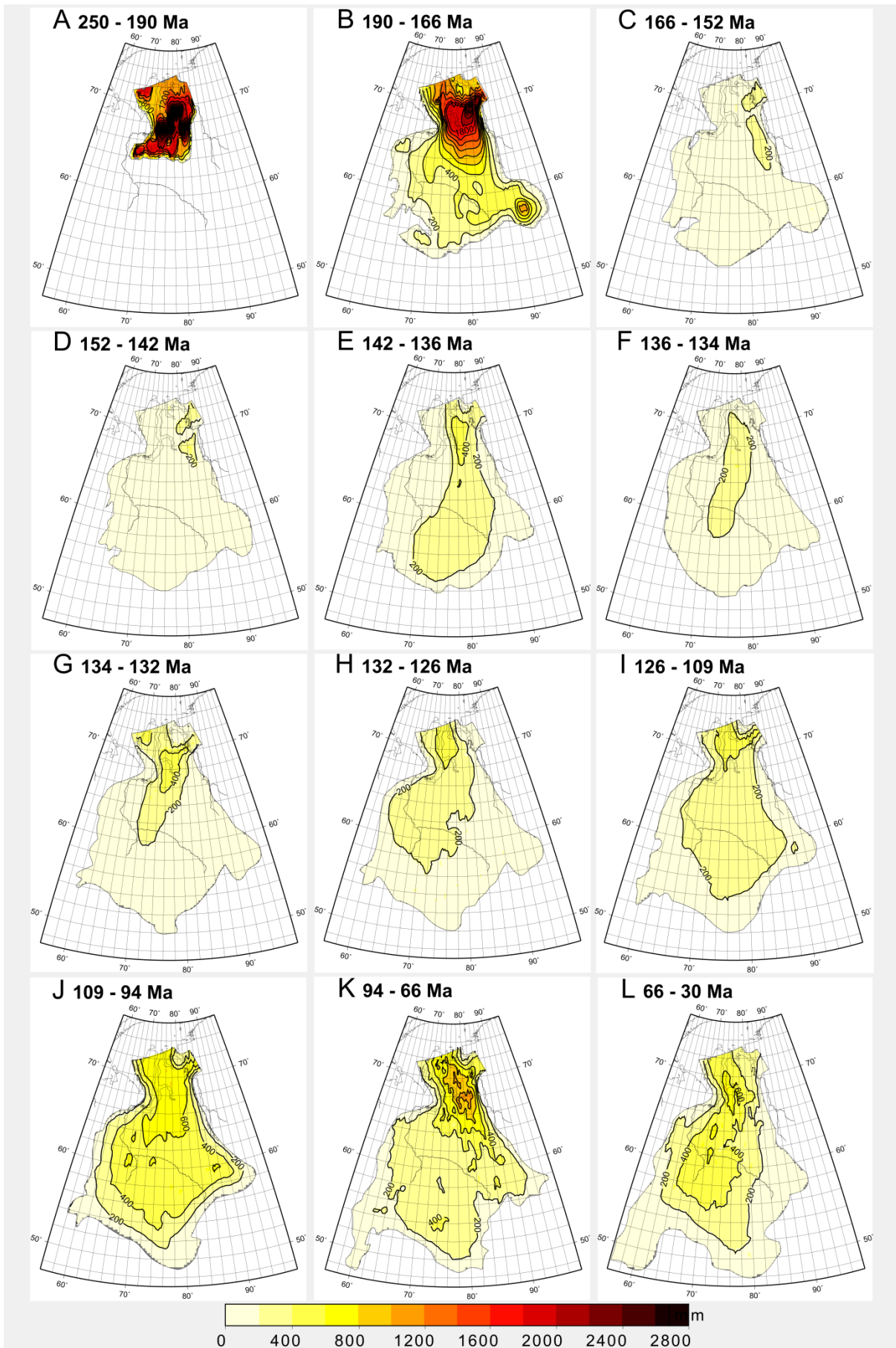
Figure 2. Isopach maps. Isopach maps showing sediment thickness in meters for 12 sedimentary cycles (A-L), digitised after Rudkevich (1976) and Rudkevich (1988). See Table 1 for the ages and names of the sedimentary cycles. Colorscale interval is 200 m. The isoline interval is 400 m for A and 200 m for B-L. Note intense sedimentation at the onset of subsidence (A, B) followed by slow-down and shift of depocenter to the East (C, D, E). The depocenter shifts back to the central (F, G) and western part of the basin (H), followed by a migration to the North (I, J). (K) shows a depocenter intensification in the Northeast. (L) is the last sedimentary cycle before the basin's uplift and erosion. The data was gridded using splines in tension, with a tension coefficient of 0.75 and a 0.25 degree resolution.

Sedimentary cycle	Age [Ma]	Lithology	Surface Porosity	Porosity Coefficient [m^{-3}]	Density [$kg * m^{-3}$]	Max. thickness [m]
A - Triassic	250-190	Sandstone	0.49	0.27	2650	3000
B – Early Jurassic (early Plinsbachean-Bathonian)	190-166	Argillaceous sandstone	0.56	0.39	2460	2500
C - Late Jurassic (Callovian-Kimmeridgian)	166-152	Argillaceous sandstone and limestone	0.56	0.39	2460	400
D – Tithonian-early Beriassian	152-142	Argillaceous	0.63	0.51	2600	400
E - Late Berriasian-early Valangian	142-136.5	Argillaceous sandstone	0.56	0.39	2460	500
F - Late Valangian	136.5-134	Argillaceous sandstone	0.56	0.39	2460	400
G - Early Hauterivian	134-132.5	Argillaceous sandstone	0.56	0.39	2460	600
H - Late Hauterivian-Barremian	132.5-126.3	Argillaceous sandstone	0.56	0.39	2460	500
I – Aptian	126.3-109.5	Argillaceous sandstone, increasing sandstone to the east	0.56	0.39	2460	500
J - Late Albian-Cenomanian	109.5-94	Argillaceous sandstone, increasing sandstone to the east	0.56	0.39	2460	800

K – Turonian-Maastrichtian	94-66	Argillaceous	0.63	0.51	2600	1000
L – Paleocene-early Oligocene	66-30	Argillaceous-siliceous sandstones	0.56	0.39	2460	800

Table 1. Summary of sedimentary parameters used in the backstripping. For the ages (Gradstein et al., 2012) was used as timescale, while the lithology was taken from Rudkevich (1976), Rudkevich et al. (1988) and sediment parameters from Allen and Allen (2013).

Stratigraphy

Figures 2, 5, 6 and 7 describe the sedimentary cover of the WSB. A peak sediment accumulation of ~2 km occurs in the Triassic and early Jurassic (Figure 2 A, 2 B), followed by at most only 400 m of sediment in the Late Jurassic period (Figure 2 C). Sedimentation was moderate in the following sedimentary cycles (Figure 2 D-G), and took place mostly in the northern and central parts of the basin. A shift of the depocenter to the West occurred in the late Hauterivian-Barremian (Figure 2 H). The last sedimentary cycle recorded was the Paleocene-early Oligocene (Figure 2 L) during which the depocenter was located roughly in the center of the basin. The basin's sedimentary deposition is also described by the burial graphs in Figure 5. Unconformities are widespread in the Late Eocene and Oligocene in all parts of the basin (Figure 6). After Oligocene erosion, sedimentation continued in the South of the basin, at the western margin and in the Yenisey delta, while the rest of the basin was in hiatus (Figure 6). In addition, a line drawing of the main seismic reflectors in Figure 7 shows the structure of the basin's sedimentary cover.

Points	P1	P2	P3	P4	P5	P6	P7	P8	P9	P10
Thickness, $[m * 10^3]$	31	33	37	37	33	35	40	33	39	39
β-factor	1.45	1.36	1.21	1.21	1.36	1.28	1.12	1.36	1.15	1.15

Table 2. Crystalline basement thickness (Cherepanova et al., 2013) and the corresponding β-factor used in the thermal subsidence analysis (McKenzie, 1978) . Other parameters include lithosphere thickness (100 km), thermal expansion coefficient of both mantle and crust ($\alpha = 3 \cdot 10^{-5} K^{-1}$), asthenosphere temperature ($T = 1853\ K$),mantle density ($\rho_m = 3330\ kg \cdot m^{-3}$), density of sea water ($\rho_w = 1000\ kg \cdot m^{-3}$), and thermal diffusivity ($\kappa = 8 \cdot 10^{-7} m^2 \cdot s^{-1}$). We assume that rifting ended 240 Ma and the unstretched crust was 45 km thick. The applied model accounts for a water-filled basin.
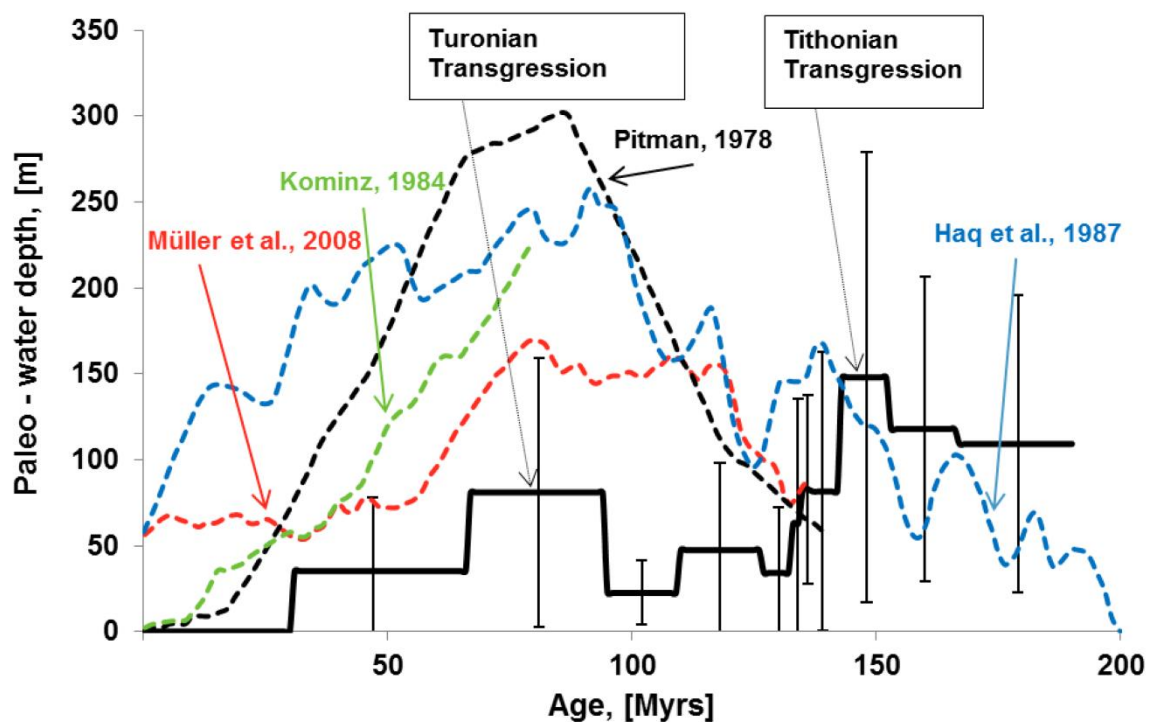
Figure 3. Mean paleo-water depth Mean paleo-water depth (the solid black line) in the basin compiled from foraminifera (Bulinnikova et al., 1978) and paleogeographic environment data (Kontorovich et al., 1975) with error bars indicating one standard deviation. Colored dashed lines show global eustatic level from different studies (Haq et al., 1987; Kominz, 1984; Müller et al., 2008b; Pitman, 1978) for comparison. Overall, the local and the global sea level curves do not coincide, although the imprint of the global sea level on the basin's local sea level is apparent in the Turonian transgressive event and in the Cenozoic gradual sea level fall.
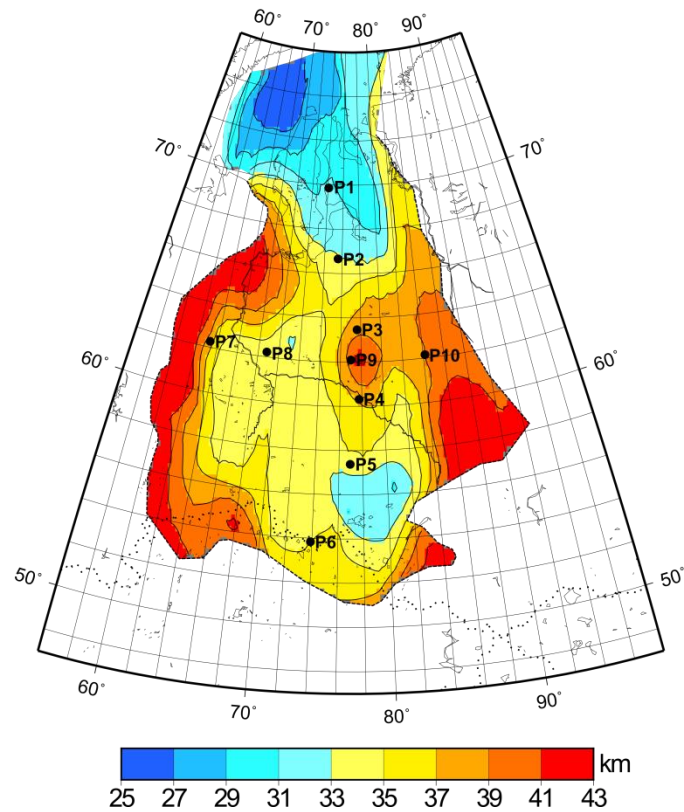
Figure 4. Crystalline basement thickness map. Thickness map of crystalline basement in the West Siberian Basin digitized from Cherepanova et al. (2013). Crustal structure is complex with maximum thickness (43 km) near cratonic borders and minimum thickness (25 km) in the northernmost part of the Basin. Black dots show location of the points (P1 to P9) for which subsidence curves are calculated in Figure 8.
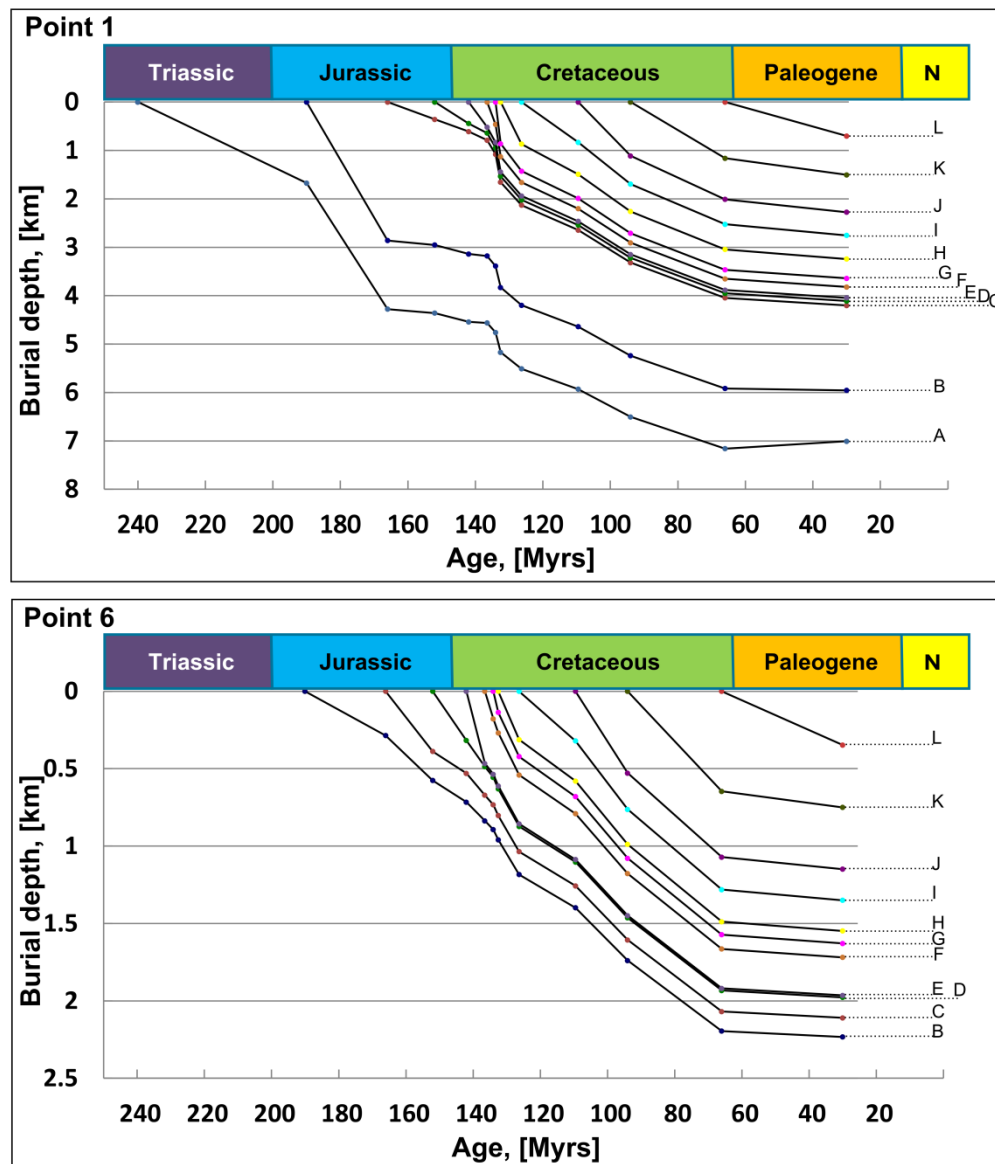
Figure 5. Burial history graphs. Burial graphs of the WSB based on the stratigraphy data from Rudkevich (1976), Rudkevich et al. (1988) for two points—one in the north (Point 1) and the other in the south (Point 6). The locations of the points are shown in Figure 4. The sedimentary cycles A-L are defined in Figure 2.
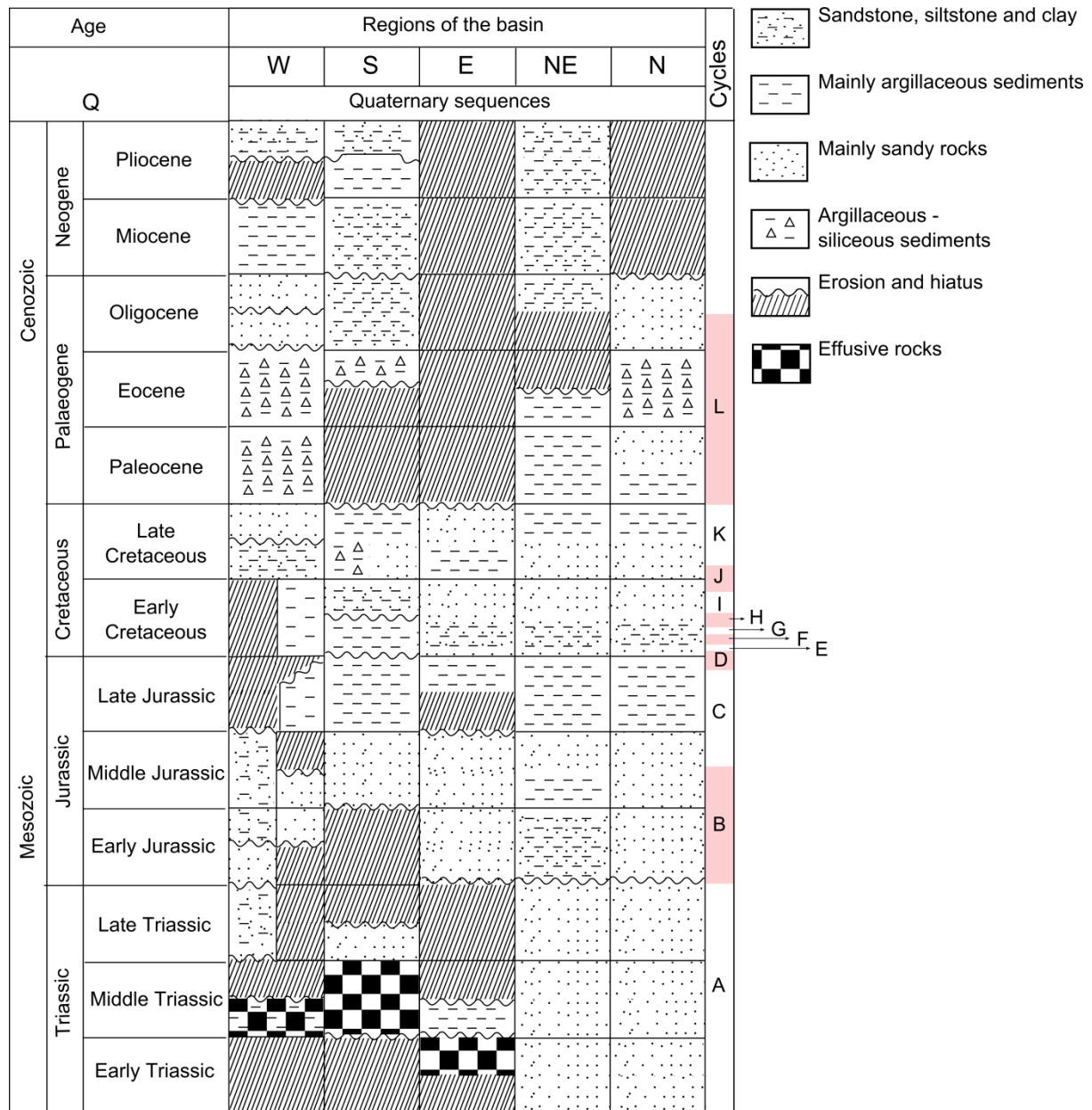
Figure 6. Unified stratigraphic chart of the WSB. The chart is simplified and redrawn after Kontorovich et al. (1975). W, S, E, NE, N stand for North, South, East, Northeast and North of the basin. On the right, the column *Cycles* shows corresponding sedimentary cycles. Unconformities interrupt sedimentary record in the early Jurassic and Oligocene in the North and the Northeast and in the Triassic, early Jurassic, early and late Cretaceous and at the Eocene-Oligocene boundary in the southern part of the basin.

Uncertainties

The main potential sources of uncertainty in our study are: the accuracy of isopach maps, paleo-water depth estimates and parameter values related to the choice of sediment type. The contours of the original isopachs are given with the interval of either 100 or 200 m depending on the map. For the 100 m scale isopach, the points in-between the contours would be either up to 50 m more than the N-th contour, or up to 50 m less than the (N+1)-th contour, so that the accuracy of the isopach is ±50 m. In the same fashion, the 200 m scale isopach have the accuracy of ±100 m. The choice of input parameters for different lithologies (e.g. initial porosity, density, porosity coefficient) also carries some uncertainty. To estimate the uncertainty, we varied the values for the initial porosity of rocks. Using porosities for each of the three lithology types that were as similar (φ_{mixed} = 0.60, φ_{shale} = 0.63, φ_{sand} = 0.55) or as different (φ_{mixed} = 0.56, φ_{shale} = 0.65, φ_{sand} = 0.45) as possible, we compared the backstripping results with the results using the mean porosity value φ_{mean} = 0.56 averaged from three present types of sediments—sandstone, argillaceous and argillaceous sandstone. The case with the most different values for the initial porosity yielded the biggest difference relative to the mean initial porosity case, with the maximum difference reaching 15 % of the tectonic subsidence for all time steps.

Additionally, the isostasy model impacts the final result. Our choice of an Airy isostasy implies maximum values of tectonic subsidence.

Maast TS - Maastrichtian transgressive surface
⬛ - Top of 250 Ma basalts
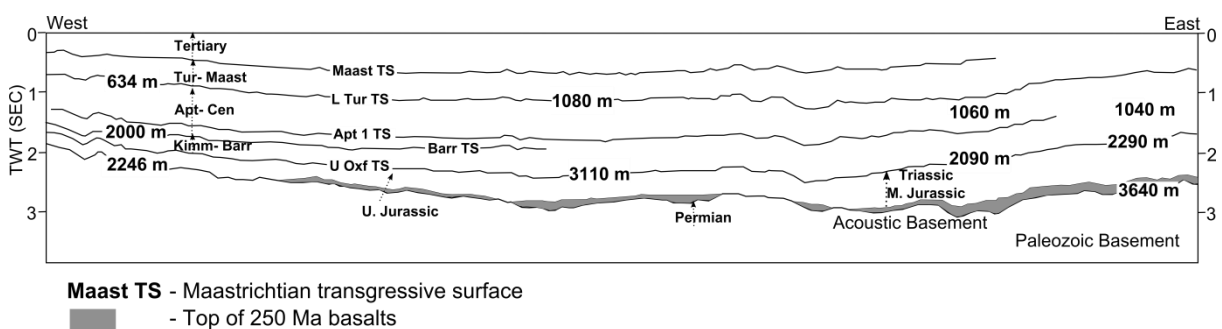
Figure 7. Seismic profile across WSB. Line drawing showing seismic profile across the WSB from West to East (redrawn after Vyssotski et al. (2006)). Location of the profile is shown on Figure 1. Total sediment thickness is consistent with our stratigraphic data.

Results

In Figure 8, we present the results of the backstripping analysis. At the Permo-Triassic boundary, the northern part of the basin subsided to about 2 km, reflecting the trend of the basement rifts (Figure 8 A). In the early Jurassic, tectonic subsidence began to affect the whole basin, with the main subsidence in the East (Figure 8 B). In the Late Jurassic, the loci of subsidence were in the eastern and southeastern parts of the basin with ~250 m of tectonic subsidence, while the central, northern and northwestern parts subsided less than 100 m (Figure 8 C). At this time subsidence propagated westwards, becoming uniform throughout the basin, and was ~100 m (Figure 8 D). Later in the Late Berriasian-early Valangian the basin underwent uplift and erosion; uplift was especially active in the center of the northern region, reaching 165 m in 5 Myrs (Figure 8 E). At the same time subsidence was active in the South, the southwestern and northeastern parts reaching 135 m (Figure 8 E). Subsidence affected the basin again in the Late Valangian, stretching as a line from the North of the basin to the South, with a peak amplitude of about 200 m (Figure 8 F). However, to the East and West of this line, there is a hiatus in sedimentation implying a relative uplift of the basin edges in these regions. In the early Hauterivian, the basin expanded westwards, and the western and northern parts of the basin experienced 200-270 m subsidence (Figure 8 G). Subsidence rates slowed in the late Hauterivian-early Barremian for subsequent stages, with the western part becoming the locus of subsidence (Figure 8 H). The Aptian and Late Albian-Cenomanian were characterised by slow subsidence, almost uniform throughout the basin, and amounting to close to 200 m in the North and centre (Figure 8 I), with the centre of subsidence migrating Southeast (Figure 8 J). In the Turonian-Maastrichtian, most of the basin was dominated by over 200 m of subsidence (Figure 8 K) until the Cretaceous-Tertiary transition when the eastern and southern margins of the basin emerged (Figure 6). In the Eocene the northwestern parts of the basin subsided (Figure 8 L), while in the middle Oligocene the basin uplifted starting from the Northeast.
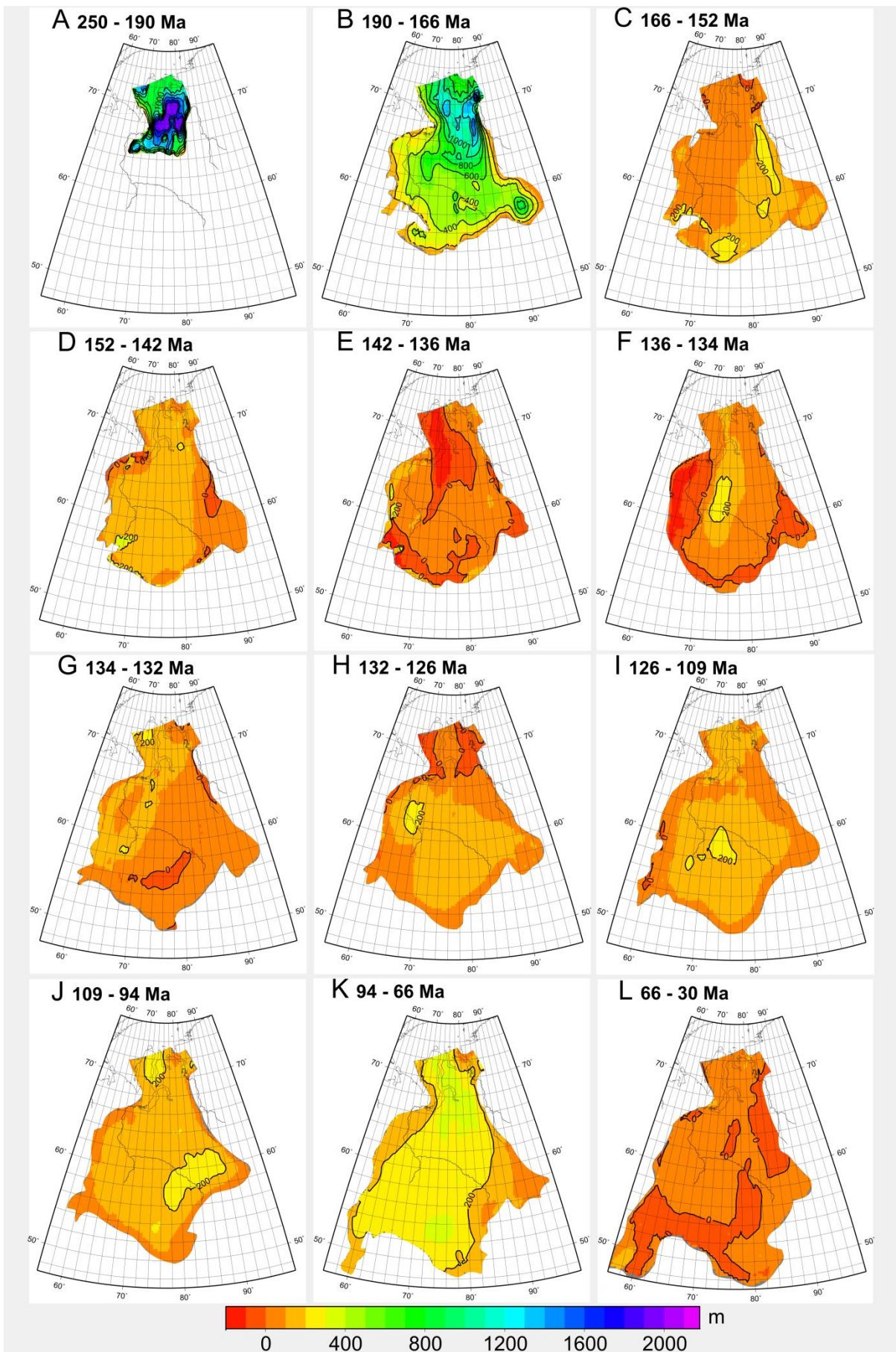
Figure 8. Tectonic subsidence maps. Maps showing tectonic subsidence in the West Siberian Basin for 12 sedimentary cycles (A-L) as defined in Figure 2. Note that the 0 contour corresponds to uplift. The colorscale interval is 100 m and isoline interval is 200 m. Initially subsidence only affects the northern part (A). The region of subsidence expands, but is still focused in the North (B) and moves later (C) to the eastern part. The uplift is apparent in the early Cretaceous (E). Later on (F, G) the subsidence locus shifts westwards, reaching the basin's western part (H). Then the subsidence locus moves to the center (I, J) and to the East (K) of the basin. (L) shows the early Paleogene change of tectonic mode in the basin associated with uplifts (red color).

We illustrate the temporal character of vertical motions in Figure 9 with two sets of points whose positions are shown in Figure 4. The first set of points crosses the basin from North to South (respectively P1-3, 9 and 4-6), while the second set crosses it from West to East (P7-10 respectively). The tectonic subsidence in the northernmost point (P1) reaches 3.5 km, while it is only around 1.6 km in the southernmost point (P6). From West to East, the maximum tectonic subsidence increases from 1.1 km (P7) to 2.0 km (P9) and then drops again to 1.6 km in the East (P10). Some of the curves also feature intermediate local maxima, indicating periods of uplift. In the North (P1 and P2), a local maximum is observed during the late Berriasian-early Valangian (period E, 142-136.5 Ma). While in the West (P7 and P8), the uplift occurs later during the late Valangian (period F, 136.5-134 Ma). Furthermore, the curves in Figure 9 show significant slowing of the tectonic subsidence in the Paleocene-early Oligocene (period L, 60-30 Ma). Lack of sediments after 30 Ma precludes estimations of tectonic subsidence from Late Oligocene to present.

For each plot in Figure 9, a single-phase lithospheric cooling model (McKenzie, 1978) for the selected points is shown using the β-factors from Table 2. A purely thermal post-rift subsidence model predicts significantly less tectonic subsidence at each point than what is calculated from the backstripping analysis (Figure 9). For example, the post-rift cooling model produces only 1.3 km of subsidence in the North (Figure 9, P1) and 0.5 km in the centre (Figure 9, P9), compared with 3.5 km and 1.6 km of backstripping-derived subsidence for the same points. In addition, the thermal cooling curve flattens at around 200 Ma, whereas the backstripping curve shows a nearly linear decrease until the Cretaceous-Paleogene boundary (66 Ma).
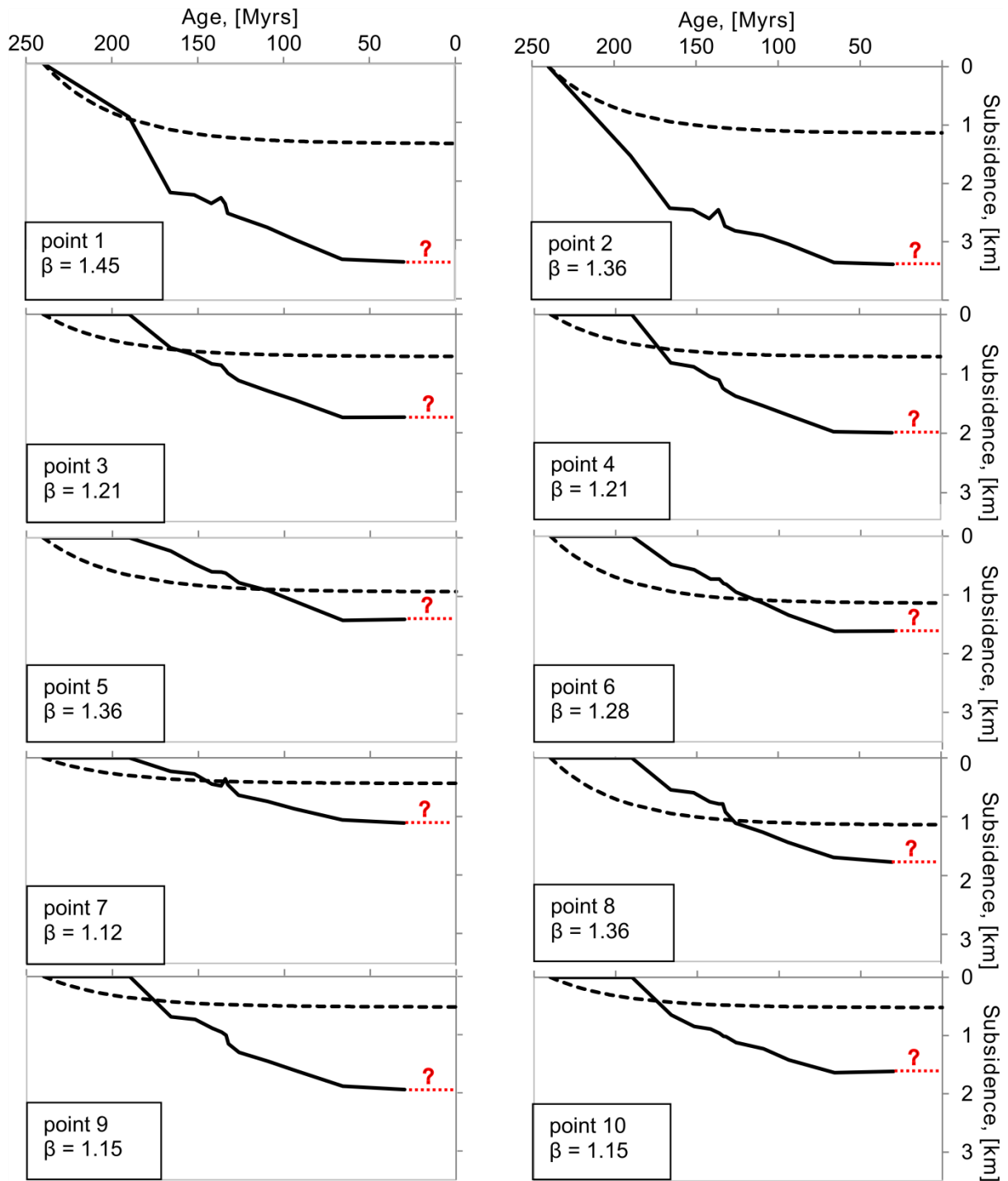
Figure 9. Tectonic subsidence analysis. Tectonic subsidence analysis for point set from Figure 4. Solid lines represent tectonic subsidence calculated by the backstripping analysis. Dashed black lines show the thermal subsidence calculated for the β-factor from Table 2. Note an increase of subsidence amount from North (P1) to South (P6). Positive peaks from 142 Ma to 136 Ma are apparent, indicating uplift. The basin uplifted ca. 30 Ma by unknown magnitude, illustrated by the red dotted line with a question mark.

Discussion

Based on a comprehensive and digitised stratigraphic dataset, our analysis shows that the WSB experienced varied and prolonged vertical motion from its inception in the Triassic to today. Relatively fast tectonic subsidence in the Triassic and early Jurassic was followed by a slowdown in Late Jurassic, with the subsidence centre moving from the North to the East. At the Jurassic-Cretaceous boundary, some regions in the basin experienced significant uplift. Later on, the subsidence moved westwards and reached the West of the basin in the Late Hauterivian. In the Paleocene, the basin's tectonic and paleogeographic environment changed: slow subsidence continued until the middle Oligocene when the basin experienced renewed uplift.

Duration of the basin's tectonic subsidence exceeds the thermal response time of the lithosphere (McKenzie, 1978). In other words, thermal subsidence of the basin is expected to attenuate ~20 Myr after its onset, when the change in depth becomes less than 10% of the total depth. However, the backstripping analysis suggests active tectonic subsidence of much longer duration. Armitage and Allen (2010) explained the protracted subsidence of intraplate basins through a mechanism that involves continuous lithospheric stretching. Specifically, they suggested that a persistent stretching with a low strain rate of $10^{-16}s^{-1}$ lasting for 50-100 Myrs and necessitating a β-factor of ~1.5 would explain the long lasting WSB subsidence. Evidence exists for faulting and fault reactivation in the basin, concentrated at Jurrasic and Oligocene time (Kontorovich, 2009). However, our backstripping analysis indicates the need for larger β-factors to explain the inferred subsidence through lithospheric extension. To satisfy the amount of subsidence reported for P1 in Figure 9, the β-factor should be ~β=3. Consequently, the thickness of stretched crust in the northern part of the basin would be as small as 15 km, in disagreement with existing crustal models (Cherepanova et al., 2013).

The Permo-Triassic emplacement of the Siberian flood basalts has encouraged the idea that the WSB's subsidence owes in part to thermal accommodation after the plume event (Holt et al., 2012; Saunders et al., 2005). It is reasonable to assume that the plume was located in the North of the basin, where the vertical motions initiated (Rudkevich, 1976) and where they take on their largest amplitude (see Figure 8). The propagation of the plume material to the periphery might have resulted in the Triassic uplift of the

southern area of the basin followed by the post-Triassic subsidence (Friedrich et al., this volume). However, in addition to the temporal decay of the thermal anomaly, the post-plume subsidence hypothesis should consider Siberia's motion across the mantle. A number of plate kinematic models is available for tectonic reconstruction of the past 100 Myrs (e.g., Seton et al. (2012)). These models rely on the choice of a reference frame, for example several fixed hotspots or moving hotspots models (Doubrovine et al., 2012; O'Neill et al., 2005; Wessel and Kroenke, 2008), all of which contributes to the uncertainty (Shephard et al., 2012).

Taking the plate reconstruction to the Permo-Triassic time requires additional assumptions (Cogné, 2003; Evans, 2009) that enable one to estimate the motion of the WSB over the mantle (Figure 10). A True Polar Wander-corrected reconstruction of Eurasia (Steinberger and Torsvik, 2008; Torsvik et al., 2008) implies that the WSB moved ~2300 km northeast since the Permo-Triassic boundary. Thus if the plume was connected to a large-scale mantle upwelling and associated dynamic topography arising from convective stresses (Braun, 2010), then the basin's prolonged subsidence would owe in part to the WSB's movement relative to this broad, mantle-anchored topographic swell.

Our analysis identifies short-lived and regional uplift events. Superimposed on the long term basin evolution, and concentrated ~142-136 Ma in the North and ~136-134 Ma in the West, they are evidenced as peaks in the tectonic subsidence curves of Figure 9. The amplitude of these peaks is about 400 m which gives a minimum estimate of the uplift intensity. Furthermore, there is evidence of intense erosion in the basin in the Cenozoic with magnitudes varying from 200 m up to 2.5 km (Igoshkin et al., 2008). Taking into account that the basin is remote from tectonic boundaries that could have influenced the basin's evolution (Ziegler et al., 1998, 1995), these short-lived, regional motions are of considerable interest as they could provide geodynamic constraints on the spatial and temporal scales of sublithospheric mantle flow. The vertical motions of the lithosphere induced by convective stresses of mantle flow are commonly assumed to be large in scale—as low as spherical harmonic degree two—and slowly changing in time. Arguments for broad spatial scales are based on seismic imaging of the deep mantle, which reveals long wavelength mantle heterogeneity (Grand, 2002; Ritsema et al., 2011; Simmons et al., 2007; Van der Hilst et al., 1997), while arguments for slow temporal

changes—implied by its relation to deep mantle heterogeneity—are drawn from geodynamic inferences that much deep mantle heterogeneity is associated with past subduction (Richards and Engebretson, 1992) and the slow convective overturn of the mantle (Bunge et al., 1998), effectively suggesting that dynamic topography evolves on time scales of 100 Myrs.

However, evidence is mounting from a variety of geologic observations for additional dynamic topography components that are shorter in spatial scale and faster changing over time. These components are indicated by episodes of regional uplift and subsidence seemingly unrelated to the large scale circulation of the mantle, which are reported from elevated passive continental margins (Japsen et al., 2012b), marginal continental basins (Autin et al., 2013; Dressel et al., 2015; Guillocheau et al., 2012), and the oceanic realm, where some locations record transient uplifts (Hartley et al., 2011). In the South Atlantic region, moreover, rapid oceanic spreading changes–on the order of 10 Myrs or so– correlate with vertical motion (Colli et al., 2014). The underlying mechanism for these changes involves variations in pressure driven upper mantle flow (Iaffaldano and Bunge, 2015; Nerlich et al., 2014) where flow velocities may exceed plate tectonic velocities by an order of magnitude (Weismüller et al., 2015). Our observations for the WSB are broadly consistent with these inferences and suggest that basins hold important archives of past mantle flow regimes, which one can constrain from retrodictions (Colli et al., 2015) or inverse mantle flow modelling techniques (Ghelichkhan and Bunge, 2016).

We close our discussion on the WSB tectonic subsidence history by considering eustatic sea level variations. An overprint of the global sea level curve on the WSB paleo-water depth is noticeable in Figure 6. Curves for eustatic sea level and the WSB paleo-water depth follow broadly similar trends in the Turonian, presumably in response to the global Cretaceous sea level high, and in the Late Cretaceous which experienced a sea level drop. While it is thus possible to attribute some basin shallowing in the Late Cretaceous to eustatic sea level effects, it is difficult to explain the basins vertical motion entirely this way. However, a better representation of the various geodynamic influences on global sea level is needed (Austermann et al., 2015) to separate the regional and global sea level signals in the WSB.
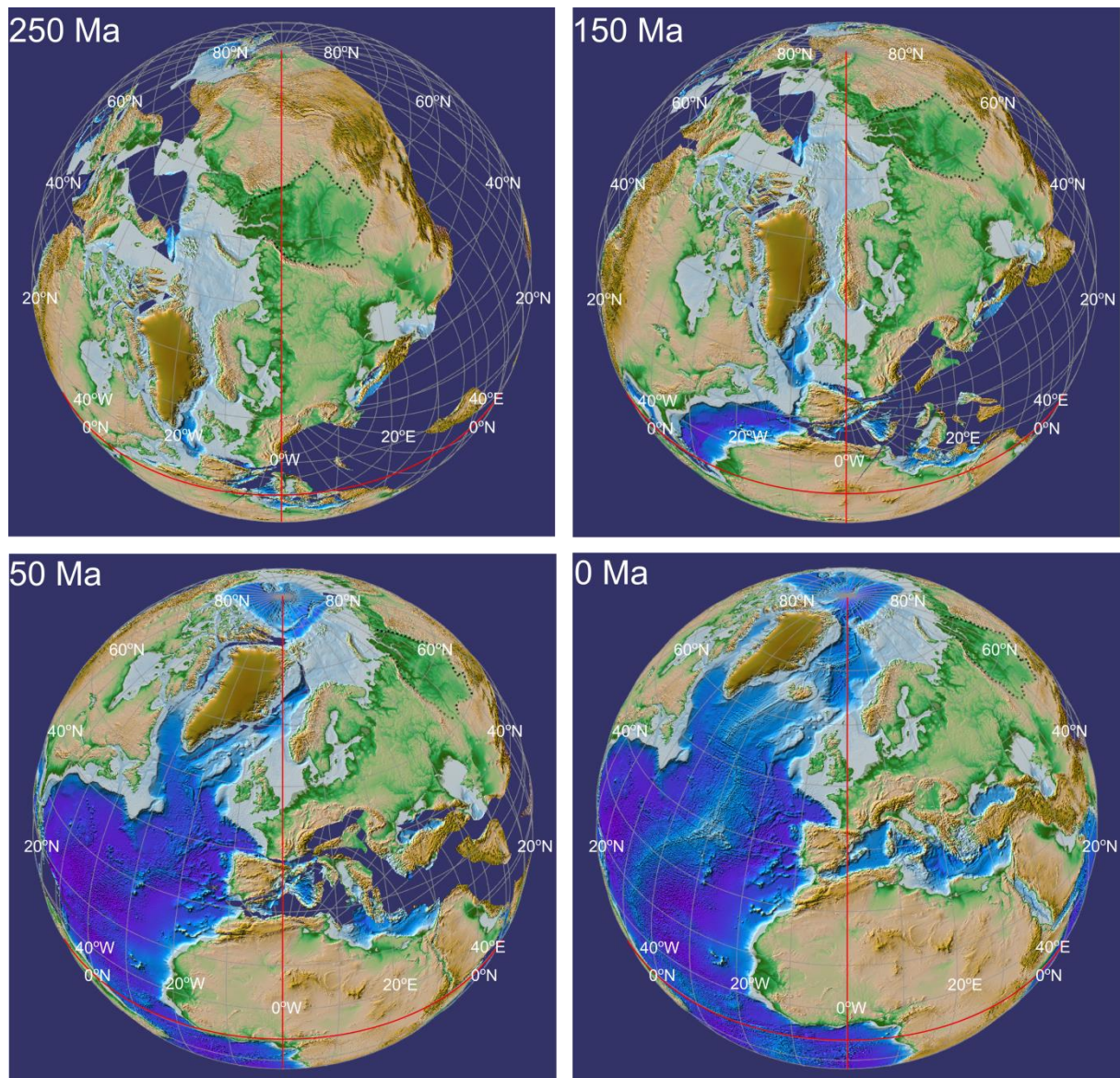
Figure 10. Tectonic reconstructions since 250 Ma. Snapshots of plate tectonic reconstructions from 4DPlates (Clark et al., 2012) since the onset of vertical motions in the WSB at 250 Ma. Dashed line shows the WSB's contour. Red lines mark positions of equator and prime meridian. We use the Plates UTIG model (Müller et al., 2008a) and the fixed hotspot reference frame. Note that Siberia experienced ~2300 km North-East motion from the initial location since 250 Ma.

Conclusions

We have reconstructed the tectonic subsidence history of the WSB for which we digitised available stratigraphic data and calculated tectonic vertical motions for 12 sedimentary cycles using a backstripping analysis. Gridded maps in Figure 8 illustrate the result of our calculations, showing alternating periods of slow subsidence, interrupted by brief uplift periods. The most intense subsidence phase was in the Triassic and in the early Jurassic. Subsidence slowed

subsequently and its locus moved to the western part of the basin. Between 142-136 Ma the basin experienced irregular uplift on the background of a global marine transgression, followed by renewed subsidence. The basin uplifted in the middle Oligocene when sedimentation stopped. Although the basin's subsidence has been interpreted as thermal subsidence in the wake of a Permo-Triassic rifting event, our results indicate a more complex history. Specifically the amplitude and prolonged duration of subsidence, its migration throughout the basin, and the occurrence of regional, short lived uplift events call for the influence of additional sublithospheric factors related to mantle flow. Our results suggest that basins hold important archives of past mantle flow regimes.

Acknowledgements

Conflict of interest

No conflict of interest declared.

References

Allen, P.A., Allen, J.R., 2013. Basin analysis: Principles and application to petroleum play assessment. John Wiley & Sons.

Anell, I., Thybo, H., Artemieva, I.M., 2009. Cenozoic uplift and subsidence in the North Atlantic region: Geological evidence revisited. Tectonophysics 474, 78–105.

Armitage, J.J., Allen, P.A., 2010. Cratonic basins and the long-term subsidence history of continental interiors. J. Geol. Soc. 167, 61–70.

Athy, L.F., 1930. Density, porosity, and compaction of sedimentary rocks. AAPG Bull. 14, 1–24.

Austermann, J., Pollard, D., Mitrovica, J.X., Moucha, R., Forte, A.M., DeConto, R.M., Rowley, D.B., Raymo, M.E., 2015. The impact of dynamic topography change on Antarctic ice sheet stability during the Middle Pliocene warm period. Geology 43, 927–930.

Autin, J., Scheck-Wenderoth, M., Loegering, M.J., Anka, Z., Vallejo, E., Rodriguez, J.F., Dominguez, F., Marchal, D., Reichert, C., Di Primio, R., others, 2013. Colorado Basin 3D structure and evolution, Argentine passive margin. Tectonophysics 604, 264–279.

Braun, J., 2010. The many surface expressions of mantle dynamics. Nat. Geosci. 3, 825–833.

Brune, S., Heine, C., Clift, P.D., Pérez-Gussinyé, M., 2017. Rifted margin architecture and crustal rheology: Reviewing Iberia-Newfoundland, Central South Atlantic, and South China Sea. Mar. Pet. Geol. 79, 257–281.

Bulinnikova, S.P., Golbert, A.V., Klimova, I.G., 1978. Paleo-bio facies of the oil and gas bearing Tithonian and Necomian sediments of the West Siberian Platform. Nedra.

Bunge, H.-P., Richards, M.A., Lithgow-Bertelloni, C., Baumgardner, J.R., Grand, S.P., Romanowicz, B.A., 1998. Time scales and heterogeneous structure in geodynamic Earth models. Science 280, 91–95.

Cherepanova, Y., Artemieva, I.M., Thybo, H., Chemia, Z., 2013. Crustal structure of the Siberian craton and the West Siberian basin: An appraisal of existing seismic data. Tectonophysics 609, 154–183.

Clark, S.R., Skogseid, J., Stensby, V., Smethurst, M.A., Tarrou, C., Bruaset, A.M., Thurmond, A.K., 2012. 4DPlates: On the fly visualization of multilayer geoscientific datasets in a plate tectonic environment. Comput. Geosci. 45, 46–51.

Cloetingh, S., Ziegler, P.A., 2007. 6.11 - Tectonic Models for the Evolution of Sedimentary Basins A2 - Schubert, Gerald, in: Treatise on Geophysics. Elsevier, Amsterdam, pp. 485–611.

Cogné, J.P., 2003. PaleoMac: A Macintosh™ application for treating paleomagnetic data and making plate reconstructions. Geochem. Geophys. Geosystems 4, 1007.

Colli, L., Bunge, H.-P., Schuberth, B.S., 2015. On retrodictions of global mantle flow with assimilated surface velocities. Geophys. Res. Lett. 42, 8341–8348.

Colli, L., Ghelichkhan, S., Bunge, H.-P., 2016. On the ratio of dynamic topography and gravity anomalies in a dynamic Earth. Geophys. Res. Lett. 43, 2510–2516.

Colli, L., Stotz, I., Bunge, H.-P., Smethurst, M., Clark, S., Iaffaldano, G., Tassara, A., Guillocheau, F., Bianchi, M.C., 2014. Rapid South Atlantic spreading changes and coeval vertical motion in surrounding continents: Evidence for temporal changes of pressure-driven upper mantle flow. Tectonics 33, 1304–1321.

Dobretsov, N.L., Polyansky, O.P., Reverdatto, V.V., Babichev, A.V., 2013. Dynamics of the Arctic and adjacent petroleum basins: a record of plume and rifting activity. Russ. Geol. Geophys. 54, 888–902.

Doré, A.G., Lundin, E.R., Jensen, L.N., Birkeland, Ø., Eliassen, P.E., Fichler, C., 1999. Principal tectonic events in the evolution of the northwest European Atlantic margin. Geol. Soc. Lond. Pet. Geol. Conf. Ser. 5, 41–61.

Doubrovine, P.V., Steinberger, B., Torsvik, T.H., 2012. Absolute plate motions in a reference frame defined by moving hot spots in the Pacific, Atlantic, and Indian oceans. J. Geophys. Res. Solid Earth 117.

Dressel, I., Scheck-Wenderoth, M., Cacace, M., 2016. Backward modelling of the subsidence evolution of the Colorado Basin, offshore Argentina and its relation to the evolution of the conjugate Orange Basin, offshore SW Africa. Tectonophysics.

Dressel, I., Scheck-Wenderoth, M., Cacace, M., Lewerenz, B., Götze, H.-J., Reichert, C., 2015. Reconstruction of the southwestern African continental margin by backward modeling. Mar. Pet. Geol. 67, 544–555.

Evans, D.A.D., 2009. The palaeomagnetically viable, long-lived and all-inclusive Rodinia supercontinent reconstruction. Geol. Soc. Lond. Spec. Publ. 327, 371–404.

Flament, N., Gurnis, M., Müller, R.D., 2013. A review of observations and models of dynamic topography. Lithosphere 5, 189–210.

Friedrich, A.M., Bunge, H.-P., Rieger, S.M., Colli, L., Ghelichkhan, S., Nerlich, R., 2017. Stratigraphic framework for the plume mode of mantle convection and the analysis of interregional unconformities on geological maps. Gondwana Res.

Ghelichkhan, S., Bunge, H.-P., 2016. The compressible adjoint equations in geodynamics: derivation and numerical assessment. GEM-Int. J. Geomath. 1–30.

Gradstein, F.M., Ogg, G., Schmitz, M., 2012. The Geologic Time Scale 2012 2-Volume Set. Elsevier.

Grand, S.P., 2002. Mantle shear–wave tomography and the fate of subducted slabs. Philos. Trans. R. Soc. Lond. Math. Phys. Eng. Sci. 360, 2475–2491.

Green, P.F., Duddy, I.R., Hegarty, K.A., 2002. Quantifying exhumation from apatite fission-track analysis and vitrinite reflectance data: precision, accuracy and latest results from the Atlantic margin of NW Europe. Geol. Soc. Lond. Spec. Publ. 196, 331–354.

Green, P.F., Japsen, P., Chalmers, J.A., Bonow, J.M., Duddy, I.R., 2017. Post-breakup burial and exhumation of passive continental margins: Seven propositions to inform geodynamic models. Gondwana Res.

Guillocheau, F., Rouby, D., Robin, C., Helm, C., Rolland, N., Le Carlier de Veslud, C., Braun, J., 2012. Quantification and causes of the terrigeneous sediment budget at the scale of a continental margin: a new method applied to the Namibia–South Africa margin. Basin Res. 24, 3–30.

Hager, B.H., Gurnis, M., 1987. Mantle convection and the state of the Earth's interior. Rev. Geophys. 25, 1277–1285.

Haq, B.U., Hardenbol, J., Vail, P.R., 1987. Chronology of fluctuating sea levels since the Triassic. Science 235, 1156–1167.

Hartley, R.A., Roberts, G.G., White, N., Richardson, C., 2011. Transient convective uplift of an ancient buried landscape. Nat. Geosci. 4, 562–565.

Heine, C., Dietmar Müller, R., Steinberger, B., Torsvik, T.H., 2008. Subsidence in intracontinental basins due to dynamic topography. Phys. Earth Planet. Inter. 171, 252–264.

Hoggard, M.J., White, N.J., Al-Attar, D., 2016. Global dynamic topography observations reveal limited influence of large-scale mantle flow. Nat. Geosci. 9, 456–463.

Holt, P.J., Hunen, J. van, Allen, M.B., 2012. Subsidence of the West Siberian Basin: Effects of a mantle plume impact. Geology 40, 703–706.

Huismans, R., Beaumont, C., 2011. Depth-dependent extension, two-stage breakup and cratonic underplating at rifted margins. Nature 473, 74–78.

Iaffaldano, G., Bunge, H.-P., 2015. Rapid Plate Motion Variations Through Geological Time: Observations Serving Geodynamic Interpretation. Annu. Rev. Earth Planet. Sci. 43, 571–592.

Igoshkin, V.J., Dolson, J.C., Sidorov, D., Bakuev, O., Herbert, R., 2008. New interpretations of the evolution of the West Siberian Basin, Russia. Implications for Exploration, in: American Association of Petroleum Geologists. Annual Conference and Exhibition, San Antonio, TX, AAPG Search and Discovery Article. 1–35.

Japsen, P., 1998. Regional velocity-depth anomalies, North Sea Chalk: a record of overpressure and Neogene uplift and erosion. AAPG Bull. 82, 2031–2074.

Japsen, P., Bonow, J.M., Green, P.F., Cobbold, P.R., Chiossi, D., Lilletveit, R., Magnavita, L.P., Pedreira, A., 2012a. Episodic burial and exhumation in NE Brazil after opening of the South Atlantic. Geol. Soc. Am. Bull. 124, 800–816.

Japsen, P., Chalmers, J.A., 2000. Neogene uplift and tectonics around the North Atlantic: overview. Glob. Planet. Change 24, 165–173.

Japsen, P., Chalmers, J.A., Green, P.F., Bonow, J.M., 2012b. Elevated, passive continental margins: Not rift shoulders, but expressions of episodic, post-rift burial and exhumation. Glob. Planet. Change 90, 73-86.

Khain, V.E., Ryabukhin, A.G., 2002. Russian geology and the plate tectonics revolution. Geol. Soc. Lond. Spec. Publ. 192, 185–198.

Kominz, M.A., 1984. Oceanic ridge volume and sea-level change-an error analysis, in: Interregional Unconformities and Hydrocarbon Accumulation. American Association of Petroleum Geologists, Tulsa, 109–127.

Kontorovich, A.E., Nesterov, I.I., Salmanov, F.K., Surkov, V.S., Trofimuk, A.A., Ervje, Y.G., 1975. Western Siberian geology of oil and gas, Nedra.

Kontorovich, V.A., 2009. The Meso-Cenozoic tectonics and petroleum potential of West Siberia. Russ. Geol. Geophys. 50, 346–357.

Kukla, P.A., Strozyk F., Mohriak W.U., 2017. South Atlantic salt basins - witnesses of complex passive margin evolution, this volume

McKenzie, D., 1978. Some remarks on the development of sedimentary basins. Earth Planet. Sci. Lett. 40, 25–32.

Morgan, W.J., 1968. Rises, trenches, great faults, and crustal blocks. J. Geophys. Res. 73, 1959–1982.

Moucha, R., Forte, A.M., 2011. Changes in African topography driven by mantle convection. Nat. Geosci. 4, 707–712.

Müller, R.D., Sdrolias, M., Gaina, C., Roest, W.R., 2008a. Age, spreading rates, and spreading asymmetry of the world's ocean crust. Geochem. Geophys. Geosystems 9.

Müller, R.D., Sdrolias, M., Gaina, C., Steinberger, B., Heine, C., 2008b. Long-term sea-level fluctuations driven by ocean basin dynamics. Science 319, 1357–1362.

Nerlich, R., Clark, S.R., Bunge, H.-P., 2014. Reconstructing the link between the Galapagos hotspot and the Caribbean Plateau. GeoResJ 1–2, 1–7.

O'Neill, C., Müller, D., Steinberger, B., 2005. On the uncertainties in hot spot reconstructions and the significance of moving hot spot reference frames. Geochem. Geophys. Geosystems 6.

Paton, D.A., van der Spuy, D., di Primio, R., Horsfield, B., 2008. Tectonically induced adjustment of passive-margin accommodation space; influence on the hydrocarbon potential of the Orange Basin, South Africa. AAPG Bull. 92, 589–609.

Pitman, W.C., 1978. Relationship between eustacy and stratigraphic sequences of passive margins. Geol. Soc. Am. Bull. 89, 1389–1403.

Praeg, D., Stoker, M.S., Shannon, P.M., Ceramicola, S., Hjelstuen, B., Laberg, J.S., Mathiesen, A., 2005. Episodic Cenozoic tectonism and the development of the NW European "passive"continental margin. Mar. Pet. Geol. 22, 1007–1030.

Reeve, M.T., Jackson, C.A.-L., Bell, R.E., Magee, C., Bastow, I.D., 2016. The stratigraphic record of prebreakup geodynamics: Evidence from the Barrow Delta, offshore Northwest Australia. Tectonics 35, 1935–1968.

Reichow, M.K., Saunders, A.D., White, R.V., Al'Mukhamedov, A.I., Medvedev, A.Y., 2005. Geochemistry and petrogenesis of basalts from the West Siberian Basin: an extension of the Permo–Triassic Siberian Traps, Russia. Lithos 79, 425–452.

Ricard, Y., Fleitout, L., Froidevaux, C., 1984. Geoid heights and lithospheric stresses for a dynamic Earth, in: Annales Geophysicae. 267–286.

Richards, M.A., Engebretson, D.C., 1992. Large-scale mantle convection and the history of subduction. Nature 355, 437–440.

Richards, M.A., Hager, B.H., 1984. Geoid anomalies in a dynamic Earth. J. Geophys. Res. Solid Earth 89, 5987–6002.

Ritsema, J., Deuss, A., Van Heijst, H.J., Woodhouse, J.H., 2011. S40RTS: a degree-40 shear-velocity model for the mantle from new Rayleigh wave dispersion, teleseismic traveltime and normal-mode splitting function measurements. Geophys. J. Int. 184, 1223–1236.

Rudkevich, M.Y., 1976. The history and the dynamics of the development of the west siberian platform. Tectonophysics 36, 275–287.

Rudkevich, M.Y., Ozeranskaya, L.S., Chistyakova, N.F., 1988. Oil-producing complexes of the West Siberian Basin. Nedra.

Said, A., Moder, C., Clark, S., Ghorbal, B., 2015. Cretaceous–Cenozoic sedimentary budgets of the Southern Mozambique Basin: Implications for uplift history of the South African Plateau. J. Afr. Earth Sci. 109, 1–10.

Saunders, A.D., England, R.W., Reichow, M.K., White, R.V., 2005. A mantle plume origin for the Siberian traps: uplift and extension in the West Siberian Basin, Russia. Lithos 79, 407–424.

Seton, M., Müller, R.D., Zahirovic, S., Gaina, C., Torsvik, T., Shephard, G., Talsma, A., Gurnis, M., Turner, M., Maus, S., 2012. Global continental and ocean basin reconstructions since 200Ma. Earth-Sci. Rev. 113, 212–270.

Shephard, G.E., Bunge, H.-P., Schuberth, B.S., Müller, R.D., Talsma, A.S., Moder, C., Landgrebe, T.C.W., 2012. Testing absolute plate reference frames and the implications for the generation of geodynamic mantle heterogeneity structure. Earth Planet. Sci. Lett. 317, 204–217.

Sigmundsson, F., 1991. Post-glacial rebound and asthenosphere viscosity in Iceland. Geophys. Res. Lett. 18, 1131–1134.

Simmons, N.A., Forte, A.M., Grand, S.P., 2007. Thermochemical structure and dynamics of the African superplume. Geophys. Res. Lett. 34,

Steckler, M.S., Watts, A.B., 1978. Subsidence of the Atlantic-type continental margin off New York. Earth Planet. Sci. Lett. 41, 1–13.

Steinberger, B., Torsvik, T.H., 2008. Absolute plate motions and true polar wander in the absence of hotspot tracks. Nature 452, 620–623.

Torsvik, T.H., Müller, R.D., Van der Voo, R., Steinberger, B., Gaina, C., 2008. Global plate motion frames: Toward a unified model. Rev. Geophys. 46.

Van der Hilst, R.D., Widiyantoro, S., Engdahl, E.R., 1997. Evidence for deep mantle circulation from global tomography. Nature 386, 578–584.

Vyssotski, A.V., Vyssotski, V.N., Nezhdanov, A.A., 2006. Evolution of the West Siberian Basin. Mar. Pet. Geol. 23, 93–126.

Weismüller, J., Gmeiner, B., Ghelichkhan, S., Huber, M., John, L., Wohlmuth, B., Rüde, U., Bunge, H.-P., 2015. Fast asthenosphere motion in high-resolution global mantle flow models. Geophys. Res. Lett. 42.

Wessel, P., Kroenke, L.W., 2008. Pacific absolute plate motion since 145 Ma: An assessment of the fixed hot spot hypothesis. J. Geophys. Res. Solid Earth 113.

Yang, T., Gurnis, M., Zahirovic, S., 2016. Mantle-induced subsidence and compression in SE Asia since the early Miocene. Geophys. Res. Lett. 43, 1901–1909.

Ziegler, P.A., Cloetingh, S., van Wees, J.-D., 1995. Dynamics of intra-plate compressional deformation: the Alpine foreland and other examples. Tectonophysics 252, 7–59.

Ziegler, P.A., Van Wees, J.-D., Cloetingh, S., 1998. Mechanical controls on collision-related compressional intraplate deformation. Tectonophysics 300, 103–129.

Chapter 2

This chapter presents a Kalkulo report on the vertical plate motions in the Barents Sea.

In previous chapter we have learned that tectonic subsidence of the West Siberian Basin and especially its northern part exhibit features indicative of dynamic topography. This chapter is dedicated to the study of a neighbouring intraplate sedimentary basin – the Barents Sea. The overview of the most recent geophysical data shows a remarkable correspondence of major tectonic events in the Barents Sea and West Siberian Basin. Due to the large spatial scale of coeval tectonic pulses, the chapter challenges ideas of local tectonic mechanisms and discusses the role of mantle convection in development of these regions.

Kalkulo report on the vertical plate motions in the Barents Sea

Introduction

Vertical plate motions play a major role in shaping sedimentary basins and formation of hydrocarbon sources (Allen and Allen, 2013). Efficient basin exploration requires understanding of the basins' vertical motions and their underlying mechanisms. Generally, basin subsidence and uplift are associated with deformation at the tectonic boundaries. However, there are various examples of sedimentary basins formed in the plate interior and their development mechanisms still remain unclear (Leighton, 1991). An example of such intra-cratonic basins is the West Siberian Basin, discussed in Chapter 1 (Vibe et al., 2017). We showed that the basin's subsidence is unlikely a result of thermal accommodation, because of its amount and prolonged duration. Moreover, the West Siberian Basin experienced irregular uplift episodes, accompanied by re-activation of faults. In order to further investigate the nature of the intraplate vertical motions we look into another intra-cratonic basin bordering the West Siberian Basin – the Barents Sea.

The Barents Sea has been actively explored since the end of the 20th century and its tectonic history is relatively well constrained (Henriksen et al., 2011b). In this chapter we aim to review the latest geophysical data on the geological structure, vertical motions and upper mantle setting in the framework of the Greater Barents Sea. We test whether the character of vertical motions in the Barents Sea can relate to that observed in the West Siberian Basin. Understanding the pattern of vertical motions potentially enables generalization of the laws, which governs development of the intraplate basins.

Geological setting

The Barents Sea occupies an area of c. 1500 M km^2 north of Europe, bordered by the Norwegian-Greenland Sea to the West and Novaya Zemlya to the East (Figrue 1). The Barents Sea is typically divided into the Western and the Eastern Barents Seas. The two parts of the Barents Sea have been distinguished due to the geo-political reasons, but also due to the significant differences in the crustal and sedimentary structures.

The Western Barents Sea comprises the highs, platforms and numerous smaller basins (Figure 1). It is situated on a Caledonian suture representing an assembly of basement terrains (Doré, 1991). The Western Barents Sea overlays a non-homogeneous crystalline crust with indications of high-density bodies, which could possibly resemble accreted Iceland arcs or oceanic terrains (Breivik et al., 2002). According to Faleide et al. (2008) in some parts of the Western Barents Sea, such as the Svalbard Platform, crustal thickness reaches 30 km. Ritzmann and Faleide (2009) suggest presence of the old, continental lithosphere in the Western Barents Sea. Tomographic model interpretation (Gac et al., 2016), however, shows that lithosphere in the Western Barents Sea is hotter and thinner, than in the Eastern Barents Sea. The type or the age of the crust in the Western Barents Sea is presumably different from the one in the Eastern Barents Sea (Sakoulina et al., 2015).
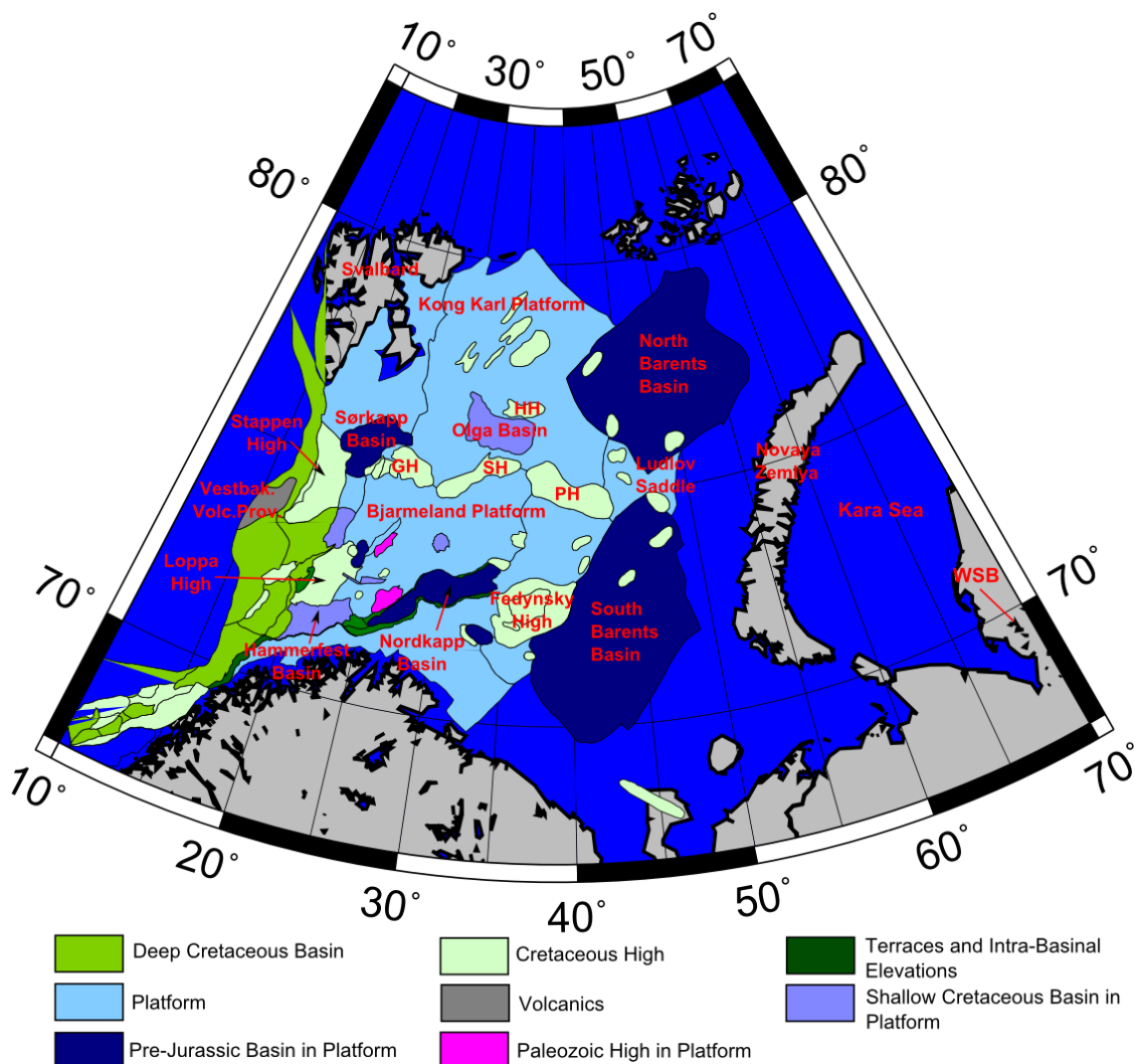
Figure 1. Geographical setting and the structural setting of the Barents Sea. The Eastern Barents Sea lies to the West of Novaya Zemlya and comprise two major basins: South Barents Basin and North Barents Basin. The Western Barents Sea occupies an area north of the Norwegian coast and comprises smaller basins, paltforms and highs. Abbreviations: GH – Gardarbanken High, SH – Sentralbanken High, PH – Polarrev High, HH – Hopen High. The shapefile is freely available at http://www.npd.no/en/Topics/Geology/Temaartikler/Structure-elements/.

The Eastern Barents Sea contains major South and North Barents basins and several highs (Figure 1). It has possibly comprised one large basin before it split up into the southern and northern parts by the Ludlov saddle in Triassic time or, according to some studies, in the middle Jurassic (Klett and Pitman, 2011; O'Leary et al., 2004). Regarding the crustal structure, the older seismic studies report that the Eastern Barents Sea rests on a combination of sub-oceanic crust and continental blocks (Verba et al., 1986). However, more recent explorations found that the Eastern Barents Sea crust is of continental nature (Ritzmann and Faleide, 2009). The continental origins of the crust are confirmed by the deep seismic investigations (Sakoulina et al., 2000). The crustal thickness data varies between different studies. The study by Sakoulina et al. (2015) documents crustal thickness of 35 km in the North Kara Basin, 50 km in the Novaya Zemlya area and 40 km in the North Kara Sea. However, The BARENTS50 crustal model by Ritzmann et al. (2007) suggest lower crustal thickness values (see Figure 2 b).

At least four mechanisms are proposed to be responsible for the formation of the Barents basins: sag-basins due to extension (Ritzmann and Faleide, 2009), foreland basin bordering due to Uralian orogeny (Otto and Bailey, 1995), thermal cooling (O'Leary et al., 2004), densification of crustal mafic heterogeneities due to buckling (Gac et al., 2013). Both western and eastern parts of the Barents Sea were shaped by several extensive rifting episodes (Doré, 1995).
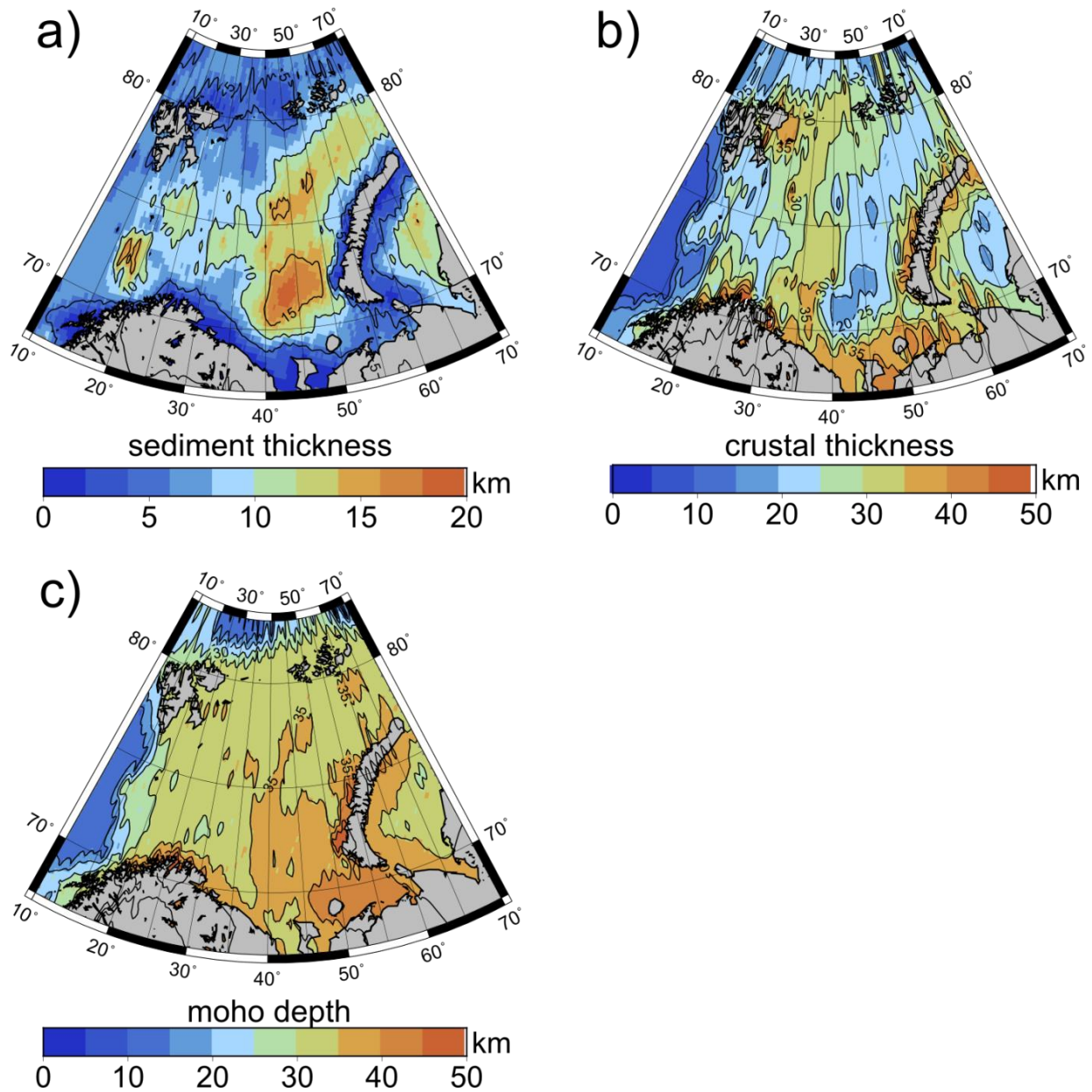
Figure 2. Sediment and crustal thickness of the Barents Sea. The maps represent different layers of the BARENTS50 crustal model by Ritzmann et al. (2007). The model is plotted using Albers Conic projection and 5 km data contours.

Tectonic history

i.   Main Paleozoic events

Gudlaugsson et al. (1998) outlined the main Paleozoic events of the Western Barents Sea history to be consolidation of the basement due to Caledonian orogeny; Devonian tectonic regime of both extension and compression; Carboniferous and Permian extensive rifting events; and gradual development of the non-fault related Permian subsidence.

The Caledonian stage began in the middle to late Silurian with a climax in the late Devonian (Aplonov et al., 1996; Doré, 1995; Klett and Pitman, 2011). In the Western Barents Sea, the main arm of the Caledonides (The Barents Caledonides) follows the NE trend of the Scandinavian-Greenland Caledonides and covers the most of the southern Western Barents Sea. Another arm of Caledonides is oriented northwards and covers the northwestern Barents Sea – the Svalbard Caledonides (Henriksen et al., 2011b). The Svalbard and Barents Caledonides define the N-S and NE-SW trends of the Barents sea fault complexes, which are thought to be basement-controlled and repeatedly activated (Doré, 1991).

The Devonian regime is documented on Svalbard, where a N-S oriented graben is filled with the early and middle Devonian strata (Friend and Moody-Stuart, 1972). Later, the strata was deformed by folding and faulting during the late Devonian "Svalbardian movements" and unconformably overlain by Carboniferous strata (Vogt, 1928). The nature of this event is not very clear (Gudlaugsson et al., 1998).

The two main extensional phases in the Western Barents Sea are agreed to be the late Devonian- middle Carboniferous and Permo-Triassic (Gabrielsen et al., 1990; Gudlaugsson et al., 1998). The first one resulted in formation of numerous extensional basins separated by local highs, such as Tromsø, Bjørnøya, Nordkapp, Fingerdjupet, Maud, Ottar and possibly Hammerfest Basins (Dengo and Røssland, 2013). Fault movements ceased in the late Carboniferous, and the relief was covered by the Carboniferous-Permian succession (Gudlaugsson et al., 1998). This platform-wide succession marked the switch from the fault-controlled syn-rift subsidence to the sag-basin type subsidence active throughout Permian. Another rifting episode occurred at the Permo-Triassic boundary and affected the northerly trending zone at the western

margin of the Barents Sea. For example, extensive erosion is documented on the Loppa High at the Permo-Triassic (Gabrielsen et al., 1993)

O'Leary et al. (2004) highlights three main rifting events in the Eastern Barents Sea in the Paleozoic: early Ordovican, middle Ordovican- Silurian and middle to late Devonian. These events are documented for both the Timan-Pechora and South Barents Basin, and it is proposed that they had similar Paleozoic structural history, but were separated by a paleo-high. Henriksen et al. (2011b) and Klett and Pitman (2011) point to another major rifting pulse also in the middle Carboniferous.

A major Permo-Triassic rifting event, which affected the Western Barents Sea, was also active in the Eastern Barents Sea, Timan-Pechora Basin and the WSB (Allen et al., 2006; Gramberg, 1997; Klett and Pitman, 2011).

ii.   Main Mesozoic events

The series of rifting events described above led to the crustal extension and formation of half-grabens, resulting in development of a sag basin in the Barents region and pronounced Triassic subsidence (Gudlaugsson et al., 1998). The subsidence was mainly focused on the Eastern Barents Sea and the Nordkapp and Hammerfest basins (Henriksen et al., 2011b). In the Western Barents Sea, Triassic subsidence rates were lower than in the East, but still very high, also suggesting that thermal subsidence might have played an important role, until the middle Triassic (Gudlaugsson et al., 1998). Interestingly, although the Triassic subsidence is partially attributed to the last stages of Uralian orogeny by most authors (Klett and Pitman, 2011; O'Leary et al., 2004; Otto and Bailey, 1995), they note that the Barents Sea does not show geometries characteristic to foreland basins.

Following Henriksen et al. (2011a) a major rifting episode in the Western Barents Sea occurred in the late Jurassic – Cretaceous, which was mostly confined to the western basins – including the Hammerfest Basin, which subsided relatively to the Loppa High. Some rifting, uplift and faulting are also recognized in the Tromsø, Bjørnøya and Harstad basins, and after the final stage of rifting these basins rapidly subsided (Faleide et al., 2008).   Faleide et al. (1993) documents major unconformities bounding the Teistengrunnen group (Callovain to late Beriassian) and numerous unconformities within the group indicating continued late Jurassic faulting. This early Cretaceous

structuring of the southwestern Barents Sea was characterized by extensional faulting with a large downthrow to the West (Faleide et al., 1993). Magmatism was also present in the form of doleritic instrusions in the Triassic – early Cretaceous shales (Gjelberg and Steel, 1995). The differential uplift and subsidence in the late Cretaceous led to the formation of deep basins
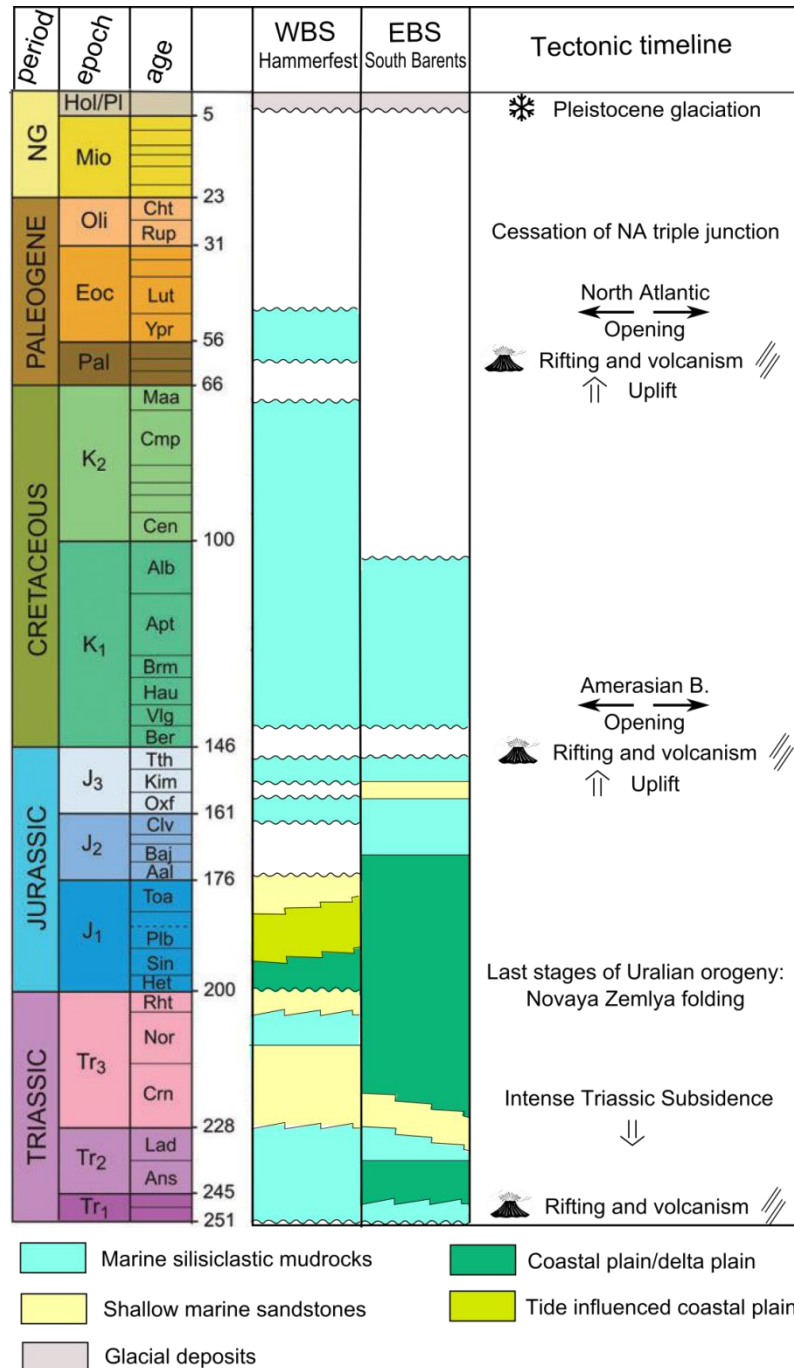
Figure 3. Stratigraphic chart of the Barents Sea. Simplified after Henriksen et al. (2011b), Worsley (2008). The right panel outlines the main tectonic events in the region and at the closest tectonic boundaries.

flanked by exposed highs and formation of the deep marine shales – Bazhenov formation or Hekkingen formation.

The Eastern Barents Sea also experienced an uplift and sub-aerial exposure of basin margins in the late Jurassic (Klett and Pitman, 2011). Notably, the regional "Late Kimerrian" unconformity marking rifting at the Jurassic- Cretaceous transition is recognized in all basins of the North Atlantic (Jacquin and de Graciansky, 1998).

Late Cretaceous strata is widespread in the Western Barents Sea, while the Eastern Barents Sea holds only the early Cretaceous strata truncated by unconformity overlain by the Quaternary sediments (Henriksen et al., 2011b).

iii.   Main Cenozoic events

Faleide et al. (1993) identifies a depositional break at the Cretaceous-Tertiary transition between the Sotbakken and Nygrunnen groups (Figure 3). The hiatus was then followed by a deposition of uniform sequence that was deposited as a sheet in the entire Barents Sea in the late Paleocene. Paleocene-Eocene sediments are found in the Western Barents Sea in the Hammerfest and Nordkapp basins, resting unconformably on the Cretaceous rocks. But the Cenozoic stratum is eroded on all the platforms around and at the Loppa high. Judging from the truncation of the early Cretaceous strata, a significant Cenozoic uplift affected the Barents Sea. Deposition was happening only along the western margin – in the Sørvestnaget basin and the Vestbakken Volcanic Province.

In the Eocene, the central segment of the Western Barents Sea underwent rifting and volcanism, followed by a down-faulting in a pull-apart setting (Faleide et al., 1993, 1991, 1988). The southern part of the Sørvestnaget basin was uplifted and eroding, shedding sediments onto the immature oceanic crust and Tromsø basin. Stappen high experienced an uplift in the early Eocene after the pronolnged susbsidence period following the Permo-Triassic uplift (Worsley et al., 2001).

In the early Oligocene, compression between Svalbard and north Greenland resulted in a fold and thrust belt on Svalbard (Henriksen et al., 2011b) and compression and inversion features are seen over all the Barents Sea. The main center of deformation and volcanism in the southwestern Barents Sea was the Vestbakken volcanic province (Faleide et al., 1993). The next uplift episode in the Barents Sea took place in the late

Cenozoic. However its timing is not very well constrained, and is debated to have happened either in the early Oligocene, or in Miocene (Reemst et al., 1994).

Dimakis et al. (1998) summarized the results of sediment balance works to derive the total value of the Cenozoic Western Barents Sea erosion. They suggest that the Barents Sea was sub-aerial prior to glaciations and erosion estimate varies from 1200 to 3500 m. The appatite fission track studies by Nyland et al. (1992) identifiy two uplift events in the Western Barents Sea, one 50-40 Ma and another 10-5 Ma.

The Eastern Barents basin and north Kara Sea were uplifted and eroded first at the late Cretaceous – Paleogene transition (Klett and Pitman, 2011; Musatov, 1998, 1989). The uplift is estimated to be on the order of 1000 m (Johansen et al., 1992; Musatov, 1999; Sobolev, 2012). N to NE striking reverse faults are identified by Gustavsen et al. (1997) and interpreted to have developed due to the compression in the Late-Cretaceous – Paleogene. The Ludlov saddle became more prominent during the late Cretaceous and Paleogene (Klett and Pitman, 2011). Another uplift, presumably, in Oligocene and Miocene, occurred along the pre-existent faults (Klett and Pitman, 2011). The total estimates of uplift range from 200-1500 m to as much as 2000-3000 m (Musatov, 1999; Ryabukhina et al., 1999).

Coeval tectonic pulses

An overview of sedimentary literature, presented above, draws our attention to the similar timing of events in Eurasian sedimentary basins.

The major Permo-Triassic rifting, which played a crucial role in the West Siberian Basin formation, also affected all parts of the Barents Sea. The Permo-Triassic extension is documented in various locations along the North Atlantic margin (Doré et al., 1999) and marks the onset of rifting activity in the North Sea Basin (Ziegler, 1992). The Permo-Triassic rifting event is responsible for the formation of large graben system in the West Siberian Basin and is thought to play the main role in the WSB's formation. The contemporary Siberian flood basalts, erupted during the rifting, link this event to important processes in mantle convection. Namely, geochemical experiments and numerical modelling results support a theory of a Permo-Triassic mantle plume under Siberia (Reichow et al., 2002; Saunders et al., 2005). However, Gramberg (1997)

suggests that the Eastern Barents rifting event is presumably younger than the West Siberian.

After the Triassic rapid subsidence of the basins, which affected both the Barents Sea and the West Siberian Basin, the late Jurasssic – early Cretaceous rifting episode occurred in both regions. The water-loaded tectonic subsidence curve of the WSB, presented in Chapter 1 (see Figure 4), shows positive peaks around the Tithonian-Beriassian transition. These peaks indicate interruption of subsidence and occurrence of uplift. Sedimentary overview (Kontorovich, 2009; Kontorovich et al., 2011) confirms a late Jurassic- Cretaceous uplift with re-activation of the existing faults in the WSB. The North Sea studies (Evans, 2003; Ziegler, 1992) recognize the late Jurassic – early Cretaceous rifting pulse, which was active for about 10 My. Notably, Ziegler (1992) highlights the absence of volcanism in the North Sea at this rifting stage, whereas magmatic intrusions are preserved in the Western Barents Sea sediments (Gjelberg and Steel, 1995). Concerning the North Sea volcanism, a large volcanic center and intense doming (with a structural relief of up to 2500 m) developed earlier, in the middle Jurassic.
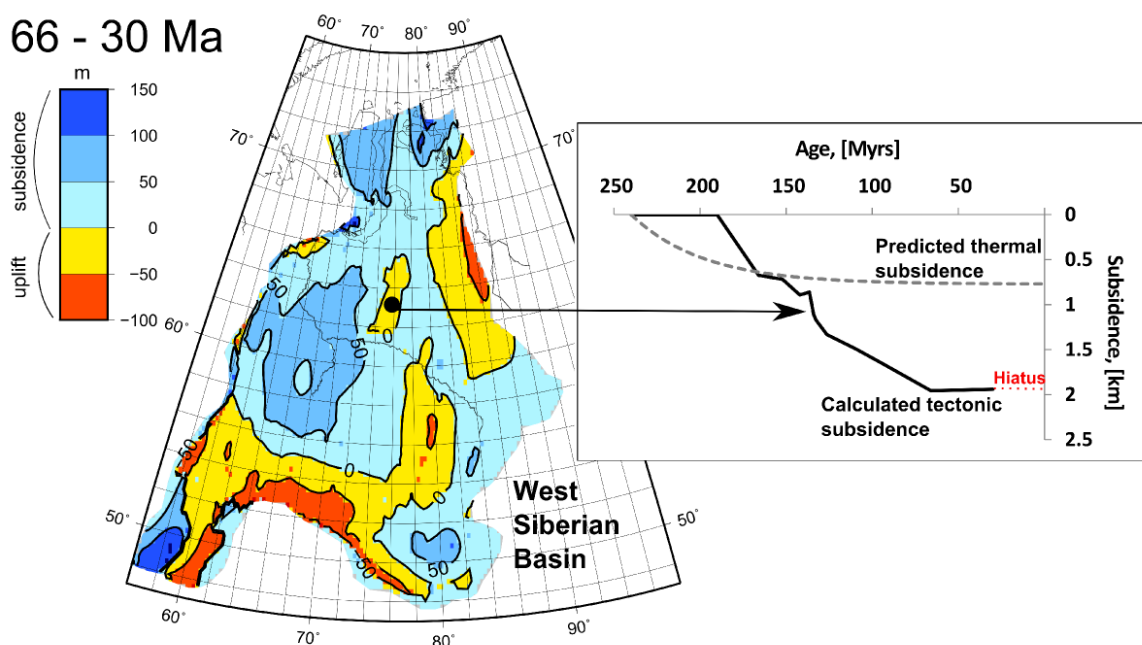
Figure 4: Irregular subsidence of the West Siberian Basin. Map from Vibe et al. (2017) showing amount of early Cenozoic tectonic subsidence and uplift in the West Siberian Basin. The plot on the right shows tectonic subsidence curve (bold black line) compared to predicted

thermal subsidence (dashed gray line). Tectonic subsidence is several times bigger than expected thermal subsidence and is interrupted by uplift events, which indicates additional development mechanisms.

Cenozoic encompassed two regional rifting episodes, documented in the Barents Sea, the West Siberian Basin and the North Atlantic. The first rifting episode occurred in the early Paleogene. As discussed above, unconformities of this time are widespread in the Barents Sea (Faleide et al., 1993; Henriksen et al., 2011a, 2011b). Rifting in the future Greenland-Norwegian Sea and at the NE Atlantic boundary reached its peak at the Cretaceous – Paleogene boundary (Skogseid et al., 2000). The British Isles were uplifted at this stage, which led to deposition of thick siliciclastic sequences in the North Sea (Evans, 2003). The West Siberian Basin also experienced re-activation of tectonic movements at the Meso-Cenozoic boundary. Our tectonic subsidence curves (Figure 4) do not show any pronounced peak at this time stage. Nevertheless, seismic cross-sections in Kontorovich (2009) demonstrate that Paleocene faulting was intense, cutting through the whole Mesozoic section. This study shows strong indications that this tectonism played a crucial role in the development of main depression in the WSB – the Koltogory-Urengoy mega-rift. To make a long story short, rifting at the Meso-Cenozoic boundary affected a very vast territory from Greenland to Siberia.

Another regional tectonic event is confined to the late Cenozoic. The Neogene uplift event in the North Atlantic and the Barents Sea left a noticeable imprint in the form of intense erosion (see Japsen and Chalmers (2000) for an overview, and also Figure 3 in Chapter 3). The exact timing of this uplift is hard to constrain, because almost all uplifted areas lack Cenozoic sediments. In addition, glacial erosion contributed heavily to the removal of Meso-Cenozoic cover. Despite that, the apatite fission track analysis for Scandinavia (Hendriks et al., 2007; Hendriks and Andriessen, 2002) indicates that Neogene witnessed an intense uplift both in Northern and in Southern Scandes. According to Rudkevich (1976) the onset of the West Siberian Basin uplift occurred already around middle Oligocene.

To sum up, the pattern of vertical motions in the Barents Sea is very similar to that in the West Siberian Basin: the Permo-Triassic rifting is followed by a very intense Triassic subsidence; re-activation of uplifts at the start and end of Cretaceous, and intense uplift from the end of Oligocene- beginning of Miocene. This pattern is observed over a distance of about 4000 km. One of the first works to notice a regional character of

tectonically generated Triassic and Jurassic sequence boundaries in the Arctic was Embry (1997). One year later, Jacquin and de Graciansky, (1998) presented the outline of global Mesozoic unconformities, recognizable in all Western European basins. Namely, these unconformities are the Hardegsen (Permo-Triassic), Early Cimmerian (early Jurassic), Mid-Cimmerian (middle Jurassic), Late Cimmerian (late Jurassic) and Laramide (Cretaceous-Paleogene) and are associated to rifting events. It is likely that the Paleocene and Miocene unconformities described in previous sections are also of the global, tectonically induced type.

Proposed Mechanisms

The rifting events observed in all of the Barents basins are usually linked to the local plate tectonic changes at the basin boundaries. Namely, the Permo-Triassic rifting is thought to be a consequence of the Uralian Ocean closure. This closure constituted the final stage of Pangean assembly which led to the subsurface heat accumulation (Doré et al., 1999; Nance et al., 1988). In the WSB, this major rifting event is agreed upon to be an effect of the mantle plume (Saunders et al., 2005). The transition from Permian to Triassic was an important stage of Earth tectonic evolution, associated with the assembly of the supercontinent Pangea, which split up again shortly (Matthews et al., 2016). This time interval is also associated with the biggest mass extinction event (Rhodes, 1967). Changes of the sea level, increased temperatures and atmospheric carbon dioxides due to the continuous volcanism are possible causes of this ecological collapse (Erwin, 1994).

The late Jurassic rifting event in the Barents Sea and in the WSB is attributed to the change of the stress field due to the opening of the Arctic basins (Faleide et al., 1993; Kontorovich, 2009). Worsley (2008) suggests that the uplift in the late Jurassic is related to the heat flow associated with the opening of the Arctic basin.

The Cenozoic Barents Sea uplift is shown by Gac et al. (2016) to be possibly due to the lithospheric shortening caused by the North Atlantic ridge push. In the WSB, according to an overview by Vyssotski et al. (2006), the Paleocene change of the depositional environments (Rudkevich, 1976) and later the uplift of the whole basin is possibly a consequence of the Indian – Eurasian collision.

However, the nature of these tectonic events is unlikely to be of a local character, for example associated with changes of tectonic stresses. The large scale of the distribution of coincident vertical motions points to a common underlying process. Jacquin and de Graciansky (1998) suggested a long-term basin subsidence as a main trigger of the eustatic changes producing the unconformities. However, this mechanism does not account for the fault re-activation associated with development of unconformities. Embry (2006) suggested that the nature of synchronous global transgression/regression events could be related to the changes of the tectonic plate velocities and directions. This idea was inspired by the study of Collins and Bon (1996), linking the eustatic changes with mantle dynamics. In Chapter 1, we found that the irregularities of the WSB's subsidence pattern are likely mantle related. This result is consistent with the theory that processes in the deep Earth generate a large-scale intraplate relief signal. Taking into account that the modern data of the Barents basement (Sakoulina et al., 2015) proposed an active dynamic component in the Barents Sea formation, observed coeval vertical motions, which connect North Atlantic and Siberia through the Barents Sea are likely to manifest some kind of mantle processes.

Mantle beneath the Barents Sea

The deep structure of the Barents crust and upper mantle are a subject of active investigations (Gac et al., 2016; Ivanova et al., 2011; Klitzke et al., 2016; Levshin et al., 2007; Minakov et al., 2017; Ritzmann and Faleide, 2009; Sakoulina et al., 2016). The main results concern the thickness and strength of the regional lithosphere, as well as its thermal state. The regional s-wave model BARMOD by Levshin et al. (2007) indicates that the lithosphere is thicker in the Eastern Barents Sea than in the Western Barents Sea. Lithospheric mantle contributes to a large degree to the increased lithospheric thickness in the Eastern Barents, and its crystalline crust is thinner than in the Western Barents Sea (Klitzke et al., 2016). Moreover, Eastern Barents Sea is characterized by a positive s-wave anomaly in the upper mantle (Levshin et al., 2007). Mantle density distribution in Figure 5 demonstrates the corresponding positive anomaly. 3D gravity model of the Barents Sea by Klitzke et al. (2016) is consistent with the density increase in the upper mantle in the East. Ritzmann and Faleide (2009) suggests that such anomaly could be a result of Siberian plume melt accumulation in the Pre-Permian rift

structures.
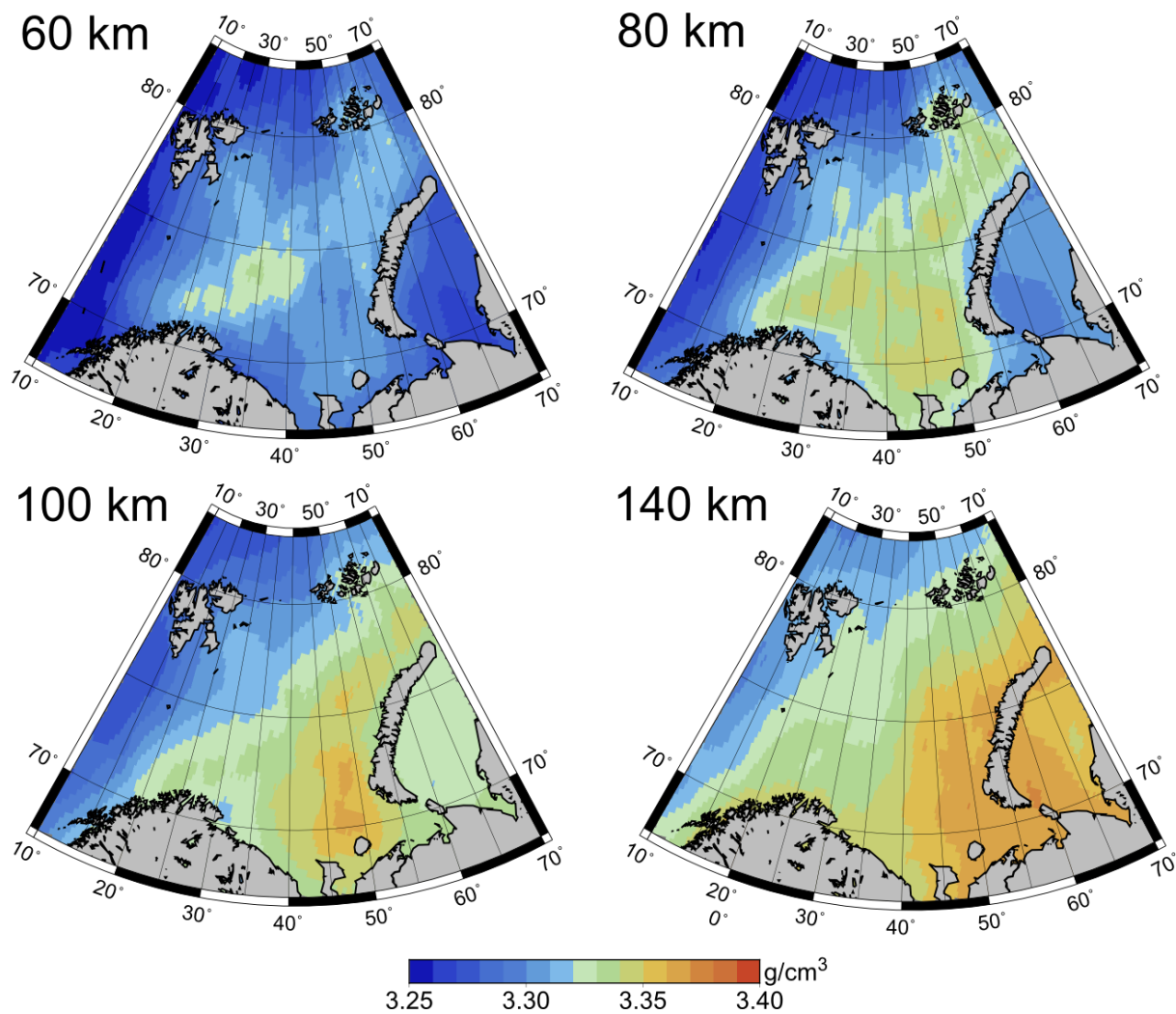
Figure 5: Mantle density at different depths. The maps represents slices of BARENTS3D model (*NORSAR(2006):BARENTS3D,* http://www.norsar.no/seismology/barents3d/ (Levshin et al., 2007; Ritzmann et al., 2007))*.* The model identifies a positive anomaly in the southeastern Barents Sea.

Computations of the lithospheric strength (Gac et al., 2016) show that the Western Barents Sea is characterized by the weak lithosphere, while the lithosphere is stronger in the East Barents Sea. This study shows that the lithospheric strength is mostly controlled by its thickness. The thermal model (Klitzke et al., 2016) shows hotter lithosphere in the West than in the East, both in terms of the mantle heat flow and the surface heat flow. For comparison, the average heatflow values are ~75 mW/m² in the West and 64 mW/m² in the East for the surface heat flow and ~45 mW/m² and ~28 mW/m² for the mantle heatflow. In the Norwegian- Greenland sea these values are 73-344 and 55-340 mW/m² respectively.

The relation of the Barents Sea tectonics to the deep processes is also expressed by the widespread dykes and associated sills in the sedimentary cover (Minakov et al., 2017). The age of the magmatism is proposed to be early Cretaceous. Two large dyke swarms are located in the Franz Joseph Land and Svalbard. Since there is no sign of underplating in the North Barents Sea, this work proposes that magma channelization from the plume located in the Arctic could be responsible for the magmatic transport into the Barents Sea. Another interesting feature that highlights the importance of deep sublithospheric processes of Barents Sea is the surprisingly flat shape of the Moho boundary in the North Barents Basin, where irregularities could have been smoothed out by the high pressure and temperature of the mantle (Sakoulina et al., 2015).

As mentioned, strong lithosphere of the East Barents Sea is characterised by colder temperature, larger thickness and anomalously high density compared to the Western Barents Sea. Importantly, such difference in lithospheric strength would entail different surface expressions of mantle dynamics. Thinner and hotter lithosphere indicating shallower depth of asthenosphere could possibly be more susceptible to stresses exerted by the mantle. Oppositely, effects of mantle dynamics would possibly be less pronounced on the colder and thicker lithosphere. Also, the style of rifting could be dependant on the rheological properties of the lithosphere. Nevertheless, there are several indications that the sublithospheric processes have played an important role in the Eastern Barents Sea development. For instance, flattened Moho structure and intense early Cretaceous igneous activity (Polteau et al., 2016) implies an active hot mantle upwelling. It seems likely that its current strong lithospheric structure is a result of a thermal contraction due to cessation of the mantle upwelling. The timing of this event would be crucial for understanding the mantle-surface interaction in both parts of the Barents Sea. Further study of the present and past mantle state under the Barents Sea has a potential to shed light on the complex development history of the study area and surrounding regions.

Concluding remarks

This chapter reviews the tectonic history of the Western and Eastern Barents Sea. The review of geological literature indicates the similar timing of major unconformities in both sub-regions. The unconformities are likely associated with the change of tectonic regimes, recognized from the re-activation and formation of faults and magmatism.

These tectonic events correspond to the Permo-Triassic, late Jurassic – early Cretaceous, late Cretaceous – Paleogene and Miocene ages. We find that this timing coincides with the timing of uplifts in the West Siberian Basins reported in Chapter 1. Since the regions feature different crustal structure and tectonic setting we propose that the vertical motions in all of these regions were strongly influenced by a common mechanism, operating on a very large scale and not related to local tectonics. A plausible mechanism is dynamic topography resulting from mantle flow associated with the North Atlantic or Arctic spreading centers. In the following Chaper 3 we will study the link between the North Atlantic topography and spreading changes.

References

Allen, M.B., Anderson, L., Searle, R.C., Buslov, M., 2006. Oblique rift geometry of the West Siberian Basin: tectonic setting for the Siberian flood basalts. J. Geol. Soc. 163, 901–904.

Allen, P.A., Allen, J.R., 2013. Basin analysis: Principles and application to petroleum play assessment. John Wiley & Sons.

Aplonov, S.V., Shmelev, G.B., Krasnov, D.K., 1996. Geodynamics of the Barents-Kara shelf: geophysical evidence. Geotectonics 30, 309–326.

Breivik, A.J., Mjelde, R., Grogan, P., Shimamura, H., Murai, Y., Nishimura, Y., Kuwano, A., 2002. A possible Caledonide arm through the Barents Sea imaged by OBS data. Tectonophysics, Deep Seismic Probing of the Continents and their Margins 355, 67–97

Collins, J.F., Bon, J., 1996. Mantle origin of global sea-level fluctuations and geomagnetic reversals: Evidence from non-linear dynamics. Proceedings of the International Symposium on Sequence Stratigraphy in S.E. Asia, 91–128

Dengo, C.A., Røssland, K.G., 2013. Extensional tectonic history of the western Barents Sea. Struct. Tecton. Model. Its Appl. Pet. Geol. 1, 91–107.

Dimakis, P., Braathen, B.I., Faleide, J.I., Elverhøi, A., Gudlaugsson, S.T., 1998. Cenozoic erosion and the preglacial uplift of the Svalbard–Barents Sea region. Tectonophysics 300, 311–327.

Doré, A.G., 1995. Barents Sea geology, petroleum resources and commercial potential. Arctic, Man and the Barents Sea Ecosystems 48, 207–221.

Doré, A.G., 1991. The structural foundation and evolution of Mesozoic seaways between Europe and the Arctic. Palaeogeogr. Palaeoclimatol. Palaeoecol. 87, 441–492.

Doré, A.G., Lundin, E.R., Jensen, L.N., Birkeland, Ø., Eliassen, P.E., Fichler, C., 1999. Principal tectonic events in the evolution of the northwest European Atlantic margin. Geol. Soc. Lond. Pet. Geol. Conf. Ser. 5, 41–61.

Embry, A.F., 2006. Episodic global tectonics: Sequence stratigraphy meets plate tectonics. Geo Expro 3, 26–30.

Embry, A.F., 1997. Global Sequence Boundaries of the Triassic and Their Identification in the Western Canada Sedimentary Basin. Bull. Can. Pet. Geol. 45, 415–433.

Erwin, D.H., 1994. The Permo–Triassic extinction. Nature 367, 231–236.

Evans, D., 2003. The Millennium Atlas: Petroleum Geology of the Central and Northern North Sea.A Project of the Geological Society of London, the Geological Survey of Denmark and Greenland and the Norwegian Petroleum Society.

Faleide, J.I., Gudlaugsson, S.T., Eldholm, O., Myhre, A.M., Jackson, H.R., 1991. Deep seismic transects across the sheared western Barents Sea-Svalbard continental margin. Tectonophysics 189, 73–89.

Faleide, J.I., Myhre, A.M., Eldholm, O., 1988. Early Tertiary volcanism at the western Barents Sea margin. Geol. Soc. Lond. Spec. Publ. 39, 135–146.

Faleide, J.I., Tsikalas, F., Breivik, A.J., Mjelde, R., Ritzmann, O., Engen, O., Wilson, J., Eldholm, O., 2008. Structure and evolution of the continental margin off Norway and the Barents Sea. Episodes 31, 82–91.

Faleide, J.I., Vågnes, E., Gudlaugsson, S.T., 1993. Late Mesozoic-Cenozoic evolution of the south-western Barents Sea in a regional rift-shear tectonic setting. Mar. Pet. Geol. 10, 186–214.

Friend, P.F., Moody-Stuart, M., 1972. Sedimentation of the Wood Bay Formation (Devonian) of Spitsbergen: regional analysis of a late orogenic basin. Oslo Universitetsforlaget.

Gabrielsen, R.H., Faerseth, R.B., Jensen, L.N., 1990. Structural Elements of the Norwegian Continental Shelf. Pt. 1. The Barents Sea Region. Norwegian Petroleum Directorate.

Gabrielsen, R.H., Grunnaleite, I., Ottesen, S., 1993. Reactivation of fault complexes in the Loppa High area, southwestern Barents Sea.

Gac, S., Huismans, R.S., Podladchikov, Y.Y., Faleide, J.I., 2012. On the origin of the ultradeep East Barents Sea basin. J. Geophys. Res. Solid Earth 117.

Gac, S., Huismans, R.S., Simon, N.S., Podladchikov, Y.Y., Faleide, J.I., 2013. Formation of intracratonic basins by lithospheric shortening and phase changes: a case study from the ultra-deep East Barents Sea basin. Terra Nova 25, 459–464.

Gac, S., Klitzke, P., Minakov, A., Faleide, J.I., Scheck-Wenderoth, M., 2016. Lithospheric strength and elastic thickness of the Barents Sea and Kara Sea region. Tectonophysics.

Gjelberg, J., Steel, R.J., 1995. Helvetiafjellet Formation (Barremian-Aptian), Spitsbergen: characteristics of a transgressive succession. Nor. Pet. Soc. Spec. Publ. 5, 571–593.

Gramberg, I.S., 1997. Barents sea Permian-Triassic paleorift and its meaning for oil and gas content of Barents-Kara platform, in: Doklady akademii nauk, 789–791.

Gudlaugsson, S.T., Faleide, J.I., Johansen, S.E., Breivik, A.J., 1998. Late Palaeozoic structural development of the South-western Barents Sea. Mar. Pet. Geol. 15, 73–102.

Gustavsen, F.B., Dypvik, H., Solheim, A., 1997. Shallow geology of the northern Barents Sea: Implications for petroleum potential. AAPG Bull. 81, 1827–1842.

Hendriks, B., Andriessen, P., Huigen, Y., Leighton, C., Redfield, T., Murrell, G., Gallagher, K., Nielsen, S.B., others, 2007. A fission track data compilation for Fennoscandia. Nor. Geol. Tidsskr. 87, 143.

Hendriks, B.W., Andriessen, P.A., 2002. Pattern and timing of the post-Caledonian denudation of northern Scandinavia constrained by apatite fission-track thermochronology. Geol. Soc. Lond. Spec. Publ. 196, 117–137.

Henriksen, E., Bjoernseth, H., Hals, T., Heide, T., Kiryukhina, T., Kloevjan, O., Larssen, G., Ryseth, A., Roenning, K., Sollid, K., Stoupakova, A., 2011a. Chapter 17 Uplift and erosion of the greater Barents Sea: impact on prospectivity and petroleum systems. Geol. Soc. Lond. Mem. 35, 271–281.

Henriksen, E., Ryseth, A., Larssen, G., Heide, T., Roenning, K., Sollid, K., Stoupakova, A., 2011b. Chapter 10 Tectonostratigraphy of the greater Barents Sea: implications for petroleum systems. Geol. Soc. Lond. Mem. 35, 163–195

Ivanova, N.M., Sakulina, T.S., Belyaev, I.V., Matveev, Y.I., Roslov, Y.V., 2011. Depth model of the Barents and Kara seas according to geophysical surveys results. Geol. Soc. Lond. Mem. 35, 209–221.

Jacquin, T., de Graciansky, P.-C., 1998. Major transgressive/regressive cycles: the stratigraphic signature of European basin development, in: de Graciansky P.-C. (Eds.), Mesozoic and Cenozoic Sequence Stratigraphy of European Basins, SEPM Spec. Pub. 60

Japsen, P., Chalmers, J.A., 2000. Neogene uplift and tectonics around the North Atlantic: overview. Glob. Planet. Change 24, 165–173.

Johansen, S.E., Ostisty, B.K., Birkeland, Ø., Fedorovsky, Y.F., Martirosjan, V.N., Christensen, O.B., Cheredeev, S.I., Ignatenko, E.A., Margulis, L.S., 1992. Hydrocarbon potential in the Barents Sea region: play distribution and potential. Arct. Geol. Pet. Potential Nor. Pet. Soc. NPF Spec. Publ. 2, 273–320.

Klett, T.R., Pitman, J.K., 2011. Geology and petroleum potential of the East Barents Sea basins and Admiralty Arch. Geol. Soc. Lond. Mem. 35, 295–310.

Klitzke, P., Sippel, J., Faleide, J.I., Scheck-Wenderoth, M., 2016. A 3D gravity and thermal model for the Barents Sea and Kara Sea. Tectonophysics 684, 131–147.

Kontorovich, V.A., 2009. The Meso-Cenozoic tectonics and petroleum potential of West Siberia. Russ. Geol. Geophys. 50, 346–357.

Kontorovich, V.A., Solov'ev, M.V., Kalinina, L.M., Kalinin, A.Y., 2011. The role of Meso-Cenozoic tectonics in the formation of hydrocarbon pools in the southern parts of the Kaimysovy arch and Nyurol'ka megadepression. Russ. Geol. Geophys. 52, 845–858.

Leighton, M.W., 1991. Interior cratonic basins. American Association of Petroleum Geologists.

Levshin, A.L., Schweitzer, J., Weidle, C., Shapiro, N.M., Ritzwoller, M.H., 2007. Surface wave tomography of the Barents Sea and surrounding regions. Geophys. J. Int. 170, 441–459.

Matthews, K.J., Maloney, K.T., Zahirovic, S., Williams, S.E., Seton, M., Müller, R.D., 2016. Global plate boundary evolution and kinematics since the late Paleozoic. Glob. Planet. Change 146, 226–250.

Minakov, A., Yarushina, V., Faleide, J.I., Krupnova, N., Sakoulina, T., Dergunov, N., Glebovsky, V., 2017. Dyke emplacement and crustal structure within a continental large igneous province, northern Barents Sea. Geol. Soc. Lond. Spec. Publ. 460.

Musatov, 1998. Cenozoic sediment cover structure and neotectonics of the Barents-Kara shelf based on the seismic data, Russ. J. Earth Sc.

Musatov, 1989. Cenozoic development of the Barents-Kara shelf relief. Geomorph.

Musatov, Y.Y., 1999. Neotectonic Criteria for Oil-Gas Productivity of Barents-Kara Shelf, Petr. Geol., 33, 107–114.

Nance, R.D., Worsley, T.R., Moody, J.B., 1988. The supercontinent cycle. Sci. Am. 259, 72–79.

Nyland, B., Jensen, L.N., Skagen, J., Skarpnes, O., Vorren, T., 1992. Tertiary uplift and erosion in the Barents Sea: magnitude, timing and consequences. Al Struct. Tecton. Model. Its Appl. Pet. Geol. Nor. Pet. Soc Spec Publ 153–162.

O'Leary, N., White, N., Tull, S., Bashilov, V., Kuprin, V., Natapov, L., Macdonald, D., 2004. Evolution of the Timan–Pechora and south barents sea basins. Geol. Mag. 141, 141–160.

Otto, S.C., Bailey, R.J., 1995. Tectonic evolution of the northern Ural Orogen. J. Geol. Soc. 152, 903–906

Reemst, P., Cloetingh, S., Fanavoll, S., 1994. Tectonostratigraphic modelling of Cenozoic uplift and erosion in the south-western Barents Sea. Mar. Pet. Geol. 11, 478–490.

Reichow, M.K., Saunders, A.D., White, R.V., Pringle, M.S., Al'Mukhamedov, A.I., Medvedev, A.I., Kirda, N.P., 2002. 40Ar/39Ar dates from the West Siberian Basin: Siberian flood basalt province doubled. Science 296, 1846–1849.

Rhodes, F.H.T., 1967. Permo-Triassic extinction. Geol. Soc. Lond. Spec. Publ. 2, 57–76.

Ritzmann, O., Maercklin, N., Inge Faleide, J., Bungum, H., Mooney, W.D., Detweiler, S.T., 2007. A three-dimensional geophysical model of the crust in the Barents Sea region: model construction and basement characterization. Geophys. J. Int. 170,

Ritzmann, O., Faleide, J.I., 2009. The crust and mantle lithosphere in the Barents Sea/Kara Sea region. Tectonophysics 470, 89–104.

Rudkevich, M.Y., 1976. The history and the dynamics of the development of the west siberian platform. Tectonophysics 36, 275–287.

Ryabukhina, S.G., Amutriyevskaya, T.V., Zayiyev, V.A., 1999. Effect of neotectonic movements on oil-gas potential of south part of Barents Sea basin.

Sakoulina, T.S., Kashubin, S.N., Pavlenkova, G.A., 2016. Deep seismic soundings on the 1-AP profile in the Barents Sea: Methods and results. Izv. Phys. Solid Earth 52, 572–589.

Sakoulina, T.S., Pavlenkova, G.A., Kashubin, S.N., 2015. Structure of the Earth's crust in the northern part of the Barents–Kara region along the 4-AR DSS profile. Russ. Geol. Geophys. 56, 1622–1633.

Sakoulina, T.S., Telegin, A.N., Tikhonova, I.M., Verba, M.L., Matveev, Y.I., Vinnick, A.A., Kopylova, A.V., Dvornikov, L.G., 2000. The results of deep seismic investigations on geotraverse in the Barents Sea from Kola peninsula to Franz-Joseph Land. Tectonophysics 329, 319–331.

Saunders, A.D., England, R.W., Reichow, M.K., White, R.V., 2005. A mantle plume origin for the Siberian traps: uplift and extension in the West Siberian Basin, Russia. Lithos 79, 407–424.

Skogseid, J., Planke, S., Faleide, J.I., Pedersen, T., Eldholm, O., Neverdal, F., 2000. NE Atlantic continental rifting and volcanic margin formation. Geol. Soc. Lond. Spec. Publ. 167, 295–326.

Sobolev, P., 2012. Cenozoic uplift and erosion of the Eastern Barents Sea–constraints from offshore well data and the implication for petroleum system modelling [Känozoische Hebung und Erosion der östlichen Barentssee–Abschätzungen aus Offshore-Bohrungsdaten und Auswirkung auf die Erdölsystem-Modellierung)]. Z. Dtsch. Ges. Für Geowiss. 163, 309–324.

Verba, M.L., Pavlenkin, A.D., Tulina, Y., 1986. Deep geological structure of the Barents Sea shelf zone (according to KSZ-82). Heterog. Deep Struct. Earth's Crust Oceans PGO Sevmorgeo Leningr, 75–88.

Vogt, T., 1928. Den norske fjellkjedes revolusjonshistorie. Nor. Geol. Tidsskr. 10, 97–115.

Vibe, Y., Bunge, H.-P., Clark, S.R., 2017. Anomalous subsidence history of the West Siberian Basin as an indicator for episodes of mantle induced dynamic topography. Gondwana Res.

Vyssotski, A.V., Vyssotski, V.N., Nezhdanov, A.A., 2006. Evolution of the West Siberian Basin. Mar. Pet. Geol. 23, 93–126.

Worsley, D., Agdestein, T., Gjelberg, J.G., Kirkemo, K., Mørk, A., Nilsson, I., Olaussen, S., Steel, R.J., Stemmerik, L., 2001. The geological evolution of Bjørnøya, Arctic Norway: implications for the Barents Shelf. Nor. J. Geol. Geol. Foren. 81.

Worsley, D., 2008. The post-Caledonian development of Svalbard and the western Barents Sea. Polar Res. 27, 298–317.

Ziegler, P.A., 1992. North Sea rift system. Tectonophysics, Geodynamics of rifting, volume 1 Case history studies on rifts: Europe and Asia 208, 55–75.

Chapter 3

At the time of writing this chapter is being submitted to GSA Geology journal as:

Repeated Cenozoic erosional events in northwestern Eurasia during episodes of faster spreading: implications for the common driving mechanism.

Yulia Vibe[a,b,*], Hans-Peter Bunge[b] , Anke Friedrich[c] and Stuart R. Clark[a]

[a] Kalkulo AS, Simula Research Laboratory, P.O. Box 134, 1325 Lysaker Norway

[b] Department of Earth and Environmental Sciences, Geophysics, Ludwig-Maximilians University of Munich, Theresienstr. 41, 80333, Munich, Germany

[c] Department of Earth and Environmental Sciences, Geology, Ludwig-Maximilians University of Munich, Luisenstr. 37/I, 80333 Munich, Germany

[*] Corresponding author

Email addresses: julia@simula.no (Y. Vibe), bunge@lmu.de (H.-P. Bunge), stuart@simula.no (S. R. Clark), friedrich@lmu.de (A. Friedrich)

The two previous chapters have shown coeval vertical motions in some areas of the northwestern Eurasia. The large scale of their spatial distribution indicates a mechanism operating on a wavelength of thousands of kilometres. Such wavelength is characteristic of the processes active in the Earth's mantle. Chapter 3 studies the correlation of the topographic evolution of northwestern Eurasia and indicators of the underlying mantle flow.

Repeated Cenozoic erosional events in northwestern Eurasia during episodes of faster spreading: implications for the common driving mechanism.

Abstract

The North Atlantic has been an important center of geological explorations since the rise of plate tectonics. The substantial amount of acquired data enables reconstructions of its spreading history. Thus, divergent plate motions of Eurasia – Greenland – North America are well constrained. Moreover, the geological data from numerous locations of the North Atlantic reports significant vertical plate motions. However their nature remains debated. Latest studies showed that the region is most likely underlain by a thin low-viscosity asthenosphere. Computational models suggest that mantle flow in such asthenosphere is dominated by pressure gradients, which can cause surface uplift. The pressure gradients are fed by ascending mantle anomalies that are also reflected in spreading velocity variations. In this work we test the hypothesis that North Atlantic vertical motions are of a regional character and are related to changes in the mantle flow. We assess the agreement between the North Atlantic uplift and spreading velocities. For this we develop the Europe scale maps of hiatus surfaces of Cenozoic epochs. We find that episodes of increased hiatus/erosion in Paleocene-Eocene and Miocene coincide with episodes of spreading rate maxima. This agreement has important implications for the understanding of the mantle convection system and its influence on the Earth surface.

Introduction

Vertical motion of the Earth's surface are a widespread phenomenon, observed at plate boundaries and in plate interiors (Japsen et al., 2012b; Leighton, 1991). It has been observed, that at certain periods of Earth history vertical motions affected very vast, thousand – kilometre – scale areas. An example is episodic burial and uplift of the adjacent continental margins along the Atlantic ridge (Japsen et al., 2012a; Japsen and Chalmers, 2000; Praeg et al., 2005; Rohrman and van der Beek, 1996). Yet, the forces driving these vertical crustal motions remain debated (Green et al., 2017.). Several

studies (Embry, 2006; Japsen et al., 2012c) propose that global changes in paleotopography could be related to changes in plate tectonic regimes and spreading rates. Colli et al. (2014) showed that such relationship is likely to hold in the South Atlantic according to a fundamental force balance model. This study linked the topographic growth of the South Atlantic passive margins to anomalously fast spreading velocities through a pressure-driven mantle flow in the asthenosphere (Höink and Lenardic, 2010; Weismüller et al., 2015).

North Atlantic is a good laboratory to test this relation between the changing topography and variations in spreading rate. The region has been extensively explored in the past decades and its tectonic history is well established (Gernigon et al., 2012; Mjelde et al., 2008). A striking feature of the North Atlantic spreading system is rapid velocity variations. Moreover, evidence of considerable vertical surface motion comes from different locations along the ridge. Studies report coeval uplift episodes in Scandinavia, the British Isles, Greenland and the Barents Sea in the early Cenozoic and in the Neogene (Henriksen et al., 2011a; Hillis et al., 2008; Japsen et al., 2005; Riis, 1996). The geological and seismological studies suggest a possible dynamic support of the North Altantic topography (Jones et al., 2012; Schoonman et al., 2017). In this paper, we test the hypothesis that there is a link between the North Altantic uplift events and the spreading velocity changes. For this, we introduce continent-scale paleo-hiatus maps, showing the extent of northwestern Eurasian erosion. We compare the area affected by erosion to the most updated knowledge of the spreading rate. If such relationship is true, our results have potential of improving our knowledge of the mantle convection system and its interaction with the Earth's surface.

North Atlantic spreading rate

The North Atlantic (Figure 1) is an expedient region to study divergent plate tectonics, due to the well-preserved and well-explored record of sea-floor magnetic lineations (Müller et al., 2008a; Pitman et al., 1971; Roest, 1987; Vogt et al., 1971). These observations enabled reconstructions of the regional and global past plate motions (Gaina et al., 2002; Seton et al., 2012; Torsvik et al., 2008b).

The seafloor magnetic record shows that the North Atlantic opening had significant spreading rate changes (Figure 1). The changes are evident when comparing the width

of the seafloor magnetic lineations to their duration. This is illustrated by the scatter plot in Figure 1 b. Under a constant spreading rate, ideally, wider isochrones reflect a longer time interval, and oppositely, narrower isochrones reflect a shorter time interval. In other words, the relationship of the isochrones' width to its duration should be linear. The outliers on Figure 1 b indicate that this is not the case. The outliers represent time intervals during which isochrones formed anomalously fast or slow, respectively. Figure 1 b shows two main episodes of spreading rate changes: in the Paleocene-Eocene and in the Miocene. The rhombi falling below the trend line correspond to the ages of 50 – 60 Ma and 10 – 20 Ma. The outliers above the trend line indicate a possible spreading slow-down and correspond to post-10-Ma-time, 40 – 20 Ma and pre-60. Moreover, rhombi N and S lay above the line, even though to a smaller degree than the latter ones, marking relatively slower spreading at 17 - 14 Ma and 48 - 44 Ma.
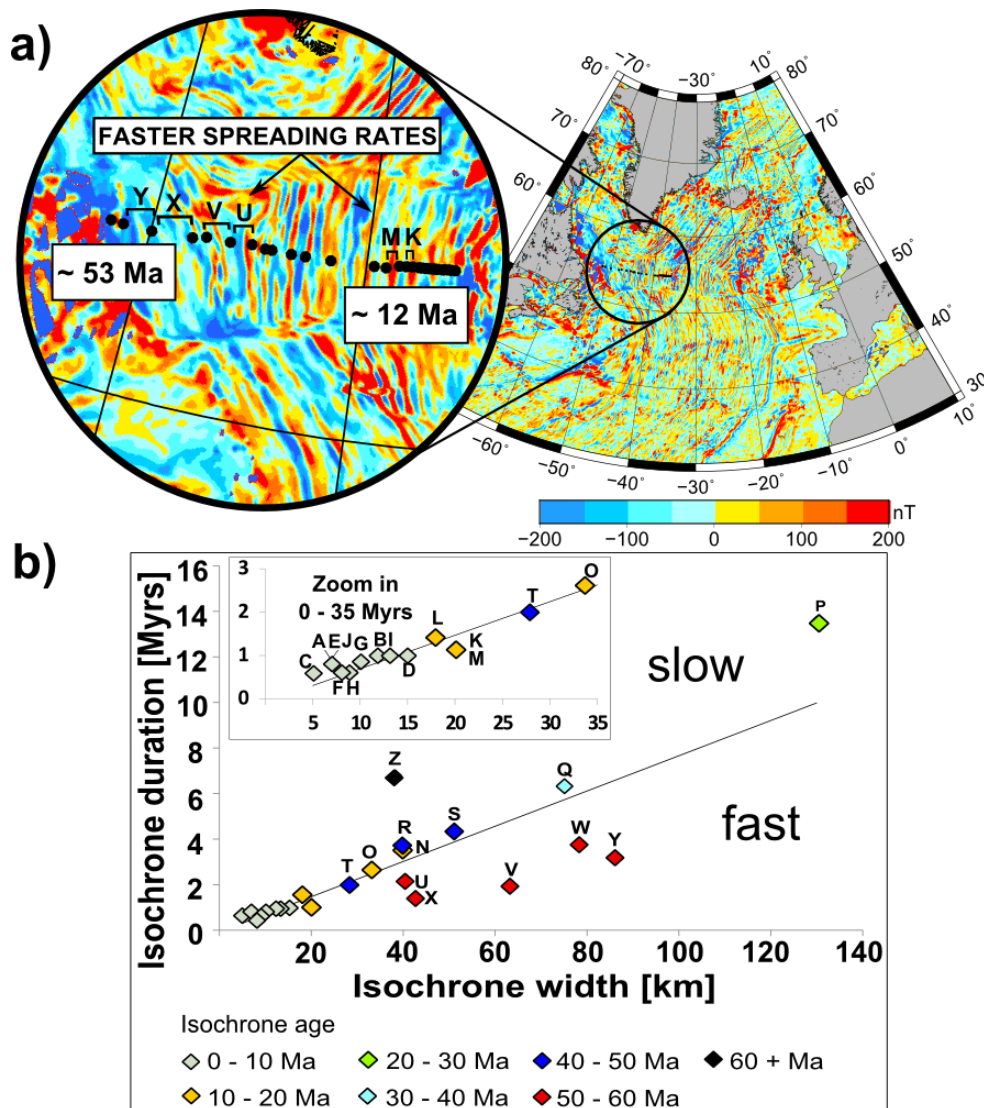
Figure 1: Geographical setting and test of isochron width and duration. Map showing magnetic lineations of North Atlantic seafloor with set of isochron picks to be tested (black dots). b) Test comparing width of lineations and their duration according to Gradstein et al. (2012). This is illustrated by the scatter plot where the trendline shows linear dependency of the width and duration for most of the isochrones. The outliers falling below the trendline indicate faster spreading rate, because larger seafloor distance is accomplished in shorter time. Thus, isochrones of Paleocene-Eocene and Miocene are revealed to have faster spreading rates: the rhombi below the trendline correspond to the chrones C22no - C27no (U, X, V, W, Y) and C5n.1ny-C5An.2no (K), 62-49 Ma and 12.2-9.8 Ma respectively. The lineations are listed in Table 1. The compilation of the picks of magnetic chrones is from the digital archive: http://www.soest.hawaii.edu/PT/GSFML/ML/index.html. The isochrones picks are located at a parallel 54°N and are marked as black dots on the magnetic anomaly (EMAG3) map of the North Atlantic.

To further constrain the trend of the North Atlantic spreading variations we calculate the rate using advanced rotational models (Figure 2). The calculation is based on the combination of Gaina et al. (2002) stage rotations for Paleogene time and Merkouriev and DeMets (2014) stage rotations for the Neogene and was performed using a quaternion-based spreading velocity code (developed by Stuart Clark). We adjusted the timescale in both models to be Gradstein et al. (2012). Figure 2 provides the spreading velocity plot of Eurasia relative to North America, computed with 1 m.y. interval from 60 Ma to present. The spreading rate is calculated for 7 points along the ridge, from 70° North to 40° North with 5° latitude increment. The high-resolution rotational data, like the one from Merkouriev and DeMets (2014) tends to be noisy, which affects the original solutions of spreading velocity. This problem is solved by employing the open-source noise-reduction software Redback (Iaffaldano et al., 2014). Redback uses Bayesian inference to find the best-fitting solutions to stage rotations and thus reduce uncertainties. The Neogene part (20 – 0 Ma) of the spreading rate curve in Figure 2 is the result of Redback noise reduction.
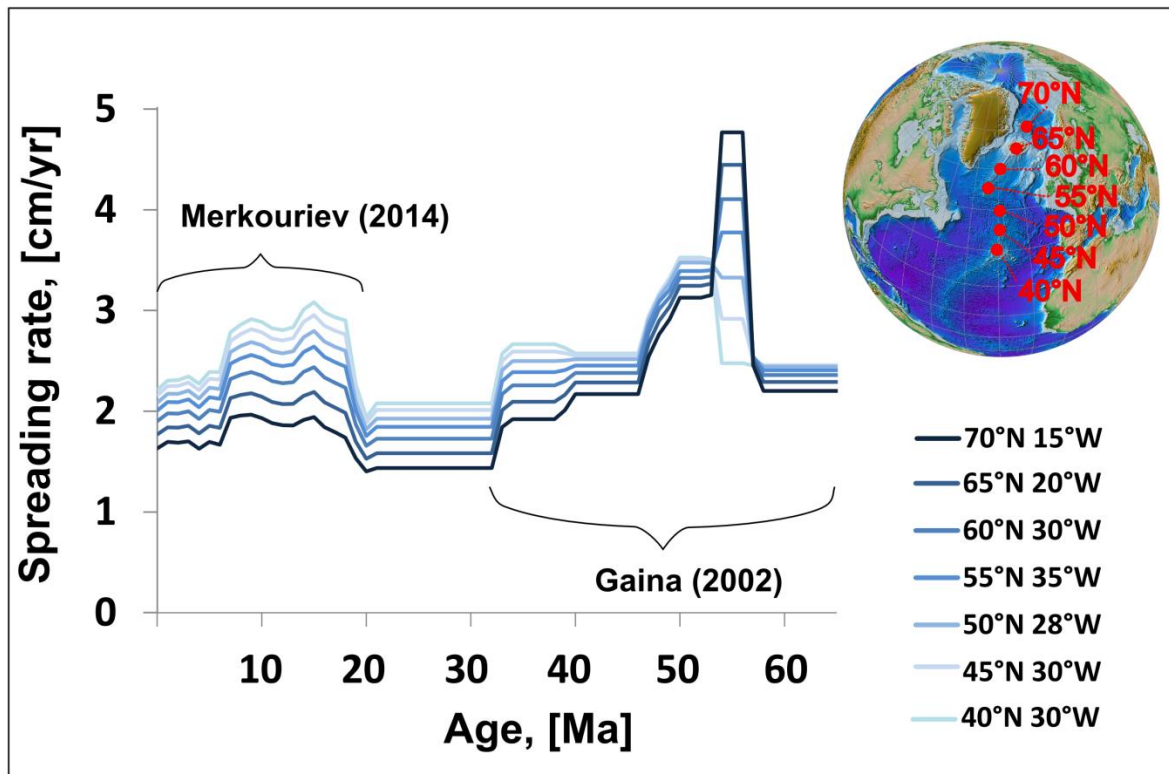
Figure 2: Spreading curves. Spreading rate of Eurasia relative to North America at seven points along the Mid-Atlantic ridge based on finite rotations for the Paleogene (Gaina et al., 2002) and for the Neogene (Merkouriev and DeMets, 2014). Noise associated with Neogene high-resolution finite rotations was minimized by Redback software (Iaffaldano et al., 2014). Spreading rate reaches local maximums around 55 Ma and around 15 Ma. Note that there is a 40 Ma increase in spreading in the South.

Proxies of vertical motion of the Earth's surface in the geological record

As mentioned above, numerous studies reported Cenozoic uplift and exhumation events in the North Atlantic region (Japsen and Chalmers, 2000). The goal of this work is to estimate the spatial pattern of Cenozoic uplift on the scale of whole Europe. For this we constrain hiatal surfaces captured at the base of distinct chronostrarigraphic series, using a method from Friedrich et al. (2017). The resulting hiatal surface maps are shown in Figure 3.

The hiatus plotting method employs the 1:5 million International Geological Map of Europe and Adjacent Areas – IGME 5000 (Asch, 2003). To constrain hiatus at the base of a certain stratigraphic sequence, we mark all intersections of the sequence base with the top surfaces of sequences older than one sequence directly underneath. Here, sequence

base surface corresponds to a set of all outcrops whose oldest age is equal to a chronostratigraphic sequence's bottom age. Accordingly, sequence top surface corresponds to an outcrop set whose youngest age is equal to a chronostratigraphic sequence's top age. These intersections stand for unconformable contacts of outcrops and indicate hiatus in their vicinity. The hiatus intensity, or amount of missing rock, is calculated as an age difference between the sequence base and a corresponding sequence top. The spatial extent of hiatus is derived by the nearest neighbor interpolation. This way, we show locations of sedimentation gaps below a certain stratigraphic sequence. This method gives insights into the paleo-topography by showing areas of erosion or non-deposition and areas of sedimentation captured at the distinct stratigraphic boundaries. For the purposes of our study, variations in relative elevation and paleo-topography serve as indicators of possible surface vertical motions.

Results

Figure 3 presents hiatal surfaces at five stage boundaries of Cenozoic, reconstructed to the past plate settings following the stage rotations of Gaina et al. (2002). The base Paleocene map (Figure 3 a) shows regions of unconformities (yellow to red) and regions of conformable deposition (dark blue) at the base of the Paleocene stage. In our study, the deposition or "no hiatus" blue areas are of a qualitative character, since we do not constrain sedimentary thickness.

The base Paleocene hiatal surface (Figure 3 a) is focused at the northern North Atlantic break-up area. In Western and Eastern Europe, Paleocene deposits, overlaying conformably the late Cretaceous outcrops, give the blue "conformable" signal over all region except the volcanic rocks in the North Rhine Graben area. On Iberian Peninsula no unconformities were detected. This is because the late Cretaceous basins are abundant in the northern and western margins of Spain with cover of much younger (Miocene) rocks. It is possible that base Paleocene hiatus is covered by these young sediments and thus, not identified by our method. Hiatus markers, buried under younger sediments comprise one of the limitations of the present method.

In Figure 3 b, the base Eocene hiatal surface covers the whole central Europe and lies over vast areas of Eastern Europe. On Greenland and Norwegian shelf Eocene deposits conformably lay over Paleocene strata manifested by the blue color on the map. The

a) Base Paleocene hiatus (~65 Ma)

b) Base Eocene hiatus (~55 Ma)
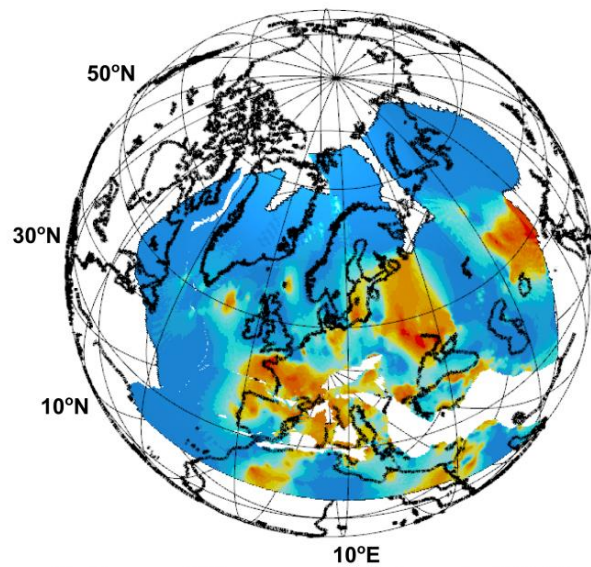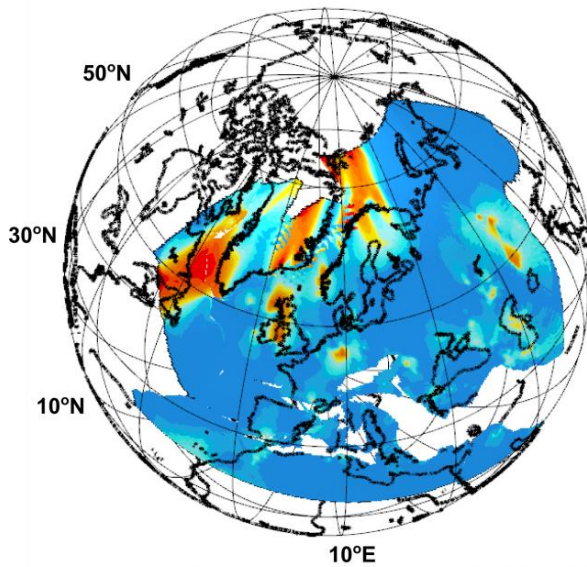
c) Base Oligocene hiatus (~35 Ma)

d) Base Miocene hiatus (~23 Ma)
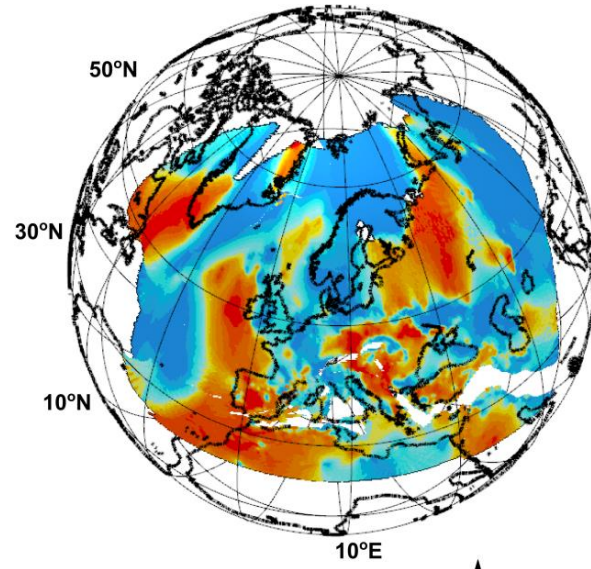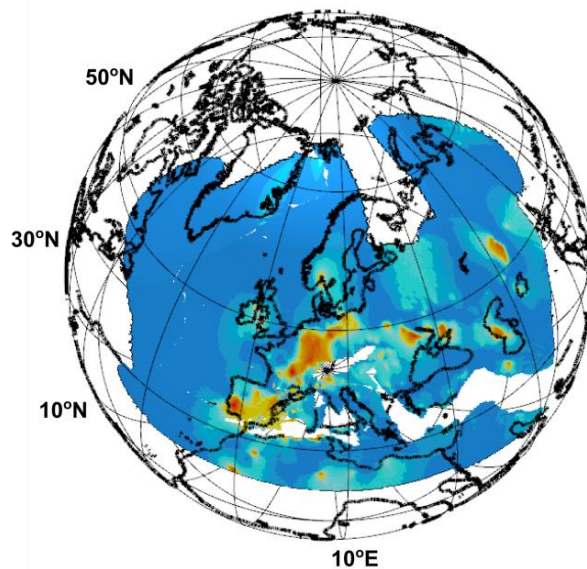
e) Base Pliocene hiatus (~5 Ma)

1 : 100 000 000   ↑ N

hiatus intensity

no hiatus   0   4   8 $\log_2$
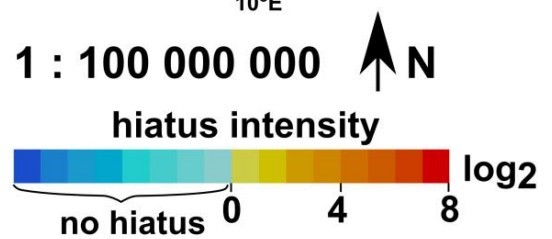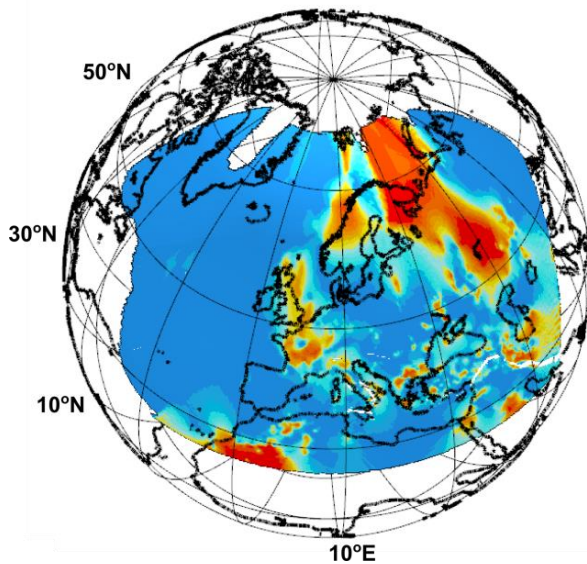
Figure 3 Hiatus maps. Maps showing hiatus intensity magnitude in logarithmic scale ($\log_2 2 = 1$ – $\log_2 256 = 8$). Present day coastlines and hiatus are reconstructed to the past tectonic setting based on the rotations from Gaina et al. (2002) using 4DPlates (Clark et al., 2012). Yellow to red areas show missing sedimentary succession at the base of respective geological time periods, while the blue areas show conformable deposition at these times.

Scandinavian mainland lacks any sediments younger than Paleozoic and therefore hiatus markers could be lost. This is another limitation of the method, which should be kept in mind. In the South of the Eastern European Platform there is a clear hiatus of moderate intensity due to the contact of the Eocene strata onto late Cretaceous rocks. Consequently, a considerable unconformity appears on the East European Platform.

The base Oligocene (Figure 3 c) is characterized only by limited hiatus areas in Germany and Iberian Peninsula. Western European margin features conformable deposition at this time. The exceptions are North of the Oslo rift and West of Scotland, where hiatus spots with moderate intensity. In Eastern Europe, Oligocene rocks are generally absent, or buried under younger Pliocene sediments. In the Northeast of Spain, Oligocene sediments cover Cretaceous rocks which spots red on the map.

The base Miocene hiatus (Figure 3 d) is widespread and is intense along the western European margin, on the Iberian Peninsula and in Eastern Europe until the Urals. In Western Greenland, vast Neogene deposits overlay Proterozoic basement reflected as high intensity hiatus. These deposits do not exist along the southeastern margin of Greenland, where Paleogene strata is deposited giving a blue color to the map. Oppositely, Miocene basins are abundant on the Iberian Peninsula, overlaying the Cretaceous and older rocks which results in high intensity base Miocene unconformities there.

At the base Pliocene boundary (Figure 3 e), moderate hiatus is located at the western margins of the North Sea, in Scandinavia, Eastern Barents Sea and France. Although, Pliocene rocks were accumulated West of Greenland, they constitute a part of the Neogene outcrops meaning that Miocene and Pliocene sequences are conformable. In addition, Greenland is covered by Quaternary cover, hindering hiatus identification of older than Quaternary stages. The same map pattern is observed along the western European margin, where Miocene and Pliocene deposits are not differentiated. The temporal resolution of the input geological map is the third limitation associated with our method, which can be improved with higher resolution input data in the future.

We find that during the fast velocity periods erosion affected significantly larger areas of northwestern Eurasia at the Paleocene – Eocene boundary and in the Miocene. Indeed, Figure 1 and 2 show that the main episodes of the spreading rate increase happened at c. 55 Ma and c. 20 Ma. The rate was at its slowest from c. 35 until 20 Ma and after 6 Ma. As expected, spreading rate varies as a function of latitude for most of the time intervals. The only exception is an additional rate increase at 40 to 34 Ma at southern latitudes (40°N curve), while for northern latitudes (from 55°N on) the spreading slows down at that time.

Figure 4 shows that hiatus intensity changes are following the trend of the North Atlantic spreading velocity variation. The spreading rate increase at 55 Ma was coeval with migration of erosion to the vast eastern areas and pronounced erosion at the East European Platform. Southern erosion was also very intense, but is an expected feature from the culmination of Pyrenean and Alpine orogenesis. The Eocene – Oligocene transition is characterized by the low hiatus values and slow spreading. The Oligocene – Miocene transition (23 Ma) exhibits a prominent unconformity located again at the ridge, which precedes a renewed spreading speed-up at ~19 Ma. Coeval with the fast Miocene spreading rate, erosion was propagating eastward. It affected eastern parts of the British Isles, the Scandes and northern parts of the East European Platform. Our findings indicate the following pattern: hiatus intensification at the ridge is followed by the increase of spreading velocity and the eastward propagation of erosion. Slow spreading rates agree with less intense hiatus.
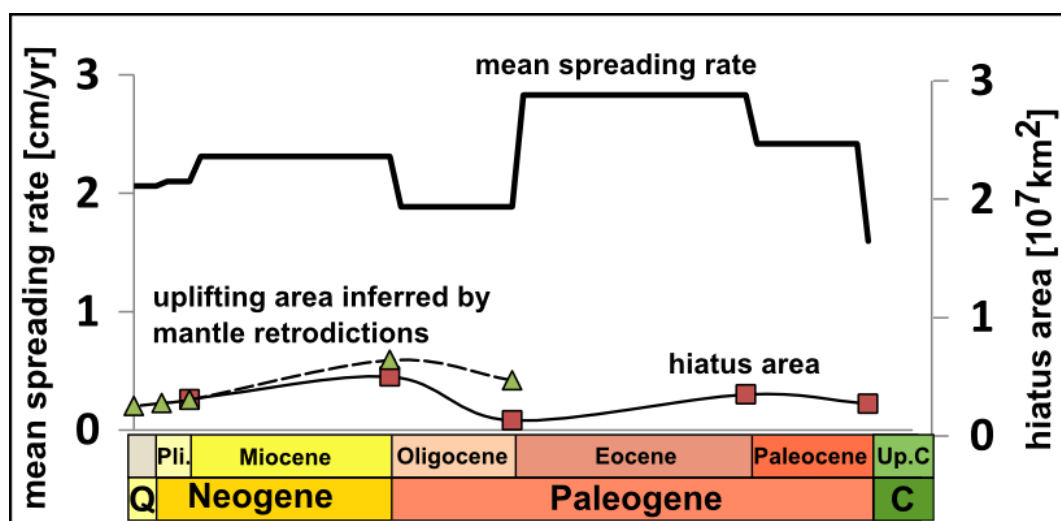
Figure 4: Link between the Spreading rate variations and hiatus magnitude. Plot showing North Atlantic spreading rate, averaged for distinct geological periods (black curve), and the variation of integral area of regions affected by hiatus in the northwestern Europe at respective time steps (black curve with red square markers). Also, Neogene uplift inferred by mantle retrodictions (Colli et al., 2015) is shown by black curve with green triangle markers. The larger area is affected by hiatus at the Paleocene- Eocene boundary, which corresponds to the maximum peak in the spreading rate around 55 Ma. The same holds for the late Oligocene-Miocene period (23 – 5 Ma) when abundant hiatus agrees with anomalously higher spreading rate and high dynamic topography. Oligocene minimum in spreading velocity corresponds to the lowest values of hiatus.

Discussion

What could link the Cenozoic northwestern European erosion and the North Atlantic spreading rate? To answer this question we have to understand the underlying mechanisms of both processes. The forces governing episodic uplifts of the passive continental margin are not very clear (Green et al., 2017). It has been long known that the driving force of plate spreading is mantle convection (Turcotte and Schubert, 2002). However, the observed spreading rate changes (Figure 2) cannot be explained by changes of large-scale mantle buoyancy, which has a time scale of 50-100 m.y.. This is the mantle transit time, which is the time required for a thermal anomaly to rise from a depth of c.1000 km by advection (Bunge et al. 1998). Such rapid spreading rate changes suggest that additional driving agents are involved.

A number of studies have looked at the effect of the far-field stresses on the spreading rate (Iaffaldano and Bunge, 2015; Janssen et al., 1995; Loomis and Morgan, 1973). Iaffaldano and Bunge (2015) estimated that Himalayan and Andean orogenic events contribute significantly to the global plate force balance and may explain up to 35% of spreading velocity variations. However, Colli et al. (2014) pointed out that some of the South Atlantic spreading rate changes are unrelated to the stress changes at the plate boundaries. Namely, this study showed that the late Cretaceous/Tertiary South Atlantic spreading rate increases most likely due to the unstable pressure-driven component in the mantle asthenosphere. Numerical models of such pressure-driven mantle flow imply a topography signal, which fits well with the geological observations of vertical plate motions of the African and South American continents.

The link between the North Atlantic spreading variations, uplift events and the asthenospheric flow has not yet been addressed. Pressure-driven mantle flow offers a

possible explanation of the Paleocene-Eocene and Miocene North Atlantic spreading changes (Figure 5). The support to this idea also comes from the full-wave tomography imaging of the low-viscosity asthenospheric channel beneath the North Atlantic (Rickers et al., 2013) and active magmatism accompanying spreading rate jumps (Breivik et al., 2014; Mjelde et al., 2008; Saunders et al., 1997; Smallwood and White, 2002). Since pressure-driven mantle flow contributes to dynamic topography, it could explain the agreement between the spreading rate trend and the erosion of the northwestern Europe (Figure 4). Furthermore, Schoonman et al. (2017) discussed the presence of several asthenospheric fingers, which stem from the Icelandic plume and extend beneath the British Isles and western Norway. An unsteady, pressure-driven flow in such thin asthenospheric channels may influence the topographic evolution of these regions. We also notice that the rapidly evolving eastward asthenospheric flow would agree well with West to East propagation of erosion observed in Figure 3.
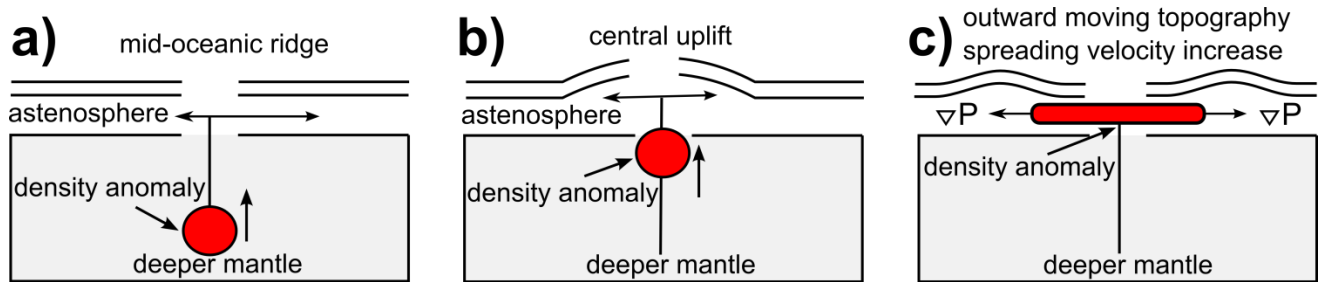
Figure 5. Schematic cartoon showing possible mechanism of coeval spreading rate increase and uplift of passive margins. The ascent of a hotter and less dense mantle material (b) causes uplift focused at the break-up area. As the density anomaly reaches asthenosphere, it causes an unstable pressure-driven flow (c). This flow results in increased spreading velocity and dynamic topography migrating away from the ridge.

Conclusions

We estimated the area of hiatus in northwestern Eurasia for five chronostratigraphic series' boundaries in the Cenozoic. The temporal variation in the spatial distribution of hiatal surfaces enables identification of changes of relative interregional elevation. This way, the study outlines the spatial and temporal variation of European topography throughout the Tertiary. Furthermore, we compare evolution of the northwestern Eurasian topography with the North Atlantic spreading rate.

Our estimates of northwestern Eurasian hiatus indicate that episodes of erosion intensification coincided with the episodes of the North Atlantic spreading acceleration. Also, northwestern Eurasian Cenozoic erosion exhibited a specific spatial pattern, where

erosion evolved eastwards from the Mid-Atlantic ridge into the continent. The underlying mechanisms of these processes are not very well understood, but are likely to result from the mantle dynamic support.

We suggest that such pattern may indicate a fast, plume-fed flow in the thin asthenospheric channel beneath northwestern Europe. The observed topographic signal may reflect a pressure-driven mantle flow, which is the dominant flow mode in a thin low-viscosity asthenosphere. Such flow serves as a link between the horizontal and vertical plate motions and could have implications for the paleo-topographic studies in Europe and in other regions.

Tables

TABLE 1. MAGNETIC LINEATIONS DATA

Lineation name in this paper	Width (km)	Time (Ma)	Isochrones Names Gradstein 2014 Timescale	Isochrone Ages Gradstein 2014 Timescale
A	7	0.8	C2	1.8-2.6
B	12	1	C2An	2.6-3.6
C	5	0.6	C2Ar	3.6-4.2
D	15	1	C3n.1n(y)-C3n.4n(o)	4.2-5.2
E	7	0.8	C3r.4r	5.2-6.0
F	8	0.6	C3A1n-C3A2n	6.0-6.7
G	10	0.8	C3A2n(o)-C4n1n(y)	6.7-7.5
H	9	0.6	C4n1n(y)-C4n2n(o)	7.5-8.1
I	13	1	C4n2n(o)-C4An(o)	8.1-9.1
J	7	0.8	C4An(o)-C5n.1n(y)	9.1-9.78
K	20	1.2	C5n.1n(y)-C5n.2n(o)	9.78-11.0
L	18	1.4	C5n.2n(o)-C5An.2n(o)	11.0-12.4

M	20	1.2	C5An.2n(o)-C5ACn(y)	12.5-13.7
N	40	3.5	C5ACn(y)-C5Dn(y)	13.7-17.2
O	34	2.6	C5Dn(y)-C6n(o)	17.2-19.7
P	130	13.6	C6n(o)-C13n(y)	19.7 – 33.2
Q	75	6.4	C13n(y)-C18n.1n(o)	33.2-39.8
R	40	3.6	C18n.1n(o)-C20n(o)	39.8-43.5
S	51	4.3	C20n(o)-C21n(o)	43.5-47.8
T	28	2	C21n(o)-C22n(o)	47.8-49.7
U	41	2.2	C22n(o)-C23n.2n(o)	49.7-51.9
V	63	2	C23n.2n(o)-C24n.3n(o)	51.9-53.9
W	78	3.8	C24n.3n(o)-C25n(o)	53.9-57.7
X	43	1.5	C25n(o)-C26n(o)	57.7-59.2
Y	86	3.3	C26n(o)-C27n(o)	59.2-62.5
Z	38	6.8	C27n(o)-C31n(o)	62.5-69.3

Table 1. Width and duration of magnetic linetations The table shows width and duration of magnetic lineations that were juxtaposed to test their linear relation in Figure 1**.** The compilation of the picks of magnetic chrones is from the digital archive: http://www.soest.hawaii.edu/PT/GSFML/ML/index.html. The isochrones picks are located at a parallel 54°N and are marked as black dots on the magnetic anomaly (EMAG3) map of the North Atlantic.

TABLE 2. GEOLOGICAL DATA

Time	Location	Source	Interpretation
Base Paleocene	British Isles	Thermochronology (Green et al., 2002; Hillis et al., 2008) Backstripping	Transient uplift of 180–425 m occurred during Paleocene times.

			analysis (Mackay et al., 2005)	
	North Sea	Stratigraphy (Anell et al., 2012; Evans, 2003)	The studies report thick deposits of presumably eroded material adjacent to the northern North Sea, the Scottish Highlands and the East Shetland Platform with thinner deposits next to southern Norway.	
	Scandes	Landform study (Lidmar-Bergström and Näslund, 2002) Thermochronolog y (Hendriks et al., 2007; Hendriks and Andriessen, 2002)	Uplift of the Scandes of the late Cretaceous-Paleocene age constrained by thermochronology.	
Base Eocene	Rhine Graben	Geodynamic study (Ziegler, 1992)	Magmatic dyke intrusions are documented in the Cretaceous-late Paleocene strata.	
	Pyrenees	Stratigraphy (Burbank et al., 1992)	The main stages of shortening in the Pyrenees took place from Paleocene to early Oligocene.	

	Porcupine	Subsidence modelling (Jones et al., 2001)	Transient uplift of 300-600 m at Paleocene- Eocene boundary.
	Faroe-Shetland	Stratigraphy (Champion et al., 2008)	Transient uplift of about 550 m in 3 Myr.
Base Oligocene	Upper Rhine Graben, Bohemian Massif	Paleotectonic maps (Dèzes et al., 2004).	Eocene activation of the fault systems with main rifting stage in the Oligocene.
Base Miocene	Porcupine	Stratigraphy (Stoker et al., 2005)	The base Miocene and middle Miocene significant unconformities recongnized in the Rockall Porcupine and Farroe-Shetland due to tectonism and formation of domes.
	Western Approaches	Paleotectonic maps (Dèzes et al., 2004)	Paris Basin and Western Approaches Basin inversions.
	Mediterranean	Geodynamic models based on sedimentary and structural data (Gunnell et al.,	28-20 Ma rifting in the Western Mediterranean and late Ruppelian unconformity in the Gulf of Lion (Southern France).

		2008; Séranne, 1999)	
Base Pliocene	British Isles	Thermochronology (Holford et al., 2005)	~1.5 km Neogene (20-0) uplift inferred by the AFT and compaction studies in the Mochras (NW Wales) borehole.
	North Sea	Stratigraphy ((Anell et al., 2012; Evans, 2003))	Middle to late Miocene hiatus of 5-12 Myr.
	Scandes	Isostatic modelling and study of landforms (Riis, 1996; Riis and Fjeldskaar, 1992; Stuevold and Eldholm, 1996; Lidmar-Bergström et al., 2013)	~1000 m of Neogene uplift in Southern Scandinavia and acceleration denudation in the northern Scandes.
		Thermochronology (Hendriks and Andriessen, 2002)	

Western	Stratigraphy	Documented hiatus in the Vestbakken
Barents Sea	(Eidvin et al.,	Volcanic Province from the early
	2014)	Miocene to late Pliocene.

Table 2. Overview of geological data related to erosion and uplift in Europe. The pattern of hiatus derived in our study is in good agreement with the results of the local studies on uplift and erosion.

Acknowledgements

References

Anell, I., Thybo, H., Rasmussen, E., 2012. A synthesis of Cenozoic sedimentation in the North Sea. Basin Res. 24, 154–179.

Asch, K., 2003. The 1: 5 Million International Geological Map of Europe and-Adjacent Areas: development and implementation of a GIS-enabled concept. Geologisches Jahrbuch, SA3, Schweizerbart'sche Verlagsbuchhandlung.

Breivik, A., Faleide, J.I., Mjelde, R., Flueh, E., Murai, Y., 2014. Magmatic development of the outer Vøring margin from seismic data. J. Geophys. Res. Solid Earth 119, 6733–6755.

Burbank, D.W., PuigdefÀBregas, C.A.I., Munoz, J.A., 1992. The chronology of the Eocene tectonic and stratigraphic development of the eastern Pyrenean foreland basin, northeast Spain. Geol. Soc. Am. Bull. 104, 1101–1120.

Champion, M.E., White, N.J., Jones, S.M., Lovell, J.P.B., 2008. Quantifying transient mantle convective uplift: An example from the Faroe-Shetland basin. Tectonics 27.

Clark, S.R., Skogseid, J., Stensby, V., Smethurst, M.A., Tarrou, C., Bruaset, A.M., Thurmond, A.K., 2012. 4DPlates: On the fly visualization of multilayer geoscientific datasets in a plate tectonic environment. Comput. Geosci. 45, 46–51.

Colli, L., Bunge, H.-P., Schuberth, B.S., 2015. On retrodictions of global mantle flow with assimilated surface velocities. Geophys. Res. Lett. 42, 8341–8348.

Colli, L., Stotz, I., Bunge, H.-P., Smethurst, M., Clark, S., Iaffaldano, G., Tassara, A., Guillocheau, F., Bianchi, M.C., 2014. Rapid South Atlantic spreading changes and coeval vertical motion in surrounding continents: Evidence for temporal changes of pressure-driven upper mantle flow. Tectonics 33, 1304–1321.

Dèzes, P., Schmid, S.M., Ziegler, P.A., 2004. Evolution of the European Cenozoic Rift System: interaction of the Alpine and Pyrenean orogens with their foreland lithosphere. Tectonophysics 389, 1–33.

Eidvin, T., Riis, F., Rasmussen, E.S., 2014. Oligocene to Lower Pliocene deposits of the Norwegian continental shelf, Norwegian Sea, Svalbard, Denmark and their relation to the uplift of Fennoscandia: A synthesis. Mar. Pet. Geol. 56, 184–221.

Embry, A.F., 2006. Episodic global tectonics: Sequence stratigraphy meets plate tectonics. Geo Expro 3, 26–30.

Evans, D., 2003. The Millennium Atlas: Petroleum Geology of the Central and Northern North Sea. A project of the Geological Society of London, the Geological Survey of Denmark and Greenland and the Norwegian Petroleum Society.

Friedrich, A.M., Bunge, H.-P., Rieger, S.M., Colli, L., Ghelichkhan, S., Nerlich, R., 2017. Stratigraphic framework for the plume mode of mantle convection and the analysis of interregional unconformities on geological maps. Gondwana Res.

Gaina, C., Roest, W.R., Müller, R.D., 2002. Late Cretaceous–Cenozoic deformation of northeast Asia. Earth Planet. Sci. Lett. 197, 273–286.

Gernigon, L., Gaina, C., Olesen, O., Ball, P.J., Péron-Pinvidic, G., Yamasaki, T., 2012. The Norway Basin revisited: From continental breakup to spreading ridge extinction. Mar. Pet. Geol. 35, 1–19.

Gradstein, F.M., Ogg, G., Schmitz, M., 2012. The Geologic Time Scale 2012 2-Volume Set. Elsevier.

Green, P.F., Duddy, I.R., Hegarty, K.A., 2002. Quantifying exhumation from apatite fission-track analysis and vitrinite reflectance data: precision, accuracy and latest results from the Atlantic margin of NW Europe. Geol. Soc. Lond. Spec. Publ. 196, 331–354.

Green, P.F., Japsen, P., Chalmers, J.A., Bonow, J.M., Duddy, I.R., 2017. Post-breakup burial and exhumation of passive continental margins: Seven propositions to inform geodynamic models. Gondwana Res.

Gunnell, Y., Zeyen, H., Calvet, M., 2008. Geophysical evidence of a missing lithospheric root beneath the Eastern Pyrenees: Consequences for post-orogenic uplift and associated geomorphic signatures. Earth Planet. Sci. Lett. 276, 302–313.

Hendriks, B., Andriessen, P., Huigen, Y., Leighton, C., Redfield, T., Murrell, G., Gallagher, K., Nielsen, S.B., 2007. A fission track data compilation for Fennoscandia. Nor. Geol. Tidsskr. 87, 143.

Hendriks, B.W., Andriessen, P.A., 2002. Pattern and timing of the post-Caledonian denudation of northern Scandinavia constrained by apatite fission-track thermochronology. Geol. Soc. Lond. Spec. Publ. 196, 117–137.

Henriksen, E., Bjørnseth, H.M., Hals, T.K., Heide, T., Kiryukhina, T., Kløvjan, O.S., Larssen, G.B., Ryseth, A.E., Rønning, K., Sollid, K., Stoupakova A., 2011. Uplift and erosion of the greater Barents Sea: impact on prospectivity and petroleum systems. Geol. Soc. Lond. Mem. 35, 271–281.

Hillis, R.R., Holford, S.P., Green, P.F., Doré, A.G., Gatliff, R.W., Stoker, M.S., Thomson, K., Turner, J.P., Underhill, J.R., Williams, G.A., 2008. Cenozoic exhumation of the southern British Isles. Geology 36, 371–374.

Höink, T., Lenardic, A., 2010. Long wavelength convection, Poiseuille–Couette flow in the low-viscosity asthenosphere and the strength of plate margins. Geophys. J. Int. 180, 23–33.

Holford, S.P., Green, P.F., Turner, J.P., 2005. Palaeothermal and compaction studies in the Mochras borehole (NW Wales) reveal early Cretaceous and Neogene exhumation and argue against regional Palaeogene uplift in the southern Irish Sea. J. Geol. Soc. 162, 829–840.

Iaffaldano, G., Bunge, H.-P., 2015. Rapid Plate Motion Variations Through Geological Time: Observations Serving Geodynamic Interpretation. Annu. Rev. Earth Planet. Sci. 43, 571–592.

Iaffaldano, G., Hawkins, R., Bodin, T., Sambridge, M., 2014. REDBACK: Open-source software for efficient noise-reduction in plate kinematic reconstructions. Geochem. Geophys. Geosystems 15, 1663–1670.

Janssen, M.E., Stephenson, R.A., Cloetingh, S., 1995. Temporal and spatial correlations between changes in plate motions and the evolution of rifted basins in Africa. Geol. Soc. Am. Bull. 107, 1317–1332.

Japsen, P., Bonow, J.M., Green, P.F., Cobbold, P.R., Chiossi, D., Lilletveit, R., Magnavita, L.P., Pedreira, A., 2012a. Episodic burial and exhumation in NE Brazil after opening of the South Atlantic. Geol. Soc. Am. Bull. 124, 800–816.

Japsen, P., Chalmers, J.A., 2000. Neogene uplift and tectonics around the North Atlantic: overview. Glob. Planet. Change 24, 165–173.

Japsen, P., Chalmers, J.A., Green, P.F., Bonow, J.M., 2012b. Elevated, passive continental margins: Not rift shoulders, but expressions of episodic, post-rift burial and exhumation. Glob. Planet. Change 90, 73–86.

Japsen, P., Cobbold, P.R., Chalmers, J.A., Green, P.-F., Bonow, J.-M., 2012c. Changes in plate motion and vertical movements along passive continental margins, in: 34th International Geological Congress, Brisbane, 5–10.

Japsen, P., Green, P.F., Chalmers, J.A., 2005. Separation of Palaeogene and Neogene uplift on Nuussuaq, West Greenland. J. Geol. Soc. 162, 299–314.

Japsen, P., Green, P.F., Lidmar-Bergström, K., Bonow, J.M., Erlström, M., 2014. Burial and exhumation history of southern Sweden estimated from apatite fission-track data, stratigraphic landform analysis and the geological record. Presented at the EGU General Assembly Conference Abstracts, 6814.

Jones, S.M., Lovell, B., Crosby, A.G., 2012. Comparison of modern and geological observations of dynamic support from mantle convection. J. Geol. Soc. 169, 745–758.

Jones, S.M., White, N., Lovell, B., 2001. Cenozoic and Cretaceous transient uplift in the Porcupine Basin and its relationship to a mantle plume. Geol. Soc. Lond. Spec. Publ. 188, 345–360.

Leighton, M.W., 1991. Interior cratonic basins. American Association of Petroleum Geologists.

Lidmar-Bergström, K., Bonow, J.M., Japsen, P., 2013. Stratigraphic Landscape Analysis and geomorphological paradigms: Scandinavia as an example of Phanerozoic uplift and subsidence. Glob. Planet. Change 100, 153–171.

Lidmar-Bergström, K., Näslund, J.O., 2002. Landforms and uplift in Scandinavia. Geol. Soc. Lond. Spec. Publ. 196, 103–116.

Loomis, T.P., Morgan, W.J., 1973. Sea-floor spreading rate changes in the South Atlantic. Mar. Geophys. Res. 2, 3–9.

Mackay, L.M., Turner, J., Jones, S.M., White, N.J., 2005. Cenozoic vertical motions in the Moray Firth Basin associated with initiation of the Iceland Plume. Tectonics 24.

Merkouriev, S., DeMets, C., 2014. High-resolution Neogene reconstructions of Eurasia-North America Plate motion. Geophys. J. Int. 198, 366–384.

Mjelde, R., Breivik, A.J., Raum, T., Mittelstaedt, E., Ito, G., Faleide, J.I., 2008. Magmatic and tectonic evolution of the North Atlantic. J. Geol. Soc. 165, 31–42.

Müller, R.D., Sdrolias, M., Gaina, C., Roest, W.R., 2008. Age, spreading rates, and spreading asymmetry of the world's ocean crust. Geochem. Geophys. Geosystems 9.

Pitman, W.C., Talwani, M., Heirtzler, J.R., 1971. Age of the North Atlantic Ocean from magnetic anomalies. Earth Planet. Sci. Lett. 11, 195–200.

Praeg, D., Stoker, M.S., Shannon, P.M., Ceramicola, S., Hjelstuen, B., Laberg, J.S., Mathiesen, A., 2005. Episodic Cenozoic tectonism and the development of the NW European "passive"continental margin. Mar. Pet. Geol. 22, 1007–1030.

Rickers, F., Fichtner, A., Trampert, J., 2013. The Iceland–Jan Mayen plume system and its impact on mantle dynamics in the North Atlantic region: Evidence from full-waveform inversion. Earth Planet. Sci. Lett. 367, 39–51.

Riis, F., 1996. Quantification of Cenozoic vertical movements of Scandinavia by correlation of morphological surfaces with offshore data. Glob. Planet. Change 12, 331–357.

Riis, F., Fjeldskaar, W., 1992. On the magnitude of the Late Tertiary and Quaternary erosion and its significance for the uplift of Scandinavia and the Barents Sea, in: Structural and Tectonic Modelling and Its Application to Petroleum Geology. Elsevier Amsterdam, pp. 163–185.

Roest, W.R., 1987. Seafloor spreading pattern of the North Atlantic between 10o and 40o N: a reconstruction based on shipborne measurements and satellite altimeter data. Geol. Ultraiectina 48, 1–121.

Rohrman, M., van der Beek, P., 1996. Cenozoic postrift domal uplift of North Atlantic margins: an asthenospheric diapirism model. Geology 24, 901–904.

Saunders, A.D., Fitton, J.G., Kerr, A.C., Norry, M.J., Kent, R.W., 1997. The north Atlantic igneous province. Large Igneous Prov. Cont. Ocean. Planet. Flood Volcanism 45–93.

Schoonman, C.M., White, N.J., Pritchard, D., 2017. Radial viscous fingering of hot asthenosphere within the Icelandic plume beneath the North Atlantic Ocean. Earth Planet. Sci. Lett. 468, 51–61.

Séranne, M., 1999. The Gulf of Lion continental margin (NW Mediterranean) revisited by IBS: an overview. Geol. Soc. Lond. Spec. Publ. 156, 15–36.

Seton, M., Müller, R.D., Zahirovic, S., Gaina, C., Torsvik, T., Shephard, G., Talsma, A., Gurnis, M., Turner, M., Maus, S., 2012. Global continental and ocean basin reconstructions since 200Ma. Earth-Sci. Rev. 113, 212–270.

Smallwood, J.R., White, R.S., 2002. Ridge-plume interaction in the North Atlantic and its influence on continental breakup and seafloor spreading. Geol. Soc. Lond. Spec. Publ. 197, 15–37.

Stoker, M.S., Hoult, R.J., Nielsen, T., Hjelstuen, B.O., Laberg, J.S., Shannon, P.M., Praeg, D., Mathiesen, A., Van Weering, T.C.E., McDonnell, A., 2005. Sedimentary and oceanographic responses to early Neogene compression on the NW European margin. Mar. Pet. Geol. 22, 1031–1044.

Stuevold, L.M., Eldholm, O., 1996. Cenozoic uplift of Fennoscandia inferred from a study of the mid-Norwegian margin. Glob. Planet. Change 12, 359–386.

Torsvik, T.H., Müller, R.D., Van der Voo, R., Steinberger, B., Gaina, C., 2008. Global plate motion frames: toward a unified model. Rev. Geophys. 46.

Turcotte, D.L., Schubert, G., 2002. Geodynamics. Cambridge University Press.

Vogt, P.R., Johnson, G.L., Holcombe, T.L., Gilg, J.G., Avery, O.E., 1971. Episodes of sea-floor spreading recorded by the North Atlantic basement. Tectonophysics, Global Tectonics and Sea-Floor Spreading 12, 211–234.

Weismüller, J., Gmeiner, B., Ghelichkhan, S., Huber, M., John, L., Wohlmuth, B., Rüde, U., Bunge, H.-P., 2015. Fast asthenosphere motion in high-resolution global mantle flow models. Geophys. Res. Lett. 42.

Ziegler, P.A., 1992. European Cenozoic rift system. Tectonophysics 208, 91–111.

Curriculum Vitae
YULIA VIBE

Birth date: 20.09.1989
Nationality: Russian

EXPERIENCE

Kalkulo
2014 - July 2017

Industrial PhD student
Analysing the physical mechanisms of geological basin development and vertical plate motions
Key Achievements:
> Building a digital geological data base of the West Siberian Basin
> High Impact Factor journal publication and conference presentations
> Promotion of the software products at the industrial exhibition EAGE
> Responsibility for the company's environment - safety delegate, fire ward and a member of the company election board

Simula Research Laboratory
2012 - 2014

Research trainee
Constructing the research project and acquiring presentation and scientific writing skills
Key Achievements:
> Successful funding proposal application
> Participation in written and oral communication courses
> Presentation at the Statoil 5DPaleoEarth Workshop and EGU conference

EDUCATION

Simula School of Research and Innovation
2011 - 2012

Master student in Computational Geoscience
Thesis work on causes of spreading velocity variations in the North Atlantic In collaboration with Statoil

Ludwig-Maximilians University of Munich and Technical University of Munich
2010 - 2012

Joint Master's Programme in Geophysics
Courses in applied mathematics and geological processes with major in Geodynamics.
Good performance over all exams (final grade 2.29 "good").

Novosibirsk State University
2006 - 2010

Bachelor's Programme in Mathematics
Programme in advanced mathematics and programming with major in applied mathematics. Excellent performance in all exams of the major.

PROFESSIONAL SKILLS

> Scientific and operational software (GMT, ArcGIS, Matlab, Gplates, 4DPlates, Inkscape, VirtualBox, Microsoft Office Package)
> Experience with programming languages (Python, C++)
> Knowledge of applied mathematics methods
> Training in presenting complex research concepts to general audience

LANGUAGES

English - Fluent
Norwegian - B2 test certificate
Russian - Native
Portuguese - B2 self- assessment
German - B1 self- assessment

List of corrections made to the submitted version.

Dear Committee,

Please, find below the list of changes that I introduced to the submitted thesis manuscript.

Note that page numbers correspond to the numbers in the headers.

Page 1, line 15 – "Alfred Wegener" changed to "Wegener"

Page 1 line 25 – "crust" changed to "lithosphere"

Page 4 line 14 – "(See Chapter 1 for more details)" changed to "(See Chapter 1)"

Page 5 line 7 – "geological" changed to "geophysical"

Page 7 line 30 –" coincident" changed to "coeval"

Page 45 line 2 – added "on" before "Caledonian suture"

Page 45line 8 – "Tomographic models" changed to "Tomographic models interpretation"

Page 54 line 4 – "global" changed to "regional"

Page 54 line 19 – "global" changed to "regional"

Page 54 line 33 – "area" to "distance"

Page 54 line 44 – "global" to "regional"

Page 65 line 6 – "at the time being of" changed to "at the time of"

In addition, I fixed the reference lists issues.

Kind regards,

Yulia